The Coupled Development of Terrain and Vegetation: The Case of Semiarid Grasslands

by

Javier Homero Flores Cervantes

C.E., Universidad Nacional Autónoma de México (2001)
S.M., Massachusetts Institute of Technology (2004)

Submitted to the Department of Civil and Environmental Engineering
in partial fulfillment of the requirements for the degree of

Doctor of Philosophy

at the

Massachusetts Institute of Technology

February 2010

Author .....
Department of Civil and Environmental Engineering
January 8, 2010

Certified by .....
Rafael L. Bras
Professsor of Civil and Environmental Engineering
Thesis Supervisor

Accepted by .....
Daniele Veneziano
Chairman, Departmental Committee for Graduate Students

The Coupled Development of Terrain and Vegetation: The Case of Semiarid Grasslands

by

Javier Homero Flores Cervantes

Submitted to the Department of Civil and Environmental Engineering
on January 8, 2010, in partial fulfillment of the
requirements for the degree of
Doctor of Philosophy in the Field of Hydrology

ABSTRACT

The distribution of vegetation in semiarid landscapes organizes as a function of moisture availability, which is often mediated by the form of the land surface. Simultaneously the processes that shape the land surface are influenced by vegetation, mainly because vegetation reduces fluvial erosion. This thesis presents the study of the bidirectional interaction between vegetation and the land form in semiarid grasslands.

Remotely sensed data and digital elevation maps are used to infer the relationship between vegetation cover and topographic attributes at two field sites in the semiarid southwestern United States. A positive relationship between drainage area (a proxy for water accumulation) and vegetation, and a negative relationship between solar radiation incidence and vegetation, are identified.

The Channel-Hillslope Integrated Landscape Development (CHILD) model is modified to include a detailed representation of soil moisture dynamics, vegetation dynamics, seasonality of the solar forcing and rainfall, spatial variability of the incidence angle of solar radiation, and intrastorm variability of rainfall intensity. The soil moisture and vegetation dynamics components of the model are calibrated and compared to observations from a small catchment in southeastern Arizona. The representation of the evolution in time of evapotranspiration, soil moisture and above ground vegetation, and of the spatial distribution of vegetation with the model, are satisfactory.

CHILD was used to simulate the evolution of the landscape under bare surface, uniform and stationary vegetation, and dynamic vegetation conditions to evaluate the effects of a dynamic vegetation cover in ten thousand years. In these simulations the emergence of bedrock outcrops that lead to significant runoff, erosion, and the accumulation of sediments and moisture downstream of the bedrock-regolith interface, had the most significant impact in the landscape. Erosion was greatest in the bedrock outcrops, and bands of sediment and moisture accumulation in their downstream ends lead to the development of bands of vegetation that augmented the accumulation of sediment and runoff infiltration.

Thesis Supervisor: Rafael L. Bras
Title: Professsor of Civil and Environmental Engineering

Acknowledgments

I gratefully acknowledge the support provided by the Department of Civil and Environmental Engineering through the Schoettler Fellowship, the support provided by the U. S. Army Research Office (agreement DAAD 19-01-1-0513), and NSF for the support provided through a biocomplexity grant (EAR 0642550).

I thank David Goodrich, Lainie Levick, Chandra Holifield and Susan Moran from the Southwest Watershed Research Center, for the LIDAR derived DEM, Landsat TM images and soil and hydrometeorological data provided for the grassland site in southeastern Arizona; and The Sevilleta Long Term Ecological Research (LTER) Program, for the DEM and grass biomass maps of the central New Mexico site made available on the internet.

I am grateful to my advisor for giving me the opportunity to work with him and be here surrounded by so many opportunities, brilliant and hardworking people, and resources. I feel privileged to be here.

I am grateful to my thesis committee members other than Rafael: Elfatih Eltahir, Erkan Istanbulluoglu, Ignacio Rodríguez Iturbe, and Kelin Whipple. Some of them came from distant cities to the thesis committee meetings, or constantly provided me with input by e-mail, to help me guide my research. Thank you.

I also wish to thank all the help from professors and colleagues through my years at MIT. Some that I want to mention are Kelin, Jack, Ole, Dara, Kris, Cynthia, Jeanette, Jim, Sheila, Gayle, Vicky and Elaine. Many thanks to current and past Bras team members, for moral and other types of support and friendship: Fred, Daniel, Nicole, Erkan, Enrique, Ola, Giacomo, Miguel, Lejo, Gaj, Gautam, Ryan, Chiara, Tony, Jingfeng, Valeri, Ujjwal, Vanessa and Fernando. Also many thanks to the parsonites, that make of this building a fine community to live in. To my friends and girlfriends, family, grandparents, sisters and parents, I want to thank you for all the love and support while I worked on this long project. You brought and bring light to my journey. Maya, Flo, Craig, Suzuko, Douglas, Janelle, Hanke, Susan, Carlos, Aiste, Heather, Ruta, Daiva, Saskia, Elena, Emily, Rebeca, Cepi, Matt, Kim, Jeanne, Shane, Ana, Daniel V., Adnan, Elsa, Sylvain, Matea, Feli, Daniel D., Ale, Thomas, Helene, Caitlin, Aidita, Marc, Juan Manuel, Tempe, Pauline, Claudia, Shinu, Victor, Paola, Mike, Lisette, Jackeline, Carolyn, Arlene, Arlyn, Francisco and Joanna, at one point or another through all my years in Cambridge you have helped me in one way (or many ways) or another. I want to thank you.

I know I wouldn't have arrived here in the first place without the help and work of many other people in Mexico before I came to Cambridge, I also want to thank them all.

TABLE OF CONTENTS

LIST OF FIGURES

LIST OF TABLES

CHAPTER 1

INTRODUCTION AND BACKGROUND

1.1 Introduction

Vegetation modifies the hydrologic and geomorphic properties of the land surface and as a result geomorphic processes modify the surface at different rates under different vegetation covers. Plant development, in turn, largely depends on topographic organization. This dependency is shown in the fact that different plant communities develop across different topographic settings. Thus, the evolution of land features such as mountains, rivers, and valleys is intimately related to the development of plants.

Despite the evident interdependence between vegetation and topography, little is known about how vegetation and topography co-evolve to produce the landscapes we observe today, if indeed they do, and to what extent the interplay between topography and vegetation affects the evolution of a landscape. The development and use of a physically based model that represents the topography-vegetation interaction during their simultaneous evolution can greatly improve our understanding of this matter. Such a model would allow a more realistic representation of both, topographic evolution and vegetation community development.

This thesis investigates the interdependence between the evolution of topography and vegetation in water-limited ecosystems by means of physically based numerical simulation. The numerical model considers the following factors: vegetation controls on water flux on a basin and on erosion-deposition processes, topography controls on moisture fluxes, and soil moisture controls on vegetation dynamics. The above factors are analyzed under a dynamic topography framework.

The spatial scale addressed in this study is that of small drainage basins, between 0.01 to 4 km^2. The temporal scales addressed are two. The evolution of topography is analyzed in thousands of years; the evolution of vegetation is analyzed in more detail at yearly time scales.

The Channel-Hilllsope Integrated Landscape Development (CHILD) model was modified to enable the representation of the interaction of vegetation and topography. The model additions of moisture and vegetation dynamics are tested by comparing its outputs to observations. Digital maps of topography and vegetation are also analyzed to search for correlations between the spatial distribution of vegetation and topographic attributes of the land surface. These correlations serve as a basis of comparison for the modeling.

The objective of this work is to evaluate the effects of the interplay between vegetation and topography in the evolution of a small drainage basin. Quantitative answers to the following questions are investigated:

1. Do current landforms result from the topography-vegetation interaction, or would landforms have evolved to their present condition without this interaction?

2. Have current vegetation communities in a landscape adapted to the present topographic conditions and reached a steady state (which corresponds to the contemporary topography and climate)? Is this steady state dependent upon or independent of the history of the topography-vegetation interaction?

3. Assuming a topography-vegetation interaction, how sensitive are the processes acting on a landscape to external disturbances in climate and land cover? How sensitive is the steady state of a landscape to these external disturbances?

1.2 Background

Ridges, hillslopes and streams are topographic elements that together with plants and soil properties constantly interact through hydrologic processes within a system enclosed in a drainage basin. Strong interdependencies exist between these topographic elements and basin hydrology, between plants and basin hydrology, and as a consequence of these first two, there is an interdependence between basin topography and plants. The above interdependencies have been extensively studied and documented, and below a brief review is presented to emphasize the relevance of each of the elements considered in the modeling work and to justify the modeling considerations.

1.2.1 Interdependence of topographic features and hydrology

Changes in landforms significantly depend on the amount and direction of water flow across a basin (basin hydrology). Conversely, flow on a basin is predominately controlled by topography [*Huang et al.*, 2002; *Rodríguez-Iturbe and Valdés*, 1979].

Rates of topographic denudation are commonly considered proportional to the shear stress that flowing water (or wind) exerts on a surface. Thus, geomorphic processes are most intense where the largest amounts of water discharge concentrate, and where flow velocities are highest (i.e., where the slope is steepest and smooth).

It is along those areas where the most rapid changes in landforms occur.

Topography directs the surface water fluxes and affects the concentrations, velocity and distribution of flow in time and space across a basin. Concave hillslopes cause convergence of flow while convex hillslopes induce divergence. Water flow velocity increases with hillslope and channel steepness. The distribution of a basins outflow in time depends on the shape of the basin and on the distribution of its channel network. For example, in elongated basins flow will be more uniformly distributed than on rounded basins [*Surkan*, 1969].

1.2.2 Interdependence of vegetation and hydrology

The establishment of vegetation on the landscape is determined in more than one way by the fluxes of water [*Rodríguez-Iturbe and Porporato*, 2005]. The availability of water in the land surface is a limiting factor in plant development, as either excess or scarcity can prevent their existence. Water availability, thus, is responsible for the variety of plant communities found on terrestrial landscapes (e.g., *Shmida and Burgess* [1988]). Fluxes of water also affect plant development. Large amounts of flux through the soil can decrease nutrient availability through leaching, thus limiting plant growth. Large amounts of flow on the surface can damage plants. As a consequence, only the few plants that survive floods or that rapidly regenerate can develop in zones where floods frequently damage vegetation [*Sigafoos*, 1961; *Scatena and Lugo*, 1995]. Evidence of this interdependence has been observed where man has altered the natural state of a basin. For example, changes in the hydrologic response of a basin due to dam control result in changes in vegetation over the course of years [*Johnson et al.*, 1976].

The fluxes of water in a basin are affected in various ways by vegetation. On a local scale vegetation affects the roughness of the surface, thus, horizontal water fluxes across the land are slower on vegetated surfaces [*Abrahams et al.*, 1995]. Vegetation also affects the vertical fluxes of water on the land by canopy interception, enhancement of the surface's infiltration capacity and water store capacity, and transpiration (e.g., *Selby* [1970]; *Wistendahl* [1958]; *Mosley* [1982]; *Aldrige and Jackson* [1968]). Because of the transformations described above, changes in vegetation immediately after fires, for example, result in new hydrologic basin responses [*Wistendahl*, 1958; *Gurnell et al.*, 1990; *Francis and Thornes*, 1990; *Moody and Martin*, 2001; *Benavides-Solorio and MacDonald*, 2001].

1.2.3 Interdependence of topographic features and vegetation

Topography can control the development and spatial distribution of vegetation, while vegetation influences erosion and deposition of soil and hence may exert a feedback on topography. As is shown below, the signals between topographic development and plant development are transmitted through the hydrologic processes of the basin.

Topographic controls on vegetation development

Vegetation development is largely controlled by the amount and distribution in time of water available to plants. Water availability is often responsible for differences among plant community (e.g., grasslands, savannas, forests) [*Rodríguez-Iturbe and Porporato*, 2005]. Therefore, vegetation development is often considered mainly a function of water stored in the soil. The amount of water stored in the soil is measured as soil moisture. Soil moisture is the percentage, in volume, of soil pores filled with water. The amount of water stored in the soil depends on climate, soil characteristics, vegetation, and topography. In relation to climate, *Shmida and Burgess* [1988] show a general link between precipitation and ecosystem type, biomass and biodiversity. Several studies have shown an increase in plant recruitment with holding capacity [*Lauenroth et al.*, 1994]. Soil depth and texture have been recognized as key factors in soil water holding capacity and vegetation development [*Porporato et al.*, 2001; *Laio et al.*, 2001a]. Vegetation affects the inputs and outputs of water from soil in several ways, for example, it significantly modulates infiltration rates [*Selby*, 1970], intercepts rainfall [*Lull*, 1964], and regulates rates of evapotranspiration (e.g., *Molchanov* [1971]). Topography affects soil moisture distribution on the hillslope scale [*Ridolfi et al.*, 2003] and on the basin scale [*Hack and Goodlett*, 1960]. Concave and topographically convergent regions are generally moister than convex and divergent regions. Aspect, the orientation of a hillslope with respect to the geographic north, is a characteristic of topography that often has been related to vegetation and soil development [*Hack and Goodlett*, 1960; *Kirkby et al.*, 1990; *Hidalgo et al.*, 1990].

Vegetation development is also controlled by erosion. Frequency of damaging floods in different sections of the landscape affect the distribution of vegetation species and age distribution of plants across a basin. *Scatena and Lugo* [1995] and *Basnet* [1992] describe species and age distribution of trees in a tropical basin in Puerto Rico, where ridges have older trees than valleys. Valleys are frequently disturbed by floods and have trees and species that reproduce rapidly. *Hack and Goodlett* [1960] and *Teversham and Slaymaker* [1976] describe patterns of plant community distribution in a basin that are correlated to the frequency of flood disturbances.

Vegetation controls on geomorphic processes

Experiments and measurements in flumes and plots have shown the impact of vegetation cover on runoff and sediment yield, where sediment yield is not only a function of the runoff produced shear stress, but also a function of the erodibility of the soil and of the deposition of soil where vegetation acts as a barrier against flow (e.g., *Abrahams et al.* [1995]; *Vacca et al.* [2000]; *Rey* [2003]; *Trimble* [1990]; *Sorriso-Valvo et al.* [1995]). Vegetation reduces soil erodibility [*Reid*, 1989; *Prosser and Dietrich*, 1995; *Prosser and Slade*, 1994] and is responsible for altering soil chemistry leading to enhanced resistance to erosion [*Angers and Caron*, 1998; *Viles*, 1990]. Plants also provide soil with cohesive strength by means of their roots [*Greenway*, 1990; *Bormann and Liekens*, 1979]. In addition, plants further reduce sediment yield due to

rain splash protection and rainfall interception [*Abrahams et al.*, 1995; *Aldrige and Jackson*, 1968]. Finally, plants offer resistance and protection against the flow of water or air, thus decreasing the shear stress exerted on the soil [*Prosser and Slade*, 1994].

In addition to the effects of vegetation on the erosion of the landscape by water flow, vegetation (together with other living organisms) enhances weathering and thus soil production. However, if the weathered material is not retained, it leads to denudation (e.g., *Yair* [1995]).

Because of the significant effect of vegetation on water flow, and as a consequence on geomorphic processes and landform evolution, a detailed representation of water flow is critical to capture the effects of vegetation on geomorphic processes. Important progress has recently been made in estimation of flow on small basins taking into account the heterogeneity of rainfall and surface properties, including soil moisture conditions [*Ivanov et al.*, 2004]. Field and numerical evidence show the importance of temporal and spatial variability in precipitation and flow across a basin on geomorphic processes [*Molnár and Ramírez*, 2001; *Sólyom and Tucker*, 2004]. These results reinforce the importance of resolving flow variation in time and space when modeling landscape evolution.

The interdependencies between topographic features and hydrology, plants and hydrology, and topographic features and plants, have profound implications on the evolution of a landscape. This work expands the understanding of the integration of all three in landscapes.

1.2.4 Modeling of landscape evolution

The interactions between landforms and vegetation through hydrologic and geomorphic processes have been described qualitatively, based mostly on field observations from small scales (e.g., the size of a plant) to larger scales (e.g., the size of a basin). These interactions are numerous, they occur in a three-dimensional space and in a wide range of temporal scales. In order to elucidate the feedbacks that are most important in landscape evolution, we need to isolate variables, change initial and boundary conditions, and measure responses to these changes in a well-controlled environment. Numerical modeling has been one of the preferred tools to do so and will be the main tool of study in the proposed work. Before describing the modeling approach for this work, a brief summary of the efforts of numerical modeling in the field of landscape evolution is provided.

Development of numerical models to simulate soil erosion and landscape evolution based on water fluxes across the surface, tectonic uplift, sediment deposition, mass wasting, and even Martian geomorphic processes is highly advanced (e.g., *Howard* [1988, 1994]; *Tucker and Bras* [1998]; *Tucker et al.* [2001]; *Willgoose et al.* [1991]). A review of contemporary basin evolution models is given in *Coulthard* [2001]. Numerical models that simulate vegetation growth by considering nutrients, climate, and internal plant dynamics on various scales have provided surprising new understanding of

plant community development and response to natural and human disturbances (e.g., *Moorcroft et al.* [2001]). Others have used numerical modeling to study specifically the interactions between vegetation growth and soil moisture (e.g., *Rodríguez-Iturbe et al.* [2001]). The modeling of hydrologic processes taking into account the effects of vegetation is constantly improving. One such model, tRIBS, considers spatial heterogeneity and temporal variability in hydrometeorological forcing (e.g., rainfall) and land surface characteristics, which include soil moisture and vegetation cover [*Ivanov et al.*, 2004]. Recent developments of this hydrologic model incorporate the dynamic development of plants. Results show that topography affects plant development by regulating soil water and energy budgets. In the model the surface and subsurface flow of water are by and large controlled by topography, and energy fluxes and water evapotranspiration are largely controlled by solar radiation, dependent on aspect and slope of the terrain. In model simulations, for example, plants grow at different rates on opposing sides of a ridge due to differences in exposure to solar radiation, and biomass production is distinctively higher in plants growing in channels than in plants growing in hillslopes. In tRIBS, however, topography does not change in time [*Ivanov et al.*, 2008a].

The study of the interaction between landforms and vegetation through geomorphic and hydrologic processes has also evolved. Some models that represent basin scale landform evolution have incorporated the effects of vegetation to a certain extent. Some examples are SIBERIA and GOLEM [*Willgoose et al.*, 1994; *Tucker and Slingerland*, 1996], Howard's [*Howard*, 1994] detachment limited model, and CHILD [*Tucker et al.*, 2001]. The last has explored the role of vegetation on landscape evolution in a simplified way, considering only the effects of vegetation on the erodibility properties of the surface. Until recently, vegetation dynamics in CHILD had been only a function of space available for growth and erosion (which kills the plants) [*Collins et al.*, 2004]. *Coulthard et al.* [2002] developed a model that represents landscape evolution at fine spatial and temporal scales (3 m grid cells and time steps within rainfall events) in which vegetation affects the flow and where vegetation growth is a function of erosion and time of recovery only. *Kirkby et al.* [2002] have developed a model (MEDRUSH) designed to estimate runoff and sediment yield from Mediterranean landscapes on scales of 100 years. In this model, a sophisticated vegetation component that modifies the soil properties and the thus the hydrologic and geomorphic processes has been included. This model, however, does not consider any topographic change. *Istanbulluoglu and Bras* [2006] devised a point model that estimates the erodibility of soil as a function of the state of vegetation on the surface. In their model vegetation growth and death is a function of plant stress due to water availability. Water availability is estimated through a soil water balance where the infiltration process, canopy interception and evapotranspiration are all functions of the state of vegetation. The principles employed by *Istanbulluoglu and Bras* [2006] to simulate the development of vegetation and vertical fluxes across the land surface are used in the modeling work proposed here. *Istanbulluoglu and Bras* [2005] analyzed the response of a landscape under a uniform vegetation cover under different tectonic uplift rates and rainfall. From such analysis it was concluded that the dominant ge-

omorphic process depends on the combination of the three elements: tectonic uplift, vegetation cover, and rainfall. *Istanbulluoglu and Bras* [2005] also simulated vegetation development in a landscape under a climate characteristic of the Oregon Range Coast using a simple vegetation development model independent of soil moisture in CHILD. They compared the landscape evolving with a vegetation cover to an unvegetated landscape. The vegetated landscape had a high and steep relief with a small drainage density that contrasted with the unvegetated landscape, which displayed low relief, gentle slopes and higher drainage density.

The modeling efforts discussed above have not captured the implications of the vegetation-topographic features interdependence described in the preceding section. This work takes advantage of all the previous modeling efforts in this area (CHILD is modified), to capture such interdependence.

1.3 Thesis outline

The thesis is comprised of 6 chapters, including this Introduction. Chapter 2 presents an analysis of the links between vegetation, radiation and topography for two sites in semi-arid grasslands, the environment that is the focus of this work. For the analysis a series of measures to quantify the distribution of vegetation as a function of topographic attributes were developed. These measures are later used to compare modeling outputs with observations in Chapters 4 and 5.

Chapter 3 presents CHILD and its new capabilities. These new capabilities include a new Barlett-Lewis rainfall generation algorithm that captures intra-storm variability, a critical component for the generation of runoff in semiarid regions. The latest version of CHILD also represents the seasonality of rainfall and of solar forcing. A characteristic of the new model is that its vegetation parameters are grounded on physical measurements that can be found literature. The fine temporal scale representation of climate and vegetation dynamics (including seasonality) allows for a direct comparison of the modeling to field or remote sensing observations of vegetation dynamics.

Moisture dynamics and their link to vegetation dynamics had been previously incorporated into the model [*Collins and Bras*, 2008]. In that work transpiration was proportional to vegetation fractional cover, and vegetation dynamics followed a logistic growth equation whose colonization rate was proportional to transpiration, and death rate was proportional to a static water stress. In this work, the links between moisture and vegetation dynamics are similar, yet the logistic equation is not used to represent the vegetation dynamics. This work uses the water use efficiency (WUE) concept, which has been frequently employed in the agricultural community and in ecological studies. In this work, furthermore, moisture and vegetation dynamics reflect the differences in solar incidence angle due to the form of the terrain.

Chapter 4 discusses the controls of climate, topography and soil properties on vegetation dynamics, and compares the vegetation and soil moisture representations

of CHILD with measurements. The goal of the chapter is to validate the representation of the vegetation dynamics in CHILD and to acknowledge its capabilities and limitations. In Chapter 4 the duration of the simulations is a few years, and the geomorphic processes are turned off.

In Chapter 5 the evolution of the landscape over 10 000 years is simulated. Five different scenarios, and two different initial topographic settings are presented. In these simulations all the processes discussed in Chapter 3 are active on the landscape, including the geomorphic processes. The goal of this chapter is to investigate the role of vegetation dynamics on the evolution of land form, erosion and sedimentation in a basin.

Finally, Chapter 6 presents a summary and the main conclusions drawn from this work.

CHAPTER 2

FEEDBACK BETWEEN VEGETATION DISTRIBUTION AND LAND SURFACE FORM

ABSTRACT

The magnitude of the bidirectional interaction between landforms and vegetation is poorly understood. This work quantifies that feedback by elucidating correlations between vegetation and topographic attributes (aspect, slope, and drainage area) in two semiarid grasslands in the southwestern U.S. (one in Arizona and the other in New Mexico). Digital elevation models (DEMs), biomass maps, and Normalized Difference Vegetation Index (NDVI) maps, with data spanning several years, are used in the investigation.

Results indicate that vegetation is inversely proportional to topography-modulated radiation; vegetation is directly proportional to drainage area; and the protection provided by vegetation cover results in steeper terrain.

At the Arizona site the effects of water accumulation along the drainage network conceal some of the topography-modulated radiation effects.

Finally, it is observed that the effects of topography on vegetation are relatively larger in the dry season preceding the monsoon, or early in the monsoon growing season.

2.1 Introduction

The heterogeneous distribution of vegetation in space affects the degree to which geomorphic processes act on the land surface. Given that geomorphic processes shape the land surface and distribute sediment, the above suggests that vegetation may affect landscape morphology. At a local scale, for example, grasses protect the surface against fluvial erosion [*Prosser et al.*, 1995] and rain splash [*Abrahams et al.*, 1995]. Furthermore, grasses increase surface roughness, reduce runoff rates [*Abrahams et al.*, 1995; *Prosser et al.*, 1995], allow for higher infiltration [*Selby*, 1993], and as a result,

diminish water erosive power. Grasses also trap sediment transported by water or wind [*Abrahams et al.*, 1995; *Lancaster and Bass*, 1998]. At basin scales, vegetation removal is known to result in large changes in water fluxes and sediment [*Bormann and Liekens*, 1979; *Bosch and Hewlett*, 1982; *Selby*, 1993].

Patterns of vegetation in the landscape are mainly a function of light, temperature, and available soil moisture [*Dick-Peddie*, 1993; *Bonan*, 2002; *Eagleson*, 2002; *Larcher*, 2003]. In this work it is argued that these factors are defined by climate at a regional scale, and by landform and soil properties at a local scale. Therefore, at the local scale, vegetation and topography are likely to have a bidirectional interaction through biological and physical processes. Various documented examples of topographic relationships with vegetation distribution exist [*Hack and Goodlett*, 1960; *Hidalgo et al.*, 1990; *Basnet*, 1992; *Scatena and Lugo*, 1995; *McMahon*, 1998], as well as studies of the effects of vegetation on geomorphic and hydrologic processes [*Prosser and Slade*, 1994; *Abrahams et al.*, 1995; *Prosser et al.*, 1995; *Prosser and Dietrich*, 1995; *Collins et al.*, 2004; *Istanbulluoglu and Bras*, 2005; *Gutiérrez-Jurado et al.*, 2007; *Istanbulluoglu et al.*, 2008]. However, the magnitude of the bidirectional interaction is not well understood.

In humid environments, light and nutrient availability are important limiting factors for plant development, and in cold environments, temperature is a limiting factor. This work focuses on grasslands in a temperate semiarid region, where water availability is the main limiting factor for plant growth. Previous observations have noted that distinct vegetation establishes on north and south facing hillslopes in mid-latitudes and semiarid regions [*Kennedy*, 1976; *Hidalgo et al.*, 1990; *Gutiérrez-Jurado et al.*, 2006]. This is attributed to the effect of differences in radiation on north and south facing hillslopes, leading to differences in soil moisture and temperatures. Recently, *Ivanov et al.* [2008a,b] reproduced distinct vegetation biomass distributions of grasses, in a complex terrain mimicking semiarid central New Mexico. Their numerical model accounted for the impact of topography on vegetation establishment and growth, taking into account the effects of topography on radiation and soil moisture distribution. Results indicated that vegetation growth is limited on south facing hillslopes because of excessive radiation, stressing the plant by depleting soil moisture, and that north-facing hillslope conditions result in more abundant vegetation growth. Results also indicated that vegetation patterns follow the drainage network when a significant amount of rainfall runs off from hillslopes into the drainage network.

Recently, two studies of a semiarid site in central New Mexico attributed differences in the geomorphic response and morphology of opposing north and south facing hillslopes to vegetation cover differences [*Gutiérrez-Jurado et al.*, 2007; *Istanbulluoglu et al.*, 2008]. This work extends the previous investigations by analyzing the relationships between vegetation distribution and topographic attributes (aspect, slope and drainage area) in two grass-dominated semiarid sites, one called Kendall, within the Walnut Gulch Experimental Watershed (WGEW) in Arizona, where mean annual precipitation is 350 mm per year, and the other in the northwestern section of the Sevilleta National Wildlife Refuge (SNWR) in New Mexico, where mean annual

precipitation is substantially smaller, 250 mm per year. At both of these sites more than 50 % of the precipitation falls during the summer monsoon, when most of the vegetation growth takes place. Conditions previous to the monsoon are generally dry.

In this study, grass species are treated as a single functional type. As a result, it identifies changes of the grass community as a single entity, not the species-specific responses of its component parts.

2.2 Field sites and data

2.2.1 Kendall site, southeastern Arizona

Kendall is a site dominated by grasses within the USDA-ARS Walnut Gulch Experimental Watershed (WGEW) (31°43′N, 110°41′W). The climate of this semiarid region is characterized by a mean annual precipitation of 350 mm, a mean annual temperature of 17.7 °C, an annual pan evaporation of 2590 mm, with a strong seasonality affecting the temporal distribution of these variables. The precipitation regime is dominated by the North American Monsoon, which occurs during the months of July through September, during which about two-thirds of the annual precipitation falls. The mean monthly temperature ranges between 8 °C in January and 27 °C in July [*Goodrich et al.*, 2008; *Keefer et al.*, 2008].

Kendall is within an alluvial fan that forms part of the San Pedro River watershed, with elevations ranging between 1500 m and 1600 m AMSL. It is dominated by C4 perennial grasses, including black, blue, hairy and sideoats gramas (*B. eripoda*, *B. gracilis*, *B., hirsuta* and *B. curtipendula*) [*Nouvellon et al.*, 2001].

2.2.2 SNWR site, central New Mexico

The second site used in this study is the grass-dominated terrain within the rectangular region of approximately 14 by 18 km in the northwest area of the Sevilleta National Wildlife Refuge (SNWR). The SNWR (34°24′N, 106°59′W) has a climate similar to that of Kendall, with more than 50 % of the annual precipitation falling during the North American Monsoon, and mean monthly temperatures ranging between $2.5°C$ in January and $25°C$ in July. However, significantly less precipitation falls in the SNWR; its mean annual precipitation is 250 mm [*Milne et al.*, 2003].

The area selected for the study, with elevations ranging between 1450 and 2500 m AMSL, is formed by alluvial deposits, eolian sand deposits, terrace deposits, and Precambrian granite and metamorphic rocks. Most of the grass-dominated rugged terrain within this rectangle is underlain by the Sierra Ladrones, and its elevation is below 1700 m AMSL. The Sierra Ladrones is an outcrop of the Sierra Ladrones Formation east of the Loma Pelada Fault [*McMahon*, 1998].

The region is covered with low-elevation grasslands and shrublands, and coniferous

woodlands and forests at the higher elevations [*Dick-Peddie*, 1993; *Milne et al.*, 2003; *Muldavin et al.*, 1998]. The area used in this study is nevertheless dominated by several grass species, including black (*Bouteloua eripoda*) and blue gramma (*Bouteloua gracilis*) (Figure 2-1).

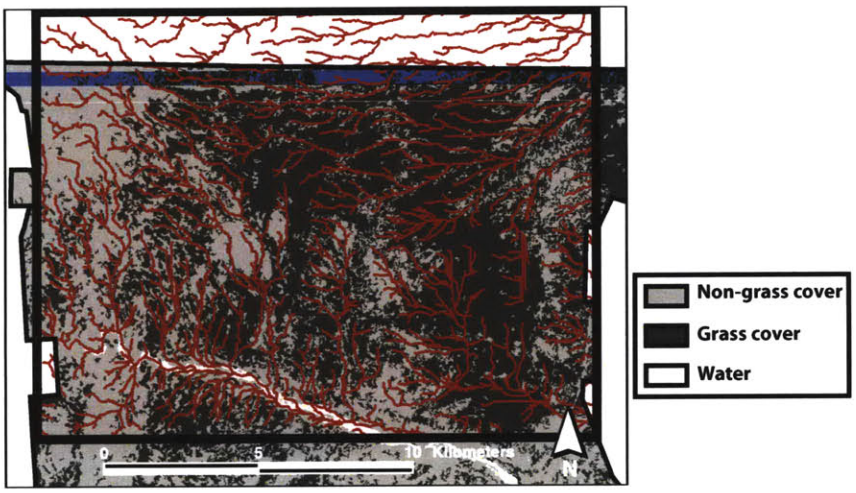

Figure 2-1: Map of the New Mexico site showing the DEM extracted drainage network with red lines, and the distribution of grassland, non-grassland covered terrain, and 'water' (the ephemeral Rio Salado).

2.2.3 Data

Data used in this analysis consist of Digital Elevation Models (DEMs) and maps of the spatial distribution of grasses. For the Arizona site (Kendall), a 1 m resolution DEM was used. This DEM was provided by personnel at the Tombstone Agricultural Research Service (ARS) office. For the New Mexico site, a 10 m DEM (EarthWatch Star-3i IFSAR product) of the region was used. This DEM is publicly available at http://sev.lternet.edu. Digital maps of slope, aspect and drainage area were obtained from the DEMs using Arcview.

Five digital maps of Normalized Difference Vegetation Index (NDVI) [*Tucker*, 1979], representative of the grass photosynthetic activity at the Kendall site, were used. These NDVI maps correspond to different dates spanning between August 24, 1990 through September 10, 1999, and have a spatial resolution of 30 m. These maps were obtained from NASA's Landsat Thematic Mapper (TM) images [*Moran et al.*, 2008]. The images were geocorrected to subpixel accuracy, and the refined empirical line (REL) method [*Moran et al.*, 2001] was used to convert dn to reflectance for the red and NIR spectral bands, as in *Holifield et al.* [2003].

Twenty-two grass biomass maps of the SNWR were used. These maps, publicly available at the SNWR website (http://sev.lternet.edu), correspond to various dates

between 1984 and 2001, and their resolution is of 28.5 m for dates before 1999, and 30 m after 1999. These maps were developed by combining ground surveys and Landsat TM derived NDVI fields [*Muldavin et al.*, 1998]. *Muldavin et al.* [1998] derived a linear regression equation between field measurements at two different grassland plots and NDVI values, using data corresponding to four different dates, between 1989 and 1990. Then, they used the linear regression and NDVI data to produce the biomass maps. Despite the growth of shrubs and trees at the SNWR study area, the biomass maps reflect the biomass corresponding to grass species. Grass pixels for these maps were identified by the analysis of the seasonal and annual variations of NDVI characteristic of grass species, which exhibit the strongest phenological dynamics in the region.

All the original data used in this work was projected in the Universal Transverse Mercator (UTM) coordinate system. Each DEM pixel was associated to the value of the NDVI/biomass pixel overlaying it. For the calculations only NDVI/biomass values of the original maps overlying terrain with uniform aspect were taken into account. The criteria to define whether the underlying terrain had a uniform aspect was the following: for the Arizona site, when the maximum difference in aspects among at least 75 percent of the overlaid pixels was 90°; for the New Mexico site, when the maximum difference in aspect among all the overlaid pixels was 90°. If the criteria was not met, the pixels were not considered in the analysis. In the case of the NDVI maps of the Arizona site, a negative or zero value for NDVI is assumed to be bare ground. Therefore, negative NDVI values are assigned a zero value.

For the analysis, annual direct solar radiation on the terrain as a function of slope and aspect is estimated following geometric relationships [*Ivanov et al.*, 2007]. First, direct solar radiation was calculated for each hour of each day of the year, by estimating the radiation intensity at the beginning of each hour and assuming that intensity for that hour. Then, those values were integrated for the whole year. The direct solar radiation intensity DSR_{rt} for each hour $[W/m^2]$ in the rugged terrain was calculated using:

$$DSR_{rt} = \cos\varphi_{\oplus\nabla} DSR_{cs} \tag{2.1}$$

where $\varphi_{\oplus\nabla}$ is the solar incidence angle, which takes into account the terrain aspect and slope [*Sellers*, 1965], and DSR_{cs} is the direct solar radiation intensity assuming a flat terrain, but taking into account atmospheric absorption and scattering, following [*Bras*, 1990].

$$DSR_{cs} = W_o \sin h_{\oplus} e^{-n(0.128-0.054\log_{10}(m))m} \tag{2.2}$$

where $W_o = 1353$ $[W/m^2]$ is the solar constant, $m = \csc(h_{\oplus})$ is the optical air mass, n is a turbidity factor of air, where $n = 2$ corresponds to clear air, and $h_{\oplus}$ is the solar altitude. In Chapter 3, calculations of direct solar radiation are described in further detail. The reader is directed there for more details regarding these calculations. Equations (2.1) and (2.2) are equivalent to equations (3.3) and (3.4) respectively. Equations (3.3) and (3.4) are presented in section 3.2.3, where the equations necessary to estimate $\varphi_{\oplus\nabla}$ and $h_{\oplus}$ are provided.

In our calculations, we assume clear air and a latitude of 32° N for the Arizona site, and a latitude of 34° N for the New Mexico site.

In addition to the annually integrated values, daily integrated values were estimated following a similar procedure.

2.3 Results and discussion

The study assumes that topography controls vegetation distribution by two means: by directing water fluxes through a drainage structure dependent on the shape of each basin, and by modulating solar radiation on rugged terrain. An inverse relationship between solar radiation and vegetation cover is expected because, in water-limited regions, solar radiation reduces soil moisture, leading to a reduction of net carbon assimilation, and inducing water and temperature stresses in plants [*Larcher*, 2003]. The above assumption implies the following:

1. Drainage area (a proxy for water accumulation in a basin) and vegetation are positively correlated.

2. The relationship between vegetation and solar radiation can be quantified through the relationships between vegetation cover and aspect, and vegetation cover and slope, because solar radiation in a rugged terrain is a function of aspect and slope. Direct annual solar radiation estimates for the New Mexico site are presented in Figure 2-2. Estimates for the Arizona site are similar. The figure shows that radiation is maximum for the south aspect, and minimum for the north aspect. Thus, moisture and vegetation are expected to be minimum for south aspects, and maximum for north aspects.

3. Steeper slopes are expected where grass provides protection against erosion [*Kirkby et al.*, 1990; *Istanbulluoglu et al.*, 2008], and thus, minimum and maximum slopes occur in south and north aspects, respectively.

4. Figure 2-2 shows that annual radiation decreases with slope in the north aspect, while it increases in the south aspect. Because of this, vegetation should increase with slope in north facing terrain, and decrease with slope in south facing terrain.

These four implications are explored below.

2.3.1 Control of the drainage structure on the spatial distribution of vegetation

Drainage area is the area upstream of any given point within a basin, and its spatial distribution is an indication of the spatial structure of the basin's drainage system. It is zero at the drainage divide, equals the basin's area at the basin's outlet, and is an indication of the amount of water (and sediment) collected at any point in the basin as a result of the lateral movement of water after rainfall. Because it is larger in valleys and channels than in the rest of the basin, more moisture and vegetation are anticipated in these regions. Often the drainage network can be identified by locating all the points in a map that have a drainage area larger than a given threshold.

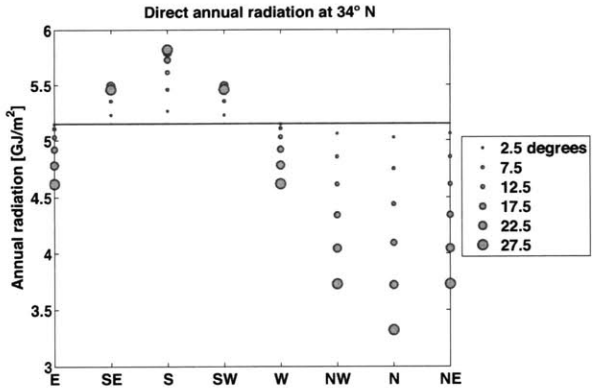

Figure 2-2: Annually integrated direct solar radiation at latitude 34° N for different aspects and slopes. Latitude 34° N corresponds to the New Mexico site (SNWR). Larger circles indicate steeper terrain. The range of slopes in the figure is representative of those observed at the study site.

Figure 2-3 shows a map of the spatial distribution of NDVI at the Arizona site, on July 24, 1999, overlaid by its drainage network. The image shows higher NDVI in the proximity of the drainage network.

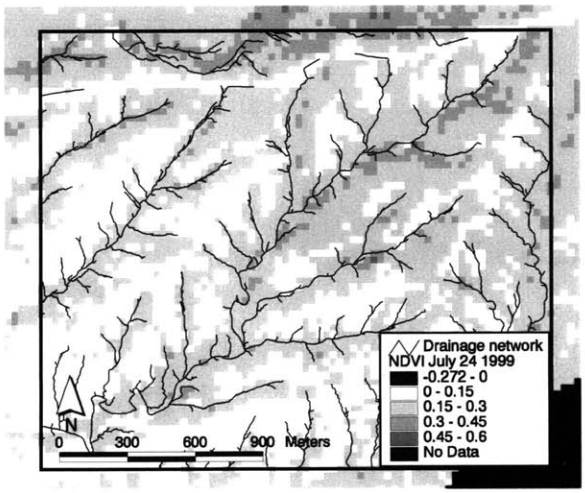

Figure 2-3: Map of NDVI on July 24 1999 at the Arizona site (Kendall, at the WGEW). The drainage network overlays the NDVI map.

To quantify the influence of drainage structure on vegetation distribution, the mean NDVI, and the mean relative NDVI as a function of drainage area, were estimated for each of the 5 NDVI maps of the Arizona site ($\overline{NDVI}^{ti}_{DA}$ and $\overline{rNDVI}^{ti}_{DA}$, respectively). Relative NDVI ($rNDVI$) is the NDVI normalized by the corresponding spatial average NDVI for each date ($\overline{NDVI}^{ti}$). The use of relative NDVI allows for a direct comparison of the spatial differences in vegetation distribution among

different dates. A logarithmic scale for the drainage area was used. Relative NDVI was averaged for drainage areas between 1 and 2 m^2, 2 and 3 m^2, and so on, until the range of 9 and 10 m^2; then it was averaged for drainage areas between 10 and 100 m^2, 100 and 200 m^2, and so forth, for each NDVI map. These calculations are illustrated in Figures 2-4a and 2-4b. Next, the relative NDVI values of different dates were averaged to obtain the 'time-averaged' relative NDVI as a function of drainage area ($\overline{rNDVI}_{DA}$), representative of the influence of the drainage structure on vegetation growth at the site. The result is shown in Figure 2-5a. Similar calculations were carried out for biomass of the New Mexico site, and are shown in Figures 2-5a, 2-6a, and 2-6b. Note that the relationship between the amount of vegetation and drainage area becomes erratic for drainage areas above 3 000 m^2 at the Arizona site, and above 300 000 m^2 at the New Mexico site, due to the small sample size for those drainage areas. The discussion below does not focus on those drainage area ranges.

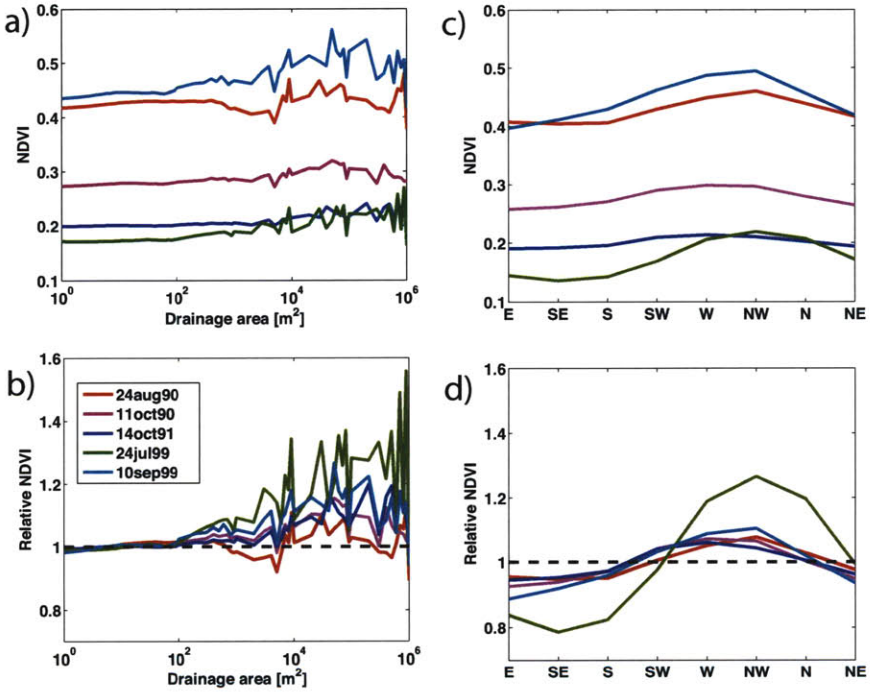

Figure 2-4: Control of the drainage structure and terrain orientation on grass growth at the Arizona site: a) and b) provide the NDVI and relative NDVI as a function of drainage area, while c) and d) provide the the NDVI and relative NDVI as a function of aspect.

Figure 2-5a implies that random samples of pixels with low drainage area are equally likely to have a $rNDVI$ (or relative biomass) larger or smaller than 1, but for pixels with higher drainage area, more sampled pixels will have, on average, a $rNDVI$ (or relative biomass) above 1, indicating a control of the drainage structure on the grassland productivity. The effects of drainage area on vegetation distribution are of a similar magnitude at both sites. At the New Mexico site, the drainage structure

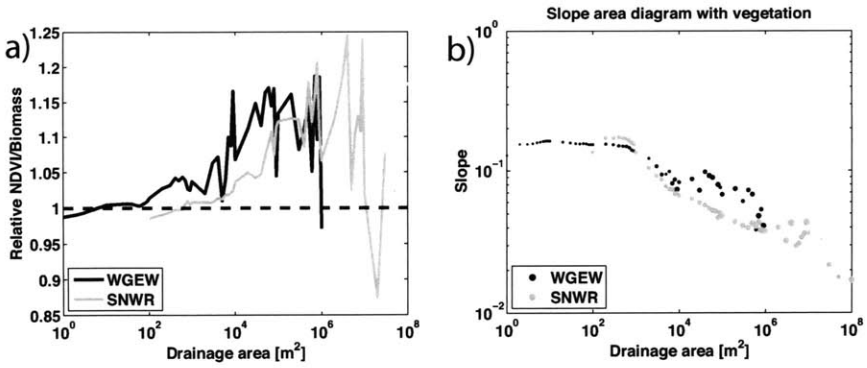

Figure 2-5: Control of the drainage structure and terrain orientation on vegetation at the Arizona (WGEW) and New Mexico (SNWR) sites: a) relative NDVI/biomass as a function of drainage area, and b) slope-area diagram. In the slope-area diagram circle diameters indicate the magnitude of the time-averaged relative NDVI/Biomass. For the Arizona site data, the smallest and largest circles correspond to values of 1 and 1.2, respectively, whereas for the New Mexico site, they correspond to values of 0.874 and 1.245, respectively.

has a more pronounced impact on the vegetation distribution in the spring, when soil is dry and biomass is relatively low (Figures 2-6a and 2-6b). At the Kendall site, few data points are available to make a similar conclusion. Nevertheless, the day with lowest $\overline{NDVI}^{ti}$, July 24, 1999, shows the largest deviation from a spatially uniform rNDVI, suggesting a high topographic effect on vegetation productivity early in the growing season (Figures 2-4a and 2-4b).

A slope-area diagram for each of the field sites was also created (Figure 2-5b). This diagram is a diagnostic tool used in geomorphology to estimate where fluvial erosion dominates, and where diffusive erosive processes such as rainsplash dominate. Slope increases with drainage area in diffusive erosion dominated terrain, whereas it decreases with drainage area in fluvial erosion dominated terrain [*Willgoose et al.*, 1991]. In the figure circle diameters indicate the magnitude of the time-averaged relative NDVI ($\overline{rNDVI}_{DA}$) (or time-averaged relative biomass). Figures 2-5a and 2-5b illustrate how on average photosynthetic activity increases with drainage area. The slope-area diagram (Figure 2-5b) shows that fluvial processes distinctively dominate in terrain with drainage areas larger than ~600 - 1000 m^2 at both sites. It also shows that at large drainage areas, abundant vegetation and small slopes coincide.

Vegetation at the sites is mainly grasses, yet, sparse woody vegetation is present. At Kendall this is particularly the case near the channels, in the valley bottoms. Thus, the contribution of woody vegetation to the NDVI signal may be important along the drainage network, but of lesser significance on the hillslopes. The effect of woody vegetation is minimal in the analysis presented here as most NDVI pixels along the drainage network are excluded as they overlay terrain with opposing aspect (see the Data section).

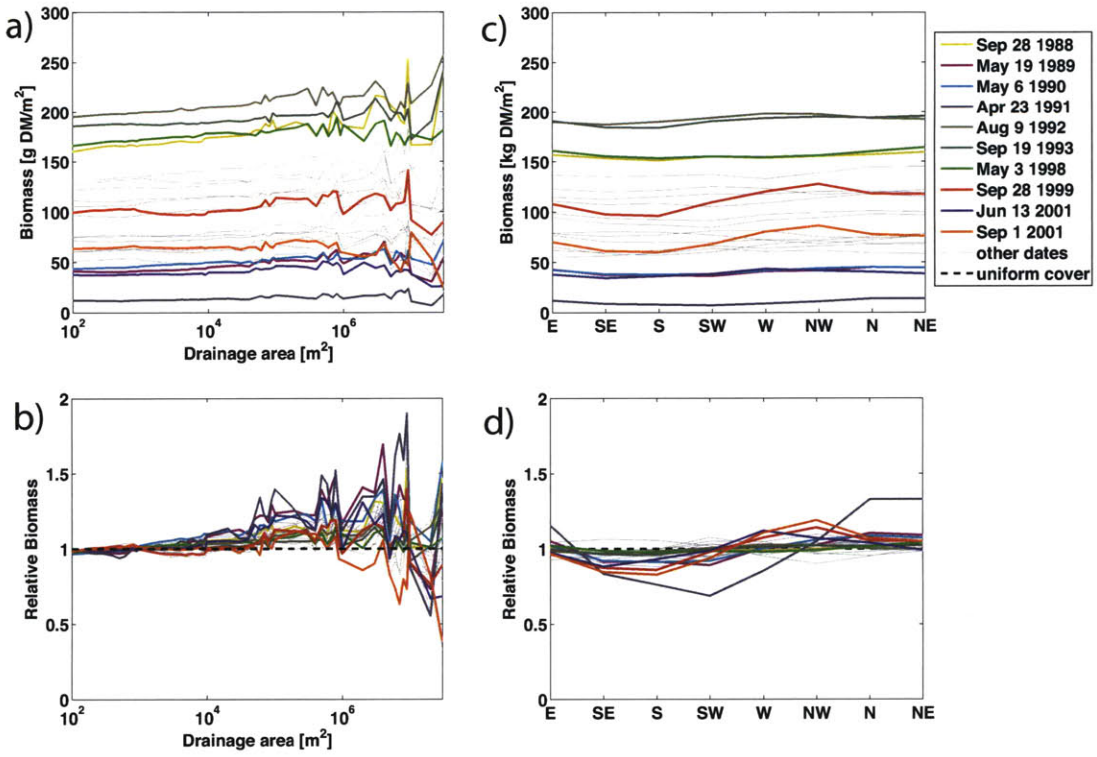

Figure 2-6: Control of the drainage structure and terrain orientation on grass growth at the New Mexico site: a) and c) provide the biomass and relative biomass as a function of drainage area, while b) and d) provide the the biomass and relative biomass as a function of aspect.

2.3.2 Control of the terrain-modulated radiation on the spatial distribution of vegetation

Vegetation distribution and aspect

To measure the effect of terrain-modulated radiation on vegetation spread, the distribution of NDVI and biomass (for the Arizona and New Mexico sites respectively) as a function of aspect was estimated analogously to the calculations of drainage area. These calculations exclude pixels with slopes smaller than 5° because that range of slopes exhibits such small differences in radiation that no effect on vegetation distribution is anticipated.

The calculations of time-averaged relative NDVI/biomass as a function of aspect, shown in Figure 2-7a, reveal that vegetation growth is sensitive to aspect. Spatial differences as a function of aspect seem larger at the Arizona site than at the New Mexico site, suggesting a stronger control of terrain-modulated radiation on vegetation growth. However, this could be the result of the use of data corresponding to different days for each site. At the Arizona site the minimum and maximum vege-

tation covering occur on the southeast and northwest aspects, respectively, instead of at the south and north aspects, as expected. This slight shift is attributed to the directionality of the drainage network towards the southwest, evident in Figure 2-3. A drainage network map for the New Mexico site is also provided for reference (Figure 2-1). As discussed in the previous section, more vegetation grows in the proximity of the drainage network, and since most of the terrain along the drainage network has a south, southwest and west aspect, the mean NDVI of those aspects is larger than if the only topographic control on vegetation distribution were the solar radiation.

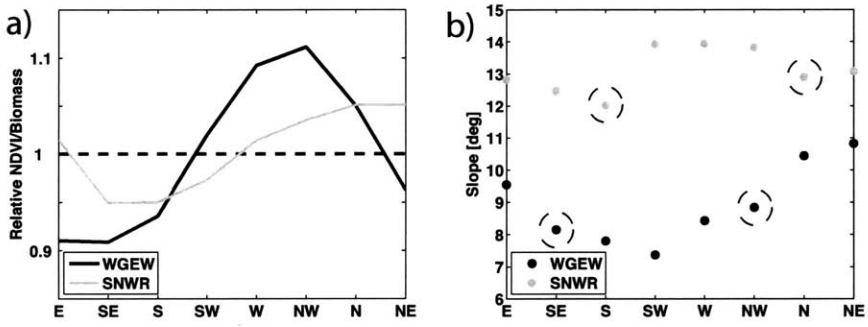

Figure 2-7: Controls of the terrain-modulated radiation on the spatial distribution of vegetation and slope. The figure shows the distribution of a) vegetation and b) slope as a function of aspect at the two field sites. NDVI is used as a proxy for ecosystem productivity at the Arizona site (WGEW), whereas biomass is used to quantify ecosystem productivity at the New Mexico site (SNWR).

The calculations of NDVI as a function of aspect for individual dates, shown in Figures 2-4c and 2-4d (and of biomass for the New Mexico site in Figures 2-6c and 2-6d), reveal that vegetation cover is relatively more sensitive to aspect in the dry season or early in the subsequent monsoon growing season, when NDVI (biomass) values are low. In the figures, the lines corresponding to the days with the lowest $\overline{NDVI}^{ti}$ (or biomass) show some of the largest deviations from a spatially uniform relative NDVI (relative biomass). Figures 2-6c and 2-6d also suggest the vegetation distribution at the New Mexico site is relatively insensitive to aspect after wet conditions (i.e. high spatially averaged biomass, generally at the end of a growing period). This is not the case at the Arizona site (Figures 2-4c and 2-4d). Perhaps this is because the maximum biomass values available for New Mexico correspond to a more abundant vegetation cover (and more extreme wet conditions) than that of the data available for Arizona. In those wet conditions, differences in solar radiation may have little effect on vegetation distribution.

Figures 2-4c and 2-6c also show that the maximum absolute differences in grass cover among aspects occur in September, at the end of the monsoon growing period. These large differences in biomass may simply be a reflection in differences in vegetation distribution at the beginning of the growing season augmented by the monsoon rains. At the Arizona site, the maximum differences in NDVI occur in September 10,

1999, approximately seven weeks after the maximum relative NDVI difference was observed (July 24, 1999) (see Figures 2-4c and 2-4d).

Slope as a function of vegetation distribution

To quantify the interaction of vegetation distribution and terrain slope, mean slope as a function of aspect was estimated. At the Arizona site, all the terrain is grass dominated, and all is considered rugged. Therefore, on all of its extension radiation can control grass cover and terrain slope. In contrast, in the New Mexico site the terrain includes significant extensions of flat terrain. Because of that, at the New Mexico site these calculations only considererd pixels in the domain that a) have an assigned grass biomass value, and b) have slopes above 5°. The calculations are shown in Figure 2-7b.

Figure 2-7b shows that at the Arizona site, the drainage directionality affects the distribution of slope as a function of aspect. The smallest slopes occur in the direction the drainage network faces (southwest), and the steepest in the opposite direction (northeast). At the New Mexico site, steep slopes develop along the west facing face of the Loma Pelada Fault. The Loma Pelada Fault runs in a north-south direction along the western edge of the Sierra Ladrones and creates a contrast in substrate erosion resistance which results in a scarp, with steep west-facing hillslopes. This causes high mean slopes in the southwest, west, and northwest aspects.

Figure 2-7b also reveals that among the aspects where the drainage network directionality and the geologic controls do not have an effect on slope, the grass cover's impact is evident. At the Arizona site, differences in grass cover among the northwest and southeast aspects are attributed only to differences in radiation. Among these two aspects, mean slope differences are attributed to differences in grass cover. As anticipated, the more vegetated northwest aspect (by about 20 %) also has a larger mean slope (by about 0.7°). Similarly, at the New Mexico site, the more vegetated north facing terrain, with approximately 10 % more biomass, is on average about 1° steeper than the south facing terrain.

Vegetation sensitivity to radiation reflected in changes in vegetation distribution as a function of slope

To explore in greater detail the effects of variable radiation as a function of topography on vegetation growth, the relative NDVI (or biomass) as a function of slope for each aspect was estimated. At the Arizona site, the time-averaged relative NDVI for slope intervals of 5° between 0° and 20° was calculated. This range of slopes covers the majority of the terrain slopes at the site. Similar calculations were carried out for the New Mexico site biomass data, for slopes between 0° and 30 °. Figures 2-8a and 2-8b show the results for the north and south aspects only. In the figures, the relative radiation as a function of slope is provided for reference. The relative radiation is the annual value normalized by the annual radiation on flat terrain.

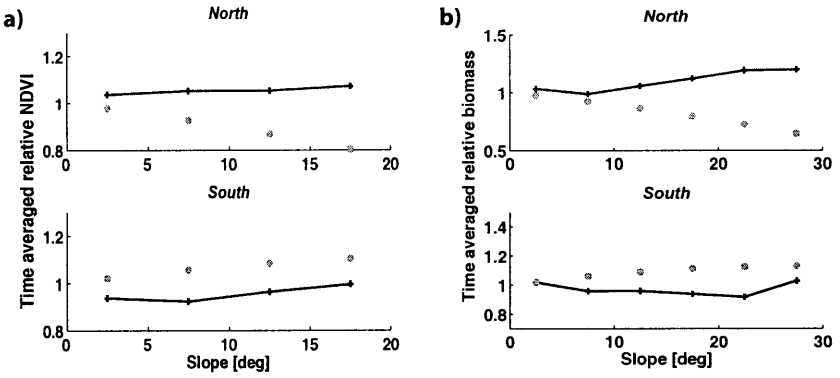

Figure 2-8: Time-averaged relative NDVI/biomass as a function of slope, for south and north aspects, at the a) Arizona and b) New Mexico sites. For reference, the relative radiation is indicated with circles. Relative radiation is the annual radiation normalized by the annual radiation on flat terrain.

At the Arizona site, relative NDVI increases slightly with slope for north and south aspects, regardless of the direction of the change in relative radiation with slope. In contrast, at the New Mexico site, biomass changes in the opposite direction than radiation as slope increases. The observations at the New Mexico site are in agreement with the idea that in this water-limited environment, soil moisture and vegetation cover decrease with radiation. At the Arizona site, on the other hand, the increase of vegetation with slope and with annual radiation in the southerly aspect disagrees with the hypothesis.

The reason for a positive correlation between photosynthetic activity and slope in the southerly aspects of the Arizona site, and the apparent insensitivity of vegetation distribution to the terrain modulated radiation, is the proximity of steep slopes to the drainage network, which is apparent in Figure 2-9. Figure 2-9 indicates that the mean distance to the drainage network for slopes of 5° is 45 m, whereas that for slopes of 20° is 15 m. The figure also shows that in contrast, at the New Mexico site mean distance to the drainage network increases with slope. As previously discussed, on average, vegetation is more abundant close to the drainage network than in the rest of the terrain, and thus, at the Arizona site, the increase of biomass with contributing area overshadows any impact that the terrain-modulated radiation may have on southerly aspects, and enhances it on northerly aspects. The steep slopes, generally banks of the channels, may not be densely vegetated, however, they fall within NDVI pixels (30 m resolution) that have a high NDVI. Notice that the fraction of terrain with slopes steeper than 10° is rather small (29% > 10°, 9% > 15°, and 3% > 20°), and so, terrain with steep slopes close to the channels has little impact on the slope-area diagram (Figure 2-5b).

Annual radiation is assumed to be representative of the year-round effects of the terrain-modulated radiation on vegetation distribution. However, that is not always the case. In contrast with the north aspect, where daily radiation consistently de-

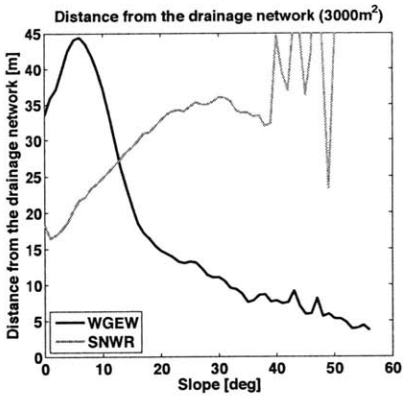

Figure 2-9: Mean distance to the drainage network from pixels with different slopes at the field sites. The drainage network is defined as terrain with a drainage area larger than 3000 m^2.

creases with slope regardless of the day of the year, in south facing terrain, daily radiation increases with slope during winter days, and decreases with slope in summer days. Moreover, the decrease in the summer is only substantial for slopes larger than 20°. The above can be seen in Figure 2-10, that shows the computed daily direct radiation for every day of the year, as a function of slope, for south and north aspects, at the New Mexico site. Such decrease in daily radiation with slope during the summer, that coincides with higher daily radiation and the growing season, is likely to result in more vegetation growth. This seems to be true at the New Mexico site, where biomass increases with slope between slope angles of 20° and 30°, independently of the (slight) increase in annual relative radiation, as seen in Figure 2-8b.

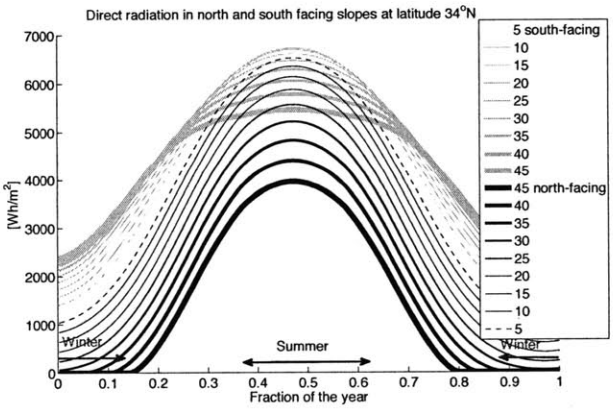

Figure 2-10: Daily direct solar radiation in south and north aspects as a function of slope, at the New Mexico site (34°N), for every day of the year.

Moisture losses due to surface or subsurface lateral redistribution could increase with terrain slope. This would reduce vegetation growth. However, apparently this

effect does not overshadow the effect of diminishing radiation on vegetation growth. Perhaps in steeper terrain it does.

2.4 Conclusions

The bidirectional interaction between the heterogeneous distribution of vegetation in space and landscape morphology in water-limited, grass-dominated, temperate environments, is investigated. Results indicate, in agreement with our initial hypothesis, that a) vegetation growth increases with drainage area; b) vegetation growth is inversely proportional to radiation, generally leading to maximum grass cover on north aspects and minimum on south aspects; c) more grass cover results in steeper slopes; and d) radiation changes as a function of slope are reflected in grass cover.

In addition, the investigation revealed that a) the effects of topography on vegetation are similar at both sites; b) in some circumstances the effects of the accumulation of moisture along the drainage network override the effects of terrain-modulated radiation; c) controls of topography on vegetation are relatively larger in the dry season preceding the monsoon or early in the monsoon; and d) in general, terrain with gentle slopes (smaller than $\sim 5°$) has more vegetation than the rest of the terrain (because at large drainage areas, where more vegetation grows, slopes are small). These results can be used to test current numerical models that assume similar environmental settings.

Possible development of this investigation is its extension to different environmental settings, where nutrients, light or temperature may be crucial limiting factors for vegetation growth, and to environments dominated by vegetation communities more complex than grasslands such as shrublands and forests.

CHAPTER 3

A MODEL OF LANDSCAPE EVOLUTION

3.1 Introduction

CHILD, the Channel-Hillslope Integrated Landscape Development model is written in C++ and uses an Object Oriented Programming approach. It was first developed 10 years ago at MIT by a group of hydrologists and geomorphologists. This program provides a framework where a 2D surface elevation field (making the domain 3D) is subject to erosion and sedimentation processes that modify it. Some of the erosion and sedimentation processes represented in the model are driven by gravity alone (diffusive processes). Others, however, are driven by a combination of water fluxes across the surface and gravity (fluvial processes). In the model, water fluxes are simulated and are produced by rainfall. The rainfall flows through the surface driven by gravity towards the lowest points in the evolving drainage system, and then exits the simulated surface.

3.1.1 The system represented with CHILD

The system represented with CHILD, schematically represented in Figure 3-1, is a landscape with the following elements: soil (moisture and depth), vegetation cover, and its elevation field. These elements are represented with circles in the figure. Three sets of internal processes modify the system properties: geomorphic processes, hydrologic processes and vegetation dynamics. These processes are represented with rectangles in the figure. This system is forced by climate (rainfall and radiation) and tectonics boundary conditions (uplifting, base level lowering). The forcing elements of the system are represented with round cornered boxes. The forcing, together with state of the system's elements and internal processes, modulate the system dynamics.

The states of soil moisture, vegetation cover, and elevation at each point in the landscape affect the hydrologic processes as indicated by curved arrows in Figure 3-1, and conversely, these processes modify those states as indicated by straight arrows.

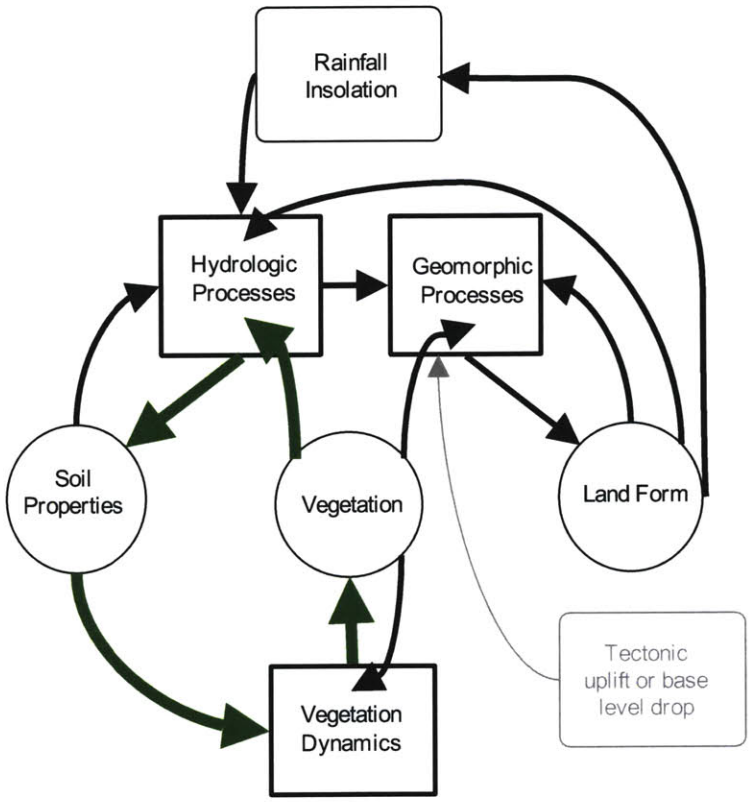

Figure 3-1: System elements (in circles) and processes (in rectangles) of the landscape considered in this work. The forcings are represented with rounded corners boxes.

The interdependence between processes and the state of the system leads to feedbacks loops. An example is illustrated with green arrows in Figure 3-1. The arrows indicate that during a storm, infiltration is higher where vegetation cover is high (vegetation affects a hydrologic process). Thus, in regions in the domain with denser vegetation cover, soil moisture input can be larger than in the rest of the domain (the hydrologic process affects the soil moisture state). The larger moisture input can sustain higher transpiration rates, and thus a higher vegetation growth rate, resulting in even more vegetation in such regions (the moisture conditions affect the vegetation dynamics, and hence, the vegetation state).

A more detailed description of CHILD follows. The climate forcing is described first, followed by the description of each of the geomorphic, hydrologic, and vegetation dynamics processes.

3.2 The climatic forcing

The main forcing process is rainfall, and two options of rainfall models are implemented in CHILD. The Poisson Pulse model [*Eagleson*, 1978] has been commonly used in simulations of the changes of the morphology of river basins in geologic timescales. This model assumes a constant rainfall intensity throughout a given rainfall event, and consists of a series of storm and interstorm sequences where the interstorm duration, storm duration and rainfall intensity are random variables with an exponential distribution. The Barlett-Lewis model [*Rodríguez-Iturbe et al.*, 1988], in contrast to the Poisson Pulse model, produces a variable rainfall intensity throughout a rainfall event, and to our knowledge has not been used before in simulations of the changes of the morphology of river basins. Rainfall is assumed to have different rainfall seasons, for example, a wet and a dry season. The way this seasonality is set for each rainfall model is slightly different, but for both models basically a different set of rainfall parameters is assigned for each rainfall season. The other forcing element of the system is insolation, whose effects are considered in the system by a temporarily, and spatially variable potential evapotranspiration (PET). Potential evapotranspiration is a measure of the ability of the atmosphere to remove water from the surface through the processes of evaporation and transpiration assuming no limitation on water supply and is a reflection of the energy available to evaporate water, and of the wind available to transport the water vapor from the ground up into the lower atmosphere. PET also depends on the capacity of the air to hold water. In this work, assuming that the available energy for evaporation and transpiration is the major responsible for PET annual variability, PET follows closely the annual cycle of insolation in the region. In the northern hemisphere latitudes, this results in a maximum PET in July (summer) and minimum PET in January (winter). Such annual cycle, represented in the model with a sinusoidal expression [*Small*, 2005], coupled to the annual pattern of rainfall, gives rise to the temporal vegetation dynamics.

The amount of solar insolation on a the land surface, accumulated throughout a year, can be as twice as much on opposing steep hillslopes at our field site. This

spatial variability in insolation resulting from the geometry of the terrain affects the amount of energy available for the processes of transpiration and evaporation from bare soil, and thus, the state of soil moisture and vegetation. Quantifying the effect of variable insolation on soil moisture and vegetation has not been fully explored but is increasingly drawing the interest of the hydrologic and geomorphological communities. Evidence of differences in vegetation between north- and south-facing slopes are abundant.

In this work we implemented a formulation that accounts for the effects of the spatial variability of insolation in the terrain. The PET at each element of the numerical grid representing the terrain is a function of both, the annual cycle of PET discussed earlier, and insolation variability in space as a function of aspect, slope and time of the year. First the PET of a flat surface, or PET_o, is calculated following the sinusoidal function that represents its annual cycle. Second the insolation at each element of the numerical grid is calculated as a function of its orientation with respect to the geographic north, its slope, and the hour and date, following geometric relationships, assuming a clear day. Then, the PET of all the elements representing the elevation field is calculated following the assumption that PET and direct solar radiation are linearly proportional. Following such assumption, PET at each element of the numerical grid, PET_i, is estimated as the product of PET_o times the ratio of the direct solar radiation in that part of the landscape and the direct solar radiation that it would receive if it were flat.

The implementation of the variability of insolation due to the geometry of the terrain results in spatial differences in the distribution of vegetation that would not be accounted for in the simulations otherwise.

3.2.1 The Poisson Pulse model

The Poisson Pulse model generates 'rectangular' pulses of rain with a mean rainfall intensity as noted above, where the rainfall intensity, storm duration and interstorm interval are random variables with an exponential distribution whose mean value describes the behavior of the rainfall generation model. We compared the landscape system behavior when using the Poisson Pulse model and when using the Barlett-Lewis model and found important differences, mainly, that the Poisson Pulse model rarely results in runoff, where as the Barlett-Lewis model frequently produces runoff with parameters corresponding to the same locality and the same month. We do not present any results in this thesis using the Poisson Pulse model and is presented here only for reference.

3.2.2 The Barlett-Lewis model

The Barlett-Lewis model generates rainfall events consisting of a series of smaller pulses of rainfall with variable rainfall intensity that provide a good representation of the rainfall intensity variability observed in rainfall events. The model works in the

following way: first it creates a rainfall event, within which rainfall pulses of different rainfall intensities are produced, until the rainfall event ends. The rainfall events are generated following a Poisson arrival process of rate λ. When a rainfall event begins, a series of 'cells' of rain with independent intensity are produced at a rate β, following also a Poisson arrival process. The duration of the rainfall event is a random variable with an exponential distribution with a parameter γ ($1/\gamma$ is the mean rainfall event duration). The duration of each cell of rain is also a random variable with an exponential distribution with a parameter η ($1/\eta$ is the mean duration of the cells of rain for a given rainfall event). In the model, β and γ are related to η through two model parameters, κ and ϕ, as follows: $\kappa = \frac{\beta}{\eta}$, $\phi = \frac{\gamma}{\eta}$. These latter two parameters make the rate of generation of cells within a storm (β), and the mean duration of a rainfall event ($1/\gamma$), vary linearly with the expected duration of the rainfall cells in a given rainfall event ($1/\eta$). This way, the rate at which cells are generated decreases with the duration of rainfall cells, and the mean duration of a rainfall event increases with the size of the rainfall cells. In other words, shorter rainfall events will have smaller and more frequent rainfall cells than longer rainfall events.

The intensity of the rainfall, x, has an expected value E[x], and in this work we assume x to be exponentially distributed. Finally, following the work of *Rodríguez-Iturbe et al.* [1988], η is a random variable with a gamma distribution with parameters α and ν, the shape and scale parameters, respectively. From this distribution, the expected value of η is $E[\eta] = \frac{\alpha}{\nu}$.

The time between the end of a rainfall event and the consecutive rainfall event is the interstorm period in this model.

Rainfall seasonality

More than one rainfall season is allowed in the Barlett-Lewis model. In this work the number of rainfall seasons is based on changes in the mean rainfall, variance of rainfall, and no-rain probability at the daily scale, at the site of interest through out the year. Months presenting similar values for these three variables are grouped toghether in a rainfall season. For the case of the Kendall site, four rainfall seasons were identified. A dry season between March and June, a monsoon season in July and August, a post monsoon season in September and October, and a winter rainfall season between November and February of the following year.

Barlett-Lewis parameters for each season are estimated from rainfall observations for 9 years at the Kendall site using a Global optimization algorithm [*Duan et al.*, 1993], and a minimization equation whose solution provides the best parameter values for the rainfall model given six statistical descriptors of the data [*Islam et al.*, 1990]. In this work the statistical descriptors used were hourly mean rainfall, hourly variance of rainfall, no-rain probability at the houlry and daily time scales, and lag-one autocorrelation at the hourly and daily time scales. The parameters used in this thesis are given in Table 3.1.

Table 3.1: Summary of the Barlett-Lewis parameters

Months	λ [1/yr]	ν [yr]	α	$E(x)$ [m/yr]	ϕ	κ
November-February	41.3163	0.002119548	39.99999	13.3885	0.0292	0.1491
March-June	17.9707	0.001603723	39.99998	42.1579	0.0104	0.0229
July-August	135.2326	0.000160139	8.22734	120.5834	0.0089	0.0116
September-October	28.1538	0.001604261	40.00000	38.8850	0.0113	0.0533

3.2.3 Insolation and PET

As discussed earlier, the variability of the capacity of the atmosphere to transpire and evaporate water from the surface (PET) is tightly linked with insolation in time and in space. The variability of this capacity through out the year is represented with the following sinusoidal function suggested by *Small* [2005].

$$PET_o = \left(\frac{PET_{max} - PET_{min}}{2}\right) \cos\left[2\pi\left(\frac{JDay - L_{PET} - 365/2}{365}\right)\right] + \overline{PET} \quad (3.1)$$

where PET_o is the daily potential evapotranspiration, for each day of the year, in mm per day, PETmax and PETmin are the maximum and minimum PET throughout the year in the region, $\overline{PET}$ is the mean annual PET in the region,, and L_{PET} is the lag of peak PET behind the peak solar forcing (in days). *Small* [2005] provides values for PETmax - PETmin, and $\overline{PET}$, for 6 states in the USA. The parameters provided in *Small* [2005] are used in this work and are given in Table A.1.

The variability of insolation in the terrain resulting from the differences in angle of incidence of solar rays on terrain facing different directions is captured in our modeling framework by adjusting the daily PET estimated with (3.1). PET_o, estimated with (3.1) represents the PET on a "flat" terrain. Next, assuming that the PET is directly proportional to isolation, and that at zero insolation PET is zero, PET on a given inclined terrain is estimated as:

$$PET_i = PET_o \frac{inso_i}{inso_o} \quad (3.2)$$

where $inso_i$ and $inso_o$ are the total insolations on the inclined and on the flat surface, respectively.

Here, the ratio $\frac{inso_i}{inso_o}$ is estimated from geometric relationships after making one assumption: that the ratio $\frac{inso_i}{inso_o}$ is approximately equal to the ratio between the direct beam of solar radiation on an inclined (S_{bi}) and on a flat surfaces (S_{bo}) on a clear day.

The total amount of solar radiation impacting a surface on the Earth, that is

the total amount of short wave radiation, is also known as global radiation. Global radiation consists of the direct beam of the sun, plus the radiation resulting from the scattering of that direct beam as it moves through the atmosphere, moves across clouds, and is reflected in other objects. Among the reflective objects is the terrain itself. Radiation resulting from the direct beam scattering is known as diffuse irradiance. The assumption that the ratio between global radiation on an inclined surface and a flat surface is approximately the same than that of the direct beam radiation yields a first approximation to the spatial variability of insolation. However such assumption neglects the variability of the proportion of diffuse irradiance in the global radiation that can be significant in northern latitudes (where direct solar radiation maybe low) and in places with a high albedo. This assumption should be revised in the future. To take into account the diffusive radiation, the sky and surface albedos must be known, as well as scattering properties of the atmosphere.

Direct beam insolation depends on several factors: the geographic location, the day of the year and the time of the day, and the orientation and inclination of the surface relatively to the Sun. Direct beam radiation at any surface can then be estimated as:

$$S_b = S \cos \varphi_{\oplus\nabla} \tag{3.3}$$

where S is the direct beam solar radiation at the ground level after crossing the atmosphere and $\varphi_{\oplus\nabla}$ is the solar angle of incidence, defined as the angle between the Sun's beam and the normal to the surface. S is estimated based on the amount of radiation reaching the top of the atmosphere, S_o, also known as the solar constant, taking into account atmospheric absorption and scattering, following [*Bras*, 1990]:

$$S = S_o \sin h_\oplus e^{-n(0.128-0.054 \log_{10}(m))m} \tag{3.4}$$

where $S_o = 1353\ [W/m^2]$ is the solar constant, $m = \csc(h_\oplus)$ is the optical air mass, n is a turbidity factor of air, where $n = 2$ corresponds to clear air, and $h_\oplus$ is the solar altitude, or angle of the Sun's beam with respect to an observer's horizon plane, in radians.

The solar angle of incidence, $\varphi_{\oplus\nabla}$, is calculated as follows:

$$\cos \varphi_{\oplus\nabla} = \cos \alpha_\nabla \sin h_\oplus + \sin \alpha_\nabla \cos h_\oplus \cos(\phi_{\oplus az} - \beta_\nabla) \tag{3.5}$$

where α_∇ is the surface's inclination in radians, β_∇ is aspect, the angle between the direction the surface faces and the geographic North, clockwise from the geographic North, in radians. Aspect is 180° (or π in radians) for a north-facing slope. $\phi_{\oplus az}$ is the Sun's azimuth from North, in radians.

The surface's inclination and aspect, α_∇ and β_∇, are obtained from the geometry of the terrain, where as the solar latitude and Sun's azimuth ($h_\oplus$ and $\phi_{\oplus az}$) depend on the time of the day, day of the year and latitude. The latter two are calculated as

follows:

$$\sin h_{\oplus} = \sin\phi \sin\delta_{\oplus} + \cos\phi \cos\delta_{\oplus} \cos\tau_{\oplus}(T_{ST}) \tag{3.6}$$

$$\phi_{\oplus az} = \arctan\left[\frac{\sin\tau_{\oplus}}{\tan\delta_{\oplus}\cos\phi - \sin\phi\cos\tau_{\oplus}}\right] \tag{3.7}$$

where ϕ is the local latitude in radians, $\delta_{\oplus}$ is the declination of the Sun (or the angular distance between the celestial equator plane and the Sun, measured from the Sun (and positive when the Sun lies north of the Earth's equator) and along the hour circle in radians, $\tau_{\oplus}$ is the hour angle of the Sun (which is the angular distance between the planes of the meridian and the Sun's hour circle), and T_{ST} is the standard time in the zone of the observer counted from midnight (in hours) [*Eagleson*, 2002].

The sun's declination $\delta_{\oplus}$ is approximated by

$$\delta_{\oplus} = \frac{23.45\pi}{180}\cos\left[\frac{2\pi}{365}(172 - JDay)\right] \tag{3.8}$$

The sun's hour angle $\tau_{\oplus}$ is calculated with

$$\tau_{\oplus} = \frac{15\pi}{180}(T_{ST} + 12 - \Delta T_{SL}), \quad if\ T_{ST} < 12 + \Delta T_{SL} \tag{3.9}$$

$$\tau_{\oplus} = \frac{15\pi}{180}(T_{ST} - 12 - \Delta T_{SL}), \quad if\ T_{ST} > 12 + \Delta T_{SL} \tag{3.10}$$

where ΔT_{SL}, the time difference between standard and local meridian, can be calculated as:

$$\Delta T_{SL} = \frac{\xi}{15}[15|\Delta GMT| - |\Phi'|] \tag{3.11}$$

In equation (3.11) ΔGMT is the time difference between the local time zone and Greenwich Mean Time, in hours, Φ' is the local longitude in degrees, and ξ is a variable equal to -1 for west longitudes and +1 for east longitudes. In this work we assume ΔT_{SL} negligible.

If we were to assume a flat surface, lets say a horizontal plane tangent to the surface of the Earth, the direct solar radiation would be solely a function of the solar altitude, and thus equation (3.3) would be

$$S_b = S \sin h_{\oplus} \tag{3.12}$$

This is consistent with equations (3.3) and (3.5) given that in a horizontal plane, α_{∇} would be zero, and thus $\cos\varphi_{\oplus\nabla} = \sin h_{\oplus}$

Equation (3.6) can be written for the case when S_b is wanted over a finite period of time. In that case

$$\sin h_{\oplus} = \Delta t \sin\phi \sin\delta_{\oplus} + \frac{12}{\pi}\cos\phi\cos\delta_{\oplus}(\sin\tau_{\oplus 1} - \sin\tau_{\oplus 2}) \tag{3.13}$$

where Δt is the time increment, and $\tau_{\oplus 1}$ and $\tau_{\oplus 2}$ are the $\tau_{\oplus}$ at the beginning and end of the time period of interest. Equation (3.13) assumes a constant ϕ and $\delta_{\oplus}$ during the time interval of integration.

Using equation (3.13)) together with equations (3.7) and (3.5) direct beam insolation for each hour of the day is estimated and then integrated over each day of the year. It is observed that the ratio $\frac{S_{bi\ daily}}{S_{bo\ daily}}$ is approximately equal to that of $\frac{S_{bi\ noon}}{S_{bo\ noon}}$. Hence it is assumed that $\frac{S_{bi\ daily}}{S_{bo\ daily}} = \frac{S_{bi\ noon}}{S_{bo\ noon}}$.

The same ratio, $\frac{S_{bi\ noon}}{S_{bo\ noon}}$, is used to estimate air temperature, as discussed in section 3.5.3

3.3 Geomorphic Processes

Geomorphic processes are responsible for moving sediments across a basin, detaching material from bedrock or regolith, transforming bedrock into regolith, uplifting bedrock. These processes cause changes in the elevation field and soil mantle depth of the land surface. These changes in elevation and soil depth in time are frequently described with the following equations:

1. Surface elevation
$$\frac{\partial z_s}{\partial t} = \frac{\partial z_R}{\partial t} + \frac{\partial h_s}{\partial t} \tag{3.14}$$

2. Bedrock elevation
$$\frac{\partial z_R}{\partial t} = U - W_R(h_s) - E_{br}(q, S) \tag{3.15}$$

3. Soil depth
$$\frac{\partial h_s}{\partial t} = \frac{\rho_R}{\rho_S} W_R(h_s) - \bigtriangledown q_s(q, S, V...) \tag{3.16}$$

These equations denote the surface elevation, z_s, as the sum of bedrock elevation and soil depth, z_R and h_s respectively. Bedrock surface rises due to tectonic uplift acting perpendicular to a horizontal surface. Tectonic uplift (which alternatively could represent base level lowering) is represented by U. Bedrock elevation is also affected by weathering and erosion, represented by W_R and E_{br} in equation (3.15). When the bedrock weathers and transforms into regolith, a change in volume occurs. Such change in volume is indicated in equation (3.16) by the ratio ρ_R/ρ_S. Equation (3.16) indicates that soil depth changes are a function of weathering of the underlying bedrock, and the sediment divergence $\bigtriangledown q_s$ at that location in the landscape. The equations above indicate the dependence of weathering on soil depth, of erosion rates of bedrock on water discharge (q) and slope (S), and sediment divergence on q, S, and vegetation cover V. The above equations represent the essence of the geomorphic processes in the numerical modeling framework. The following sections discuss the representation of uplift, weathering, erosion and sediment transport.

3.3.1 Uplift and Weathering

Uplift and weathering are processes that involve changes in the vertical direction only. Uplift is assumed uniform and constant, and ranges between 0.001 to 1 mm per year. Weathering is soil depth dependent, and follows an exponential decay as soil depth increases [*Heimsath et al.*, 1997]:

$$W_R = W_{Ro} e^{K_W h_s} \tag{3.17}$$

where W_{Ro} is the weathering rate on exposed bedrock and K_W an empirical coefficient.

3.3.2 Erosion and sediment transport

Erosion consists of the detachment and removal of soil or rock by the action of water, wind, biological activity and gravity. The detachment and removal occur through different processes that may be grouped as (a) fluvial erosion, due to overland water flow; (b) diffusion, which groups erosion processes dependent on slope gradient such as rain splash erosion; and (c) mass wasting, which includes processes such as landsliding. Other categories such as wind erosion could be added to the list, and these types of erosion maybe important. However this work only considers fluvial erosion and diffusion.

The removal of sediment or bedrock from one location results in its deposition somewhere else and in the possibility of accumulation of sediment in some parts of the landscape. Therefore, the representation of sediment transport across the landscape, or a hillslope, will determine the new distribution of sediment in the landscape. To represent these erosion and sediment transport processes CHILD simulates the terrain with a grid of "cells" interconnected through a "drainage network". The computation of erosion and sediment processes follows the draiinage network general direction.

Each of the cells represents a location in the landscape with soil, vegetation, and elevation properties corresponding to that location. The drainage network connects these cells following the path a drop of water would follow from each cell in the grid to the "outlet" of the grid, assuming each drop of water would follow the "steepest descent" route. The outlet of the grid is the cell with the lowest elevation. Thus, the grid represents a closed boundary watershed, where all cells "drain" through that outlet. No "sinkholes" are permitted in the grid.

Sediment due to fluvial erosion and diffusion move in the downward direction, following the drainage direction. The calculations are made first in the cells higher up in the network, and then in the cells downstream, however, making sure that all the calculations above any given cell are complete. This assures that the sediment budget at any cell has accounted for any possible sediment coming from any upstream cells. The upstream cells constitute the *contributing drainage area* of that cell. The contributing drainage area is often referred to simply as the *drainage area.* The drainage area also constitutes the terrain surface that will collect the rainfall that

will "drain" through the given cell.

Equations (3.14), (3.15) and (3.16) show the interplay between uplift, weathering, bedrock erosion and sediment flux divergence at each point in the landscape. This interplay connects all the cells of landscape through the drainage network. It is important to note that such connection occurs only through the sediment divergence term. Uplift is independent of the rest of the processes, and weathering is dependent on all of them through their effect on soil depth. Fluvial erosion and diffusion erosion encompass the bedrock erosion and sediment flux divergence and are impacted by every geomorphic process. Fluvial erosion and diffusion erosion are discussed below

A few differences exist between fluvial erosion and diffusion erosion. Fluvial erosion occurs only during rainfall events, causes both bedrock erosion and sediment flux (represented by sediment divergence in equation (3.16)), and is driven by water flux and terrain steepness or slope. Diffusion erosion, unlike fluvial erosion, is assumed to occur all the time, only cause sediment flux (and not bedrock erosion), and is driven only by terrain steepness (and not by water flux).

3.3.3 Fluvial erosion

A distinction is made between fluvial erosion from bedrock and from soil. Bedrock is only eroded where soil has been previously removed and the bedrock is exposed to the action of running water. This requires an algorithm that allows for the erosion of soil during a rainfall event until it has been completely removed, and then for the erosion of bedrock, if the bedrock to be eroded is previously soil covered. Fluvial erosion also requires the satisfaction of two conditions before it takes place: (a) that the flow of water has enough erosive power to detach bedrock particles or sediment particles from a surface; and (b) that the flow of water has enough capacity to transport the detached particles to a downstream location. Erosion at each cell in the grid representing the surface will be equal to the minimum of the two capacities, that of detachment and that of transport. In some circumstances, flow will have the capacity to transport sediment, but not to detach it. In those circumstances fluvial erosion is said to be detachment limited. In some other cases, the flow will have more material that it can transport, most likely because it is already carrying sediments from upstream locations. In these circumstances fluvial erosion is said to be transport limited.

In the numerical framework, the amount of sediment transported from upstream cells (q_{in}) into any given cell is computed first. Then, the amount of sediment being removed from the cell is computed as

$$q_{s\ out} = \min[q_{avail}, E_{sd}, E_{st}] \tag{3.18}$$

where q_{avail} is the sediment available for transport, and E_{sd} and E_{st} are the flow's sediment detachment and transport capacity respectively. In this framework, bedrock

erosion only occurs if all the sediment is depleted by the flow, that is if

$$q_{s\ out} = q_{avail} \tag{3.19}$$

Once $q_{s\ in}$ and $q_{s\ out}$ are known, the sediment divergence is computed as

$$\nabla q = q_{s\ out} - q_{s\ in} \tag{3.20}$$

In these equations, the quantities of sediment are the average fluxes of sediment per unit area of each cell, per unit of time, so strictly the rates are those of the average sediment transport per unit area. These rates are in units of $[m/year]$.

In CHILD small time steps within a rainfall storm prevent numerical instabilities in the calculations of erosion. The erosion rates may change throughout the storm as sediment moves through the system and the form of the landscape slowly changes.

Detachment limited equations

Commonly the capacity of the flow to detach sediments is given by the following equation:

$$q_d = \kappa_d(\tau - \tau_{cr})^{p_d} \tag{3.21}$$

where q_d is the detachment capacity per unit area in a node $[m^3/(m^2 s)]$, and where τ_{cr} is a critical shear stress threshold [Pa] above of which erosion occurs, and κ_d ($[m/(Pa\ s)]$ if $p_d = 1$) and p_d are empirical parameters. The same form of the equation above is frequently used for bedrock erosion (e.g. *Tucker and Bras* [2000]).

In CHILD the same equation is used, but the notation is slightly different. For bedrock it is

$$E_{BR} = \kappa_B(\tau - \tau_{cr})^{p_{db}} \tag{3.22}$$

where as for soil, it is:

$$E_{sd} = \kappa_S(\tau - \tau_{cr})^{p_{ds}} \tag{3.23}$$

where κ_B and κ_S are the bedrock and soil detachment erodibilities, in units of $[m/(Pa^{p_{db}} year)]$ and $[m/(Pa^{p_{ds}} year)]$ respectively, τ is the shear stress experienced by the rock or soil due to the flow of water in $[Pa]$, τ_{cr} is the critical shears stress of the rock or soil, in $[Pa]$, and p_{db} and p_{ds} are constant exponents. Range of values for κ_S are given below in 3.3.6. The parameters used in the simulation are given in Table A.2.

Detachment only occurs above τ_{cr}, a critical shear stress that depends on vegetation density for soil mantled terrain. Shear stress calculations are discussed in the following subsection. The critical shear stress increases under vegetation cover due to the bonding effect of plant roots and organic matter on regolith material. We assume τ_{cr} to increase linearly with vegetation cover as follows:

$$\tau_{cr} = \tau_{cb} + V\tau_{cv} \tag{3.24}$$

where τ_{cb} is the critical shear stress on a bare surface, τ_{cv} is the increase of the critical shear stress under a fully vegetated surface, and V is the vegetation cover fraction, ranging from 0 to 1. Fluvial erosion is further affected by vegetation when vegetation affects the runoff, runon and infiltration processes in a catchment, as is discussed in the Hydrologic Processes section.

Transport limited equations

The transport capacity is estimated with an equation similar to that of detachment capacity, equation (3.21). However detachment is calculated as a change in volume per unit area in time (e.g., $\frac{m^3}{m^2 years}$, yielding $m/year$) and transport capacity is estimated as volume per unit width (e.g., $\frac{m^3}{m\ years}$, yielding $m^2/year$) because of the nature of the physical process represented: detachment is the capacity of shear stress to detach particles from a surface, and transport capacity is that of the flow to move sediment along the flow path of a given width. The form of the equation for transport capacity commonly used, also used in CHILD is

$$q_s = \kappa_f(\tau - \tau_{cf})^{p_f} \tag{3.25}$$

where κ_f, in units of $[\frac{m^2}{Pa^{(p_f)}{}_s}]$, and p_f are parameters estimated from sediment transport of granular materials theories. τ_{cf}, in units of $[Pa]$, is the critical shear stress for transport. E_{st} is obtained as,

$$E_{st} = \frac{q_s W}{A} \tag{3.26}$$

where W and A are the width of the flow of water running through a given cell and the area of the cell, in m and m^2 respectively. By multiplying q_s by W, the total sediment transport capacity Q_s $[m^3/s]$ is obtained, and then that divided by A $[m^2]$ results in the average capacity of the flow to transport a volume of sediment per unit area per time from each cell, in m/s. In CHILD the critical shear stress for detachment of sediments is constant and spatially homogeneous.

The coefficient κ_f, in contrast to κ_B and κ_S, the empirical erodibility coefficients of the detachment limited fluvial erosion equations, is a coefficient that can be estimated as a function of the size of the sediment that water will move. Following *Meyer-Peter and Müller* [1948], and assuming d_{50} as the representative diameter of sediments to be mobilized,

$$\kappa_f = K\frac{\sqrt{g(sg-1)d_{50}^3}}{(\rho_w g(sg-1)d_{50})^{P_f}} \tag{3.27}$$

where K is an empirical coefficient equal to 8 [dimensionless], g is gravity $[m/s^2]$, sg specific gravity of the grain (2.65 for quartz, dimensionless), ρ_w is the density of water $[kg/m^3]$, and P_f is the empirical coefficient (1.5, dimensionless) of the Meyer-Peter and Müller formulation. d_{50} is the maximum size for the smallest 50% of a sediment sample, and corresponds to the median diameter $[m]$.

As an example, for a d_{50} of $1mm$, $\kappa_f = 1.56e{-}5\ [m^2/(Pa\ s)]$, or $492\ [m^2/(Pa^{1.5}\ year)]$.

The Meyer-Peter and Müller formulation was originaly proposed for bedload transport, but the same form of the equation is used to represent total sediment transport.

3.3.4 Shear stress

The flow of water over a surface exerts a shear stress between that results in the detachment and transport of particles on the surface. Such detachment and transport are represented by the equations in the preceding subsection. Other elements of the flow, such as turbulence, and the capacity of water to dilute minerals from the material at the surface, are not commonly considered in geomorphologic formulations and neither in this work.

Therefore, it is sufficient to estimate the shear stress at the surface to estimate the fluvial geomorphic work on the terrain. Shear stress (τ), in Pa units, is calculated assuming shear stress is equal to the water weight vectorial component tangent to the surface. A further assumption is that the angle of inclination of the surface, θ, is relatively small so that $\sin\theta = S$, with S being the slope of the inclined surface in the direction of the flow.

$$\tau = \rho g h S \tag{3.28}$$

where ρ is water density (in kg/m^3), g gravity (in m/s^2), and h flow depth (in m). The flow depth h can be obtained making use of Mannings relationship between flow velocity v and flow depth

$$v = \frac{1}{n} y^{2/3} S^{1/2} \tag{3.29}$$

where v is in $[m/s]$, n is Mannings roughens coefficient $[s/m^{1/3}]$, and y is the hydraulic radius $[m]$. The hydraulic radius is the ratio between the cross sectional area of the flow and the wetted perimeter. Assuming that the flow depth is relatively small compared to the width of flow, y is assumed equal to flow depth h. Then substituting h for y in (3.29), v for q/h, q being the flow per unit width in $[m^2/s]$, and solving for h yields

$$h = n^{0.6} q^{0.6} S^{-0.3} \tag{3.30}$$

Finally, substituting (3.30) in (3.28) yields

$$\tau = \rho g n^{0.6} q^{0.6} S^{0.7} \tag{3.31}$$

Equation (3.31) estimates the total shear stress exerted on the surface. However, shear stress on a terrain surface may be distributed among plants and soil particles following the conceptualization of *Einstein and Barbarossa* [1952] for partitioning the boundary shear stress into grain and form roughness components based on their relative contribution to flow roughness (skin friction concept). The shear stress on

the sediments can be formulated as:

$$\tau_{eff} = F_\tau \tau \tag{3.32}$$

where F_τ is the shear stress partitioning ratio, the ratio between shear stress acting solely on the grains of the soil at the surface and the total shear stress on the surface. For modeling cropland erosion, *Foster* [1982] hypothesized that F_τ is the ratio of the Darcy-Weisbach friction factor for soil to the total friction factor composed of bare soil, vegetation cover and crop residue. By relating flow friction factor to vegetation cover, *Istanbulluoglu and Bras* [2005] expressed effective shear stress as a function of vegetation cover. Their formulation was verified using data from *Prosser et al.* [1995], which reports flow velocities, depths and soil loss measurements under different grass cover conditions and varying water discharge in a field flume in Tennessee Valley, CA. We use *Istanbulluoglu and Bras* [2005] formulation

$$F_\tau = \left[\frac{n_s}{n_s + n_v}\right]^{1.5} \tag{3.33}$$

with

$$n_v = n_v^R \left(\frac{V}{V_R}\right)^{\omega} \tag{3.34}$$

where n_s is the roughness of a bare surface, n_v roughness resulting from vegetation, V is vegetation cover, V_R is a reference vegetation cover, n_v^R is the roughness corresponding to the reference vegetation cover, and ω is an empirical exponent that *Istanbulluoglu and Bras* [2005] calibrated to 0.5. Substituting equations (3.31) and (3.33) into (3.32), and assuming $n = n_s + n_v$, the effective shear stress is given by

$$\tau_{eff} = \frac{\rho g n_s^{1.5}}{(n_s + n_v)^{0.9}} q^{0.6} S^{0.7} \tag{3.35}$$

In CHILD the form of the effective shear stress τ_{eff} equation is slightly different:

$$\tau_{eff} = \kappa_t \left(\frac{n_s^{1.5}}{(n_s + n_v)^{0.9}} q_{CHILD}^{mb} S^{nb}\right) \tag{3.36}$$

where the exponents m_b and n_b are 0.6 and 0.7 respectively, and the coefficien $\kappa t = \rho g \Upsilon_s$, groups the constants ρ and g. Υ_s is a factor that converts the units of flow in used in CHILD (q_{CHILD}) $[m^2/year]$ to units of $[m^2/s]$. Υ_s is equal to the number of seconds in a year to the power of $(-mb)$.

The flow per unit width in CHILD (q_{CHILD}) is calculated assuming a channel width computed empirically using the well-known scaling relationship between channel width and discharge[*Leopold and Maddock*, 1953; *Leopold et al.*, 1964], as discussed in *Tucker et al.* [2001]. The scaling relationship is summarized as:

$$W = W_b \left(Q/Q_b\right)^{\omega_s} \tag{3.37}$$

$$W_b = \kappa_w Q_b^{\omega_b} \tag{3.38}$$

where W is the channel width, W_b the bankfull channel width, Q the flow, Q_b the bankfull flow, both in $[m^3/sec]$, and ω_s, ω_b and κ_w empirical exponents and coefficients. Here it is assumed that $\omega_s = \omega_b$, and equations (3.37) and (3.38) are reduced to the expression used by *Tucker and Slingerland* [1997]

$$W = \kappa_w Q^{\omega_s} \tag{3.39}$$

with $\kappa_w = 10\ [m/(m^3/sec)^{0.5}]$ and $\omega_s = 0.5$.

3.3.5 Diffusion

Diffusive processes consist of sediment movement due to gravity and environmental disturbances such as animal activity and rain splash, which increase in magnitude as the slope steepens. In contrast to fluvial erosion, diffusion only occurs on soil mantled terrain and is independent of water runoff. Rain splash diffusion generally increases with rainfall intensity, however a layer of water resulting from the rain may protect the soil from the impact of rain drops. In our formulation diffusion is assumed to be only dependent on the slope of the terrain, however, estimating diffusion as a function of biological activity, vegetation cover, rainfall intensity and other factors is an open area of research. The amount of sediment transported due to diffusion in the downward direction from each grid cell representing a surface is given by

$$q_{diff\ out} = \min[q_{avail}, \kappa_{diff} S] \tag{3.40}$$

where κ_{diff} is an empirical coefficient, and is of the order of $0.01 m^2/year$ for semiarid environments (e.g., *Roering* [2008]). Recently, however, new formulations for this diffusion process are emerging in the scientific literature (e.g., *Roering* [2008]).

The movement of sediment from one location due to diffusion implies its deposition in a neighboring location. Thus, in the modeling framework the mass balance of soil at each cell due to diffusion must take into account the incoming and outgoing sediments. This results in a sediment divergence term similar to that of fluvial erosion (3.20):

$$\nabla q_{diff} = q_{diff\ out} - q_{diff\ in} \tag{3.41}$$

where $q_{diff\ in}$ is the sediment due to diffusion on the neighboring cell that "drain" to the cell of interest.

Mass wasting processes are gravity driven, as diffusion, but in contrast to the gradual nature of diffusive processes, they occur sporadically and result in sudden movements of material. Examples of this type of processes are landslides and channel bank collapse. Landslides occur in relatively steep terrain, where as bank collapse occurs in regions of cohesive soils and relatively flat terrain where channels incise. Channel extension due to bank collapse is more likely to occur than landslides in the field sites studied in this work. Bank collapse and headcut retreat erosion processes

have been studied using CHILD, the reader is refered to *Istanbulluoglu et al.* [2005] and *Flores-Cervantes et al.* [2006]. In the current framework, however, diffusion is assumed to account for all gravity driven processes. Given that the soils at the study site are not highly cohesive, the gravity erosion processes are expected to be rather continuous instead of episodic, and thus be well represented by diffusion. In the future, a higher deegree of complexity can be added by relaxing this assumption and modeling channel extension due to bank failures and plunge pool erosion, among other type of mass wasting processes.

Interesting theoretical derivations can be made relating the form of a hillslope and the diffusion equations used. That is out of the scope of this work but we refer the reader to *Roering* [2008].

3.3.6 Values of the parameters for the empirical detachment limited equations for soils

Large efforts have been carried out to estimate the parameters of equations of the form of (3.21) to allow for the modeling and estimation of erosion. These efforts include thousands of measurements of water flow and erosion throughout several decades. A recent review of this data by *Knapen et al.* [2007] presented a series of base values of κ_d and τ_{cr} for soils, for the case of $p_d = 1$, as depicted in Figure 3-2. Values for erosion of bedrock are also obtained from observations. In the current formulation we simply use a value of erodibility several orders of magnitude smaller than that of soils.

The reported ranges of values of k_d and τ_{cr} vary by 3 orders of magnitude. Table 3.2 summarizes data from 4 different studies, including that of *Knapen et al.* [2007], in units that yield detachment rate in $[m^3/(s\ m^2)]$, equivalent to $[m/s]$. Some of the data is in units that yield detachment in $[kg/(s\ m^2)]$, including data in Figure 3-2. The $[kg/(s\ m^2)]$ units are transformed to $[m/s]$ by dividing them by the soil density, which is assumed 1250 $[kg/m^3]$ for the values presented in Table 3.2.

Table 3.3 shows the values estimated by *Nearing et al.* [1999] under the assumption that p_d is different from 1. Note how the value of κ_d is two orders of magnitude lower when p_d is different than 1, even though the data set from where the parameter was estimated is the same as that of *Laflen et al.* [1991]. The type of soil they sampled was gravelly sandy loam (percentages of clay, silt, sand and rock fragments are: 10, 8, 39 and 43) of the Lucky Hills in Walnut Gulch, AZ, and is the same area sampled by Laflen et al., in 1991.

Table 3.4 shows the values used in *Flores-Cervantes et al.* [2006], which were different for laboratory and a field conditions. Sandy loams, clays and clay loams from Montana were used in the laboratory experiments reported in the table.

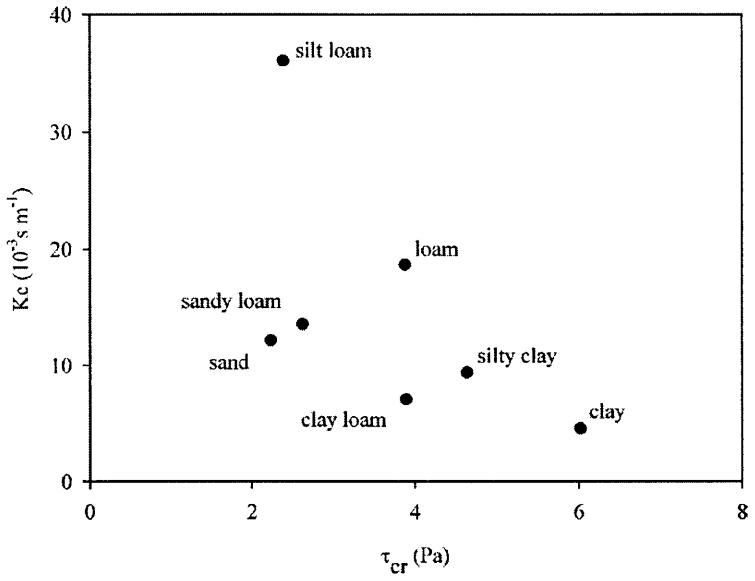

Figure 3-2: Parameter values of κ_d and τ_{cr} for different textures, assuming $p_d = 1$, from *Knapen et al.* [2007]

3.4 Hydrologic (water fluxes) processes

The flux of water across a land surface is tightly linked to vegetation dynamics and geomorphic processes. Therefore water fluxes across the landscape can be seen as a bridge between the spatial patterns of vegetation and land surface form.

Changes in the form of the landscape result from the flux of water along a landscape as has been discussed in section 3.3. Where water flows, and with what intensity it flows, depends on the form of the land surface. Water follows certain paths controlled in the modeling framework by the evolving "drainage network" described in section 3.3.2. In the drainage network, more water flows through its branches the closer they are to the outlet: relatively little water flows close to the ridges and more water flows along the hollows and valleys of the landscape. In this network, in addition, the intensity of the flux increases with the steepness of the terrain. This organization in surface water fluxes lead to organized erosion and sedimentation patterns that give rise to a new land surface form. The bi-directional interaction between surface hydrology and geomorphology is schematically represented in Figure 3-3 with dashed arrows.

The bi-directional interaction between hydrologic and geomorphic processes mentioned above is affected by the state of vegetation in two ways. First, vegetation restricts erosion and sediment transport as previously discussed in section 3.3. Second, and alluding to the bridge that hydrologic processes create between vegetation

Table 3.2: Range of values of κ_d and τ_{cr} for soils from different studies

κ_d $[\frac{m}{Pa\ s}]$	τ_{cr} $[Pa]$	Type of study	Type of value	Source
4.72e-7	0.5	Field [3 x 10 m]	mean	*Laflen et al.* [1991]
6.36e-6	5	Field [0.14 x 3.05 m]	mean	*Nearing et al.* [1999]
1e-9 4e-6	0.001 - 400	River beds	Range	*Hanson and Simon* [2001]
1e-9 1e-6	0.5 - 400	River beds, Mississipi	Range	*Hanson and Simon* [2001]
2e-9 4e-6	0.001 - 200	River beds, Nebraska	Range	*Hanson and Simon* [2001]
2e-8 8e-7	0.1 - 40	River beds, Iowa	Range	*Hanson and Simon* [2001]
8.8e-6	7	Lab, field, and river bed	Mean	*Knapen et al.* [2007]
4e-6	2	Lab, field, and river bed	Median	*Knapen et al.* [2007]
4.8e-6	3	Field	Mean	*Knapen et al.* [2007]
8.8e-6	3	Lab	Mean	*Knapen et al.* [2007]
3.2e-6 3e-5	2-6	Cropland soils	Range	*Knapen et al.* [2007]

Table 3.3: Values of κ_d when p_d is different from 1 for the Lucky Hills site in Walnut Gulch, AZ

κ_d $[\frac{m}{Pa\ s}]$	τ_{cr} $[Pa]$	p_d	Type of study	Source
3e-8	0	2.377	Field [0.14 x 3.05 m plot]	*Nearing et al.* [1999]

and land form patterns, vegetation changes the organization of the flow of water. Plants modify the surface properties in such a way that the surface's infiltration capacity increases around them [e.g., *Selby* [1993]], reducing runoff and water's erosive power. These uni-directional interaction between vegetation and geomorphological processes, one acting directly and the other one by way of the hydrologic processes, are schematically represented in Figure 3-4 with thick solid arrows.

The distribution of vegetation in the landscape is sensitive to the distribution of soil moisture in the landscape, and thus, to the processes governing the fluxes of water that regulate the moisture state of the landscape. The dependence of vegetation on soil moisture is discussed in detail below in section 3.5. This distribution of vegetation, in turn, as mentioned in the preceding paragraph, affects infiltration rates of the surface and as a consequence runoff generation. In addition, vegetation transpires moisture from the soil, and protects the surface against bare soil evaporation, thus exerting a control on the fluxes of moisture out of the soil. The bi-directional interaction between water fluxes and vegetation is schematically represented in Figure 3-3 with dotted arrows.

The bi-directional interaction between vegetation dynamics and hydrologic processes is influenced by the land surface form and the soil depth in several ways, some of them already mentioned. Both, land surface form and soil depth are direct con-

Table 3.4: Differences between laboratory and field conditions in κ_d

κ_d $[\frac{m}{Pa\ s}]$	τ_{cr} $[Pa]$	p_d	Type of study	Source
8e-5	1.75	1	Modeling of a flume	*Flores-Cervantes et al.* [2006]
8e-8	1.75	1	Modeling of the field	*Flores-Cervantes et al.* [2006]

sequences of erosion and sedimentation processes. Three ways in which land surface form and soil depth affect the bi-directional interaction are: (a) land form controls the surface fluxes of water and as a consequence vegetation distribution; (b) soil depth distribution controls the water storage capacity in the landscape and thus the spatial distribution of the potential for the establishment of vegetation; (c) land form regulates the amount of insolation in the terrain due to differences in the incidence of solar radiation, and thus, land form regulates the available energy for transpiration and evaporation. The variability in insolation results in topography dependent patterns of vegetation. The effects of land form and soil depth on vegetation mentioned above are schematically illustrated in Figure 3-4, and they all demonstrate the bridge that hydrologic processes provide for an interaction between topography and vegetation.

The representation of all of the above interactions within the model presented in this work will be discussed in this section.

An important effect of vegetation on water fluxes not considered in this thesis is that a vegetative cover changes the flow hydraulics and hence the flow hydrograph. In this work steady state flow is assumed. Vegetation increases the terrain's surface roughness. A higher surface roughness results in a slower water flow velocity. A slower water flow velocity results in a moderate, and long duration water flux through a catchment, in contrast to an intense, and short lived water flow event. Given an identical rainfall, a long duration water flow event of moderate intensity contrasts with a short-lived water flow event of high intensity in at two important ways: (1), shear stress on the surface is less, and so geomorphic activity could be negligible; (2) more water is allowed to infiltrate, reducing erosion and increasing the terrain capacity to sustain vegetation.

The steady state flow assumption greatly simplifies the numerical model, reduces complexity and saves computer time. This assumption is reasonable to the extent that a steady state flux is representative of the surface water flux of a catchment. A steady state flux is reasonable for relatively small watersheds subject to long duration rainfall. The assumption may also be reasonable over the long solution horizons considered here. Nevertheless, it would be desirable to relax the steady state assumption and explicitly account for these effects of vegetation on water hydraulics in the future.

Hydrologic processes, or water fluxes, can be divided into two categories, the surface runoff processes (rainfall-runoff-runon-infiltration) that occur in the timescales of the duration of a storm, and the soil moisture dynamics (infiltration-lateral moisture redistribution-leakage-evaporation, transpiration), that occur in the timescales of the

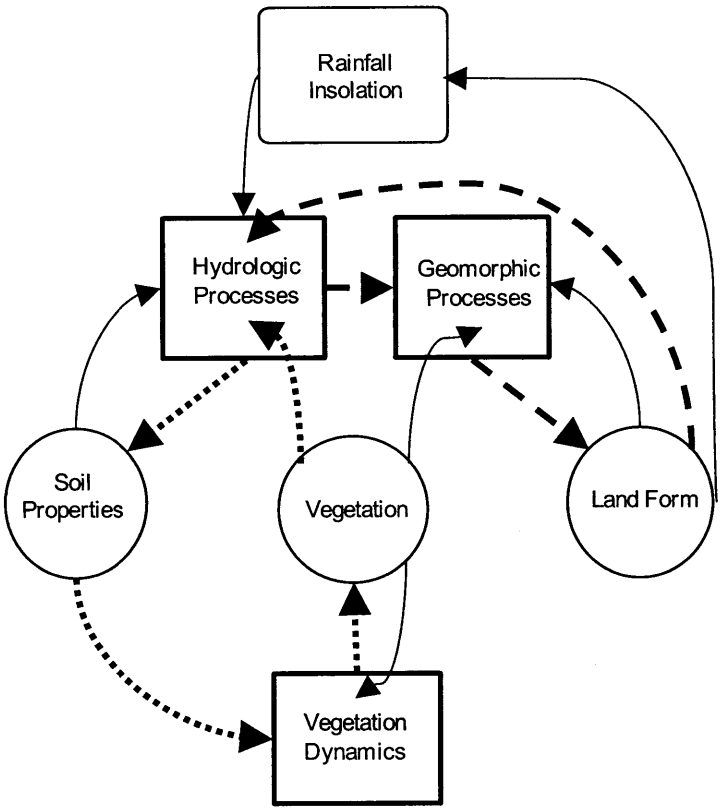

Figure 3-3: Schematic representation of the bi-directional interaction between geomorphological and hydrological processes, shown by thick dashed arrows, and the schematic representation of the bi-directional interaction between vegetation dynamics and hydrological processes, shown by thick dotted arrows.

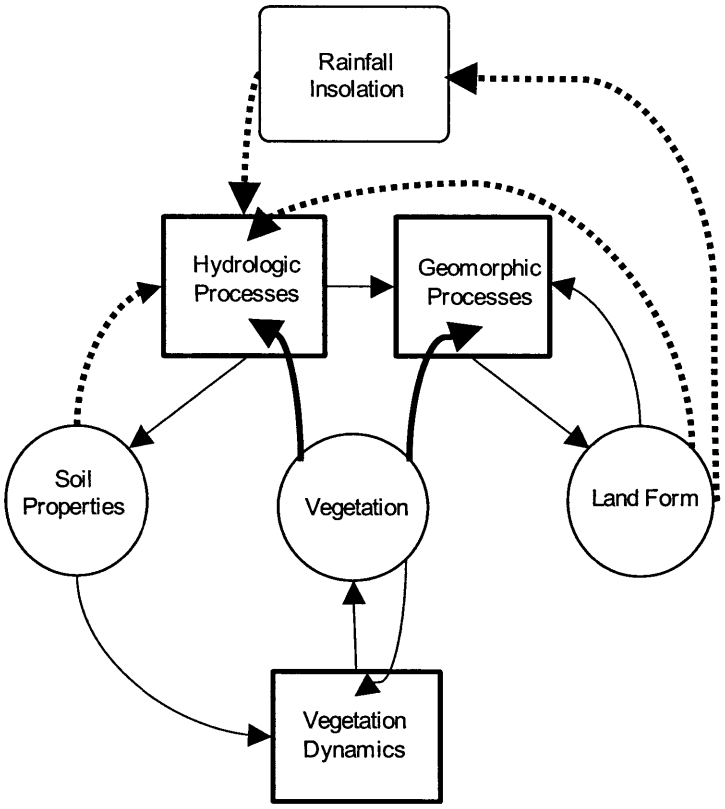

Figure 3-4: Impacts of vegetation on the bi-directional interaction between geomorphological and hydrological processes (see Figure 3-3), represented with thick solid arrows, and impacts of the land surface form and soil depth on the bi-directional interaction between vegetation dynamics and hydrological processes (see Figure 3-3), represented with thick dotted arrows.

duration of the period between storms (interstorm). These two sets of processes are linked by the infiltration process.

3.4.1 Surface runoff processes

Some rainfall infiltrates, some remains stored on leaves or terrain depressions, and the rest becomes surface runoff. Infiltration excess runoff occurs when rainfall intensity exceeds the infiltration rate and thus the excess rainfall becomes surface runoff. Storage excess runoff occurs when the soil saturates during a rainfall event and thus any rain after that becomes surface runoff. Return flow consists of the runoff generated by water flowing out of the ground after recently having infiltrated in a neighboring higher location. The present work only considers the first two cases of surface runoff generation.

The fluxes of water are computed in a similar way to the fluxes of sediment discusses in section 3.3: the calculations are made following the drainage patterns starting from the highest elevations and then moving in the downstream direction until the outlet of the catchment is reached. This way, all the runoff flowing into a cell from upstream cells has been accounted for when estimating the corresponding infiltration, runoff generation, and water flux out of that cell.

In this work rain is assumed to fall uniformly over the whole domain, and runoff calculations are made with the assumption of a steady state flux in mind. This simplifies calculations because under that assumption, all fluxes are assumed to be constant and equal to the amount of water raining upstream of any given cell, along the drainage network, minus the infiltration happening also upstream of that given cell along the drainage network, plus the rainfall falling in that cell minus the infiltration occurring at that cell. This can be expressed mathematically by:

$$Q_{out} = (P - I_r)A + Q_{in} \tag{3.42}$$

where P is precipitation intensity in $[m^3/year]$, I_r infiltration rate in $[m/year]$, A area represented by the node element or cell in $[m^2]$, and Q_{in} the flux of water coming into the analyzed cell from neighboring cells in $[m^3/year]$. Infiltration is represented by

$$I_r = \min\left(I_c, P, \frac{h_s n_p (1-s)}{\Delta t}\right) \tag{3.43}$$

where I_c is the infiltration capacity in $[m/year]$, and the term $h_s n_p(1-s)$ represents the storage capacity of the soil to store moisture. This term is the soil depth h_s times the soil porosity n_p, times the fraction of that porosity not filled with water $(1-s)$. The time increment of the calculation is Δt. It is generally speaking the duration of the rainfall of a given intensity and in CHILD is given in $[years]$. The relative soil moisture is represented by s. Dividing by Δt converts the store in the soil into a rate of the amount of moisture the soil can receive during Δt.

In this work infiltration capacity is dependent on vegetation cover. Following

Dunne et al. [1991] it is estimated as:

$$I_c = I_{cb} + V\ I_{cv} \tag{3.44}$$

where I_{cb} and I_{cv} are the infiltration capacities in a bare surface and a vegetated surface, respectively.

3.4.2 Soil moisture dynamics

Soil moisture dynamics are assumed to act uniformly across each model element, where moisture balance is accounted by applying appropriate input and output fluxes in the vertical and horizontal directions, including infiltration, bare soil evaporation, transpiration, leakage and lateral moisture redistribution. The output fluxes are accounted in the same way as in *Collins and Bras* [2008]. Infiltration is accounted for during each rainfall event, and the rest of the fluxes are calculated at the end of the interstorm period or every two weeks, whatever occurs first. Vegetation is also updated every time moisture is updated. Moisture is calculated with a mass balance equation

$$n_p\ Z_r \frac{\partial s}{\partial t} = I_r - E - T - L - \Phi \tag{3.45}$$

where Z_r is the root zone depth in $[m]$, and E evaporation from bare soil, T transpiration, L leakage and Φ lateral moisture redistribution, in $[m/year]$ (the rest of the variables have been previously defined). In this equation, propagation of the wetting front in the soil is ignored, and the soil moisture of the entire root zone is represented by one value. If the root zone depth is assumed equal to the soil depth, that is $Z_r = h_s$, then equation 3.45 becomes

$$n_p\ h_s \frac{\partial s}{\partial t} = I_r - E - T - L - \Phi \tag{3.46}$$

and indicates a link between the spatial distribution of soil depth on the landscape to that of moisture.

Figure 3-5 graphs soil moisture loss rate for a typical water-limited ecosystem soil and vegetation conditions [*Collins*, 2006] using common expressions for evaporation from bare soil, transpiration, and leakage losses functions of root zone soil moisture. Lateral fluxes are considered part of the leakage losses. Water loss terms in equation (3.45) are strongly related to soil moisture, type of soil, vegetation, evaporation demand and transpiration demand.

The evaporation and transpiration demands are function of the PET previously defined in section 3.2. Starting from initially saturated root zone soil moisture ($s = 1$), leakage takes place until soil moisture falls to field capacity, s_{fc}, a soil property below which drainage is zero. Evaporation from bare soil increases linearly with soil moisture from zero below a threshold minimum soil moisture (the hygroscopic soil moisture, s_h, dependent on soil type) to its potential rate at soil moisture saturation (scaled by bare

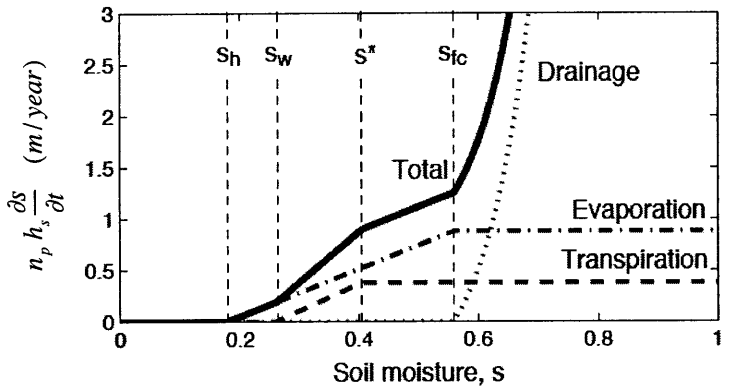

Figure 3-5: Soil moisture loss rates as a function of soil moisture for typical soil and vegetation characteristics of semiarid ecosystems [*Collins*, 2006].

surface area $(1-V)$). However, for reasons of analytical tractability, for soil moisture larger than the soil's field capacity, s_{fc}, the evaporation rate remains constant . For values above the field capacity, leakage becomes the dominant process of moisture loss. Transpiration is at its potential rate (scaled by the vegetation cover V) when relative soil moisture is between s_* and 1. The soil moisture threshold s_* depends on soil and vegetation characteristics. In terms of vegetation, s_* represents soil moisture threshold that marks the beginning of plant water stress as plants start closing their stomata to conserve water [*Porporato et al.*, 2001]. Below s_*, transpiration linearly decreases with soil moisture, s, until it reaches the wilting point, s_w, at which plant wilting starts and transpiration ceases.

The following description of the representation of leakage losses in CHILD is extracted from *Laio et al.* [2001a].

> "Leakage losses are assumed to happen by gravity at the lowest boundary of the soil layer, neglecting possible differences in matric potential between the soil layer under consideration and the one immediately below. The loss rate is assumed to be at its maximum when soil is saturated and then rapidly decay as the soil dries out, following the decrease of the hydraulic conductivity $K(s)$. The decay of the hydraulic conductivity is usually modeled using empirical relationships of different forms [e.g., ...*Hillel* [1998]]. Here the hydraulic conductivity is assumed to decay exponentially from a value equal to the saturated hydraulic conductivity

K_s at $s = 1$, to a value of zero at field capacity, s_{fc}. The exponential form, chosen for reasons of mathematical tractability, has been commonly employed in the literature as an alternative to the more customary power law ... The assumed behavior of leakage losses is thus expressed as"

$$L(s) = K(s) = \frac{K_s}{e^{\beta(1-s_{fc})} - 1}\left[e^{\beta(s-s_{fc})} - 1\right], \quad s_{fc} < s \leq 1 \tag{3.47}$$

In (3.47), β is a coefficient which is used to fit the expression to the commonly used power law expression $K(s) = K_s s^c$ [*Hillel*, 1998], where $c = 2b+3$ and b defined from empirically determined soil-water retention curves of the form $\Psi_s = \overline{\Psi}_s s^{-b}$, where Ψ_s is the matric potential and $\overline{\Psi}_s$ and b experimentally determined parameters. Following a criterion that minimizes the discrepancies between (3.47) and $K(s) = K_s s^c$, β is defined as $\beta = 2b+4$. This way, the value of β depends on the type of soil, and varies between 12 for sand to around 26 for clay.

"... From a physical viewpoint, the modeling of leakage driven by a unit vertical gradient due to gravity implies no interaction with the underlying soil layers and the water table. Such simplifications pose some restrictions in the use of the model, even though in most water-controlled ecosystems the contribution due to capillary rise from the water table or deeper soil layers, if any, is generally of secondary importance".

This work considers the role of topography in redistributing soil moisture (the only consideration of lateral fluxes) when s_{fc} is exceeded. Moisture flux is divided in vertical and horizontal flow components assuming anisotropy between the plane parallel to the surface and that normal to the surface, following the work of *Cabral et al.* [1992].

$$q_l = L(\cos S \sin S)(a_r - 1) \tag{3.48}$$

where q_l is the lateral redistribution and a_r is the anisotropy ratio. The horizontal component is thus that corresponding to moisture redistribution, and the rest is assumed leakage. Lateral moisture redistribution is assumed to occur in the same direction that the surface flow, that is, in the steepest descent direction. Mass is conserved in the lateral redistribution of flow. Moisture moving from one cell to the other modifies moisture stored in the new cell. When the downstream element to where the lateral moisture transfer is directed saturates, the fraction of the lateral flux that could not be transferred is assumed to drain downwards. All the vertical fluxes, that is leakage, evaporation, transpiration and infiltration, are recorded for each time step of the simulation.

Analytical expressions for the soil moisture dynamics used here are provided by Collins [*Collins*, 2006]. He shows analytical expression for soil moisture losses combining E, T and L as a function of s, and also the evolution of soil moisture in time.

3.5 Vegetation dynamics

Effects of vegetation on geomorphic and hydrologic processes have been outlined in the preceding sections of this chapter, and some of the ways in which hydrologic processes (and indirectly the forms of the landscape as they affect hydrologic processes) affect vegetation have been indicated as well. Here, the way vegetation growth is represented in the model is discussed. In this work vegetation growth is drastically simplified. Vegetation is assumed to be only one species, its state is quantified by a single metric, the proportion of vegetation cover that is assumed uniform across each modeling element. Growth and mortality are assumed dependent only on soil moisture availability through time. Limitation of vegetation growth due to limitation on photosynthetic sunlight, nutrients availability, or other environmental stress such as herbivores or insects are not taken into account. Age is not considered. This characterization of vegetation best suits grasses in open land. The existence of other species, competition between species, propagation of seeds and cycles of reproduction and establishment, are out of the scope of this work.

Vegetation and soil moisture dynamics are tightly coupled, particularly in semiarid settings. Here we represent these dynamics at each element of the numerical grid. In CHILD, a water mass balance is kept and water enters and exits the soil following processes of infiltration, transpiration, evaporation from bare soil, leakage, and lateral soil moisture flux.

Vegetation growth occurs as a function of transpiration. The concept of water use efficiency (WUE) has been frequently used in the agricultural community and also on ecological studies, and it relates the amount of water transpired by a plant to the amount of carbon it assimilates, in grams per meter squared. Because transpiration depends on soil moisture availability and the amount of vegetation on the land, through the WUE it is possible to readily link vegetation growth to the soil moisture state. In addition, the WUE has been estimated from transpiration and carbon assimilation of plants in the field and in laboratories, at different scales, and for different plants and plant communities. Thus we can parameterize this vegetation dynamics formulation directly with measurements.

In this formulation, the carbon assimilated by plants is distributed between above ground biomass (green leaves) and below ground biomass (roots), following an allometric rule that results in the growth of the above ground biomass at the beginning of the growing season, and of the below ground biomass by the end of the growing season. The above and below ground biomass pools are independently tracked. A constant rate of biomass senescence, and losses of carbon due to plant respiration are assumed.

This formulation is used with parameters obtained from published studies of vegetation dynamics, and is compared to observations over a period of 7 years. This comparison is presented in Chapter 4. The simulations were forced with daily observed rainfall.

In order to better capture the observed vegetation dynamics with the model, a

couple of restrictions to the WUE formulation were added to represent the phenological characteristics of grasses at the field site. These are the following: a) carbon assimilation is limited to spring and summer; b) "flush" of carbon from the roots to the leaves is allowed during the spring and summer until a minimum above ground biomass threshold is exceeded, and this flush is proportional to the root biomass; c) senescence rate doubles when the plant has been above a threshold 30-day-averaged-water-stress.

3.5.1 Water Use Efficiency

Water use efficiency (WUE) is the ratio between biomass produced by a plant and the amount of water transpired by a plant. The ratio varies with species, but also within a given plant specimen through time and even from one leave to another. The more water use efficient a plant is, the higher the WUE will be. WUE has been used in the agricultural literature as the ratio between biomass produced by a crop and the total amount of water evapotranspired during a day, or during a growing season. These type of measurements used in agriculture include the water loss due to evaporation from the bare soil and are very useful for estimating the costs in terms of water to produce certain type or crop. In the biological sciences and ecology literature instantaneous measurements on a single leaf report a WUE in better agreement with the definition of WUE assumed here. The instantaneous amount of biomass synthesized by a plant and the amount of water it transpires can be measured in a leaf with a gas analyzer. Each gram of dry biomass in a plant is constituted by about 0.4 grams of carbon. With this conversion, and a measure of the gas fluxes of water and carbon dioxide in and out of a leave representative of a given plant or plant community for a given period of time, a WUE can be estimated. Various values of WUE for grasses and grass communities were published as a result of the African Savanna Biome Programme. Those values are presented in Table 3.5. WUE can also be theoretically estimated by relating the diffusivity of CO_2 and H_2O, atmospheric temperature and water vapor deficit, using the following equation (after *Williams and Albertson* [2005])

$$WUE = \frac{g_c(1-\alpha)C_a}{g_v(f^* - f)}\mu \tag{3.49}$$

where g_c and g_v are air diffusivities of CO_2 and H_2O vapor respectively, in $[m^2/s]$, C_a is ambient CO_2 concentration in $[\frac{1}{\mu mol\ s}]$, f^* and f are the saturated specific humidity of air and the specific humidity of the air in $[\frac{kg\ H_2O}{kg\ air}]$, α is the ratio of intercellular to ambient CO_2 concentration [dimensionless], and μ $[1.5x10^{-6}\frac{gCO_2}{g\ air}]$, is a factor related to unit conversion. However, this equation assumes infinite amounts of biomass production in a very humid environment, and thus its use is limited. In humid environments other factors limit biomass production. In this work, a constant WUE value is assumed. This is a relatively good approximation in grasslands [*Ponton et al.*, 2006], which are the focus of this study.

Table 3.5: Measured values of water use efficiency (WUE) for grasses and grass communities [*Scholes and Walker*, 1993]

	Details	$\frac{gH_2O}{gCO_2}$	$\frac{gDM}{gH_2O}$	$\frac{gC}{kgH_2O}$
Grasses (single leaf, instantaneous)				
Eragrostis pallens	Growth chamber	40	0.017	6.82
Digitaria eriantha	Growth chamber	43	0.016	6.34
	Field	336	0.002	0.81
Chenchrus ciliaris	Field	526	0.001	0.52
Eragrostis lehmanniana	Field	1470	0.0005	0.18
Whole grass plant, full growing season				
Unstressed	Pots in Field	52	0.013	5.24
Stressed	Pots in Field	47	0.015	5.8
Grass community, full season	Field	127	0.005	2.14
Trees and grass, long-term	Field	420	0.002	0.65

DM stands for dry matter, conventionally used to describe quantities of vegetation in ecosystem studies [*Scholes and Walker*, 1993]

3.5.2 Gross Primary Productivity

With this WUE assumption, the rate of net productivity of a plant or a plant community , NPP, in grams of dry mass per unit square meter (or $\frac{gDM}{m^2yr}$), can be estimated as:

$$NPP = T\, WUE \rho_w \tag{3.50}$$

where T is the transpiration rate per unit area $[m/year]$.

3.5.3 Biomass of green leaves, roots and death biomass

Biomass in a plant will increase as the photosynthetic activity of the plant synthesizes carbon and it distributes it between its different components, for example between above ground biomass and below ground biomass, or between its structural and non-structural components, such as branches and leaves of a tree. In the case of grasses, it is reasonable to account for the amount of biomass distributed between the leaves (above ground biomas, B_g) and roots (below ground biomass B_r). At the same time that the plant grows, part of it dies. Dead above ground biomass may remain standing for several days or weeks, as well as dead roots. The pool of dead above ground biomass is also monitored. This above ground death biomass certainly affects the erosion processes. In this work dead biomass is added to the total amount of the above ground biomass to estimate the effect of vegetation on erosion. However, dead biomass is not taken into account in the soil moisture dynamics calculations, where only the green above ground biomass fraction of the total above ground biomass is considered.

The dynamics of grasses represented in the present work are governed/regulated by the following two differential equations, with biomass in $[gDM/m^2]$:

$$\frac{dB_g}{dt} = NPP\left(\phi_{\oslash}\left(1 - \frac{B_g}{B_{gmax}}\right)\right) - d_g B_g \tag{3.51}$$

$$\frac{dB_r}{dt} = NPP\left(1 - \phi_{\oslash}\left(1 - \frac{B_g}{B_{gmax}}\right)\right) - d_r B_r \tag{3.52}$$

where $\phi_{\oslash}$ is a phenology parameter discussed below, $B_{g\ max}$ is the green grass biomass that would fully cover the ground, and d_g and d_r are the senescence rates of green leaves and roots. The terms in the parenthesis represent the partitioning of the NPP between above and below ground biomass (i.e., shoots and roots).

In this model, the partitioning of biomass between roots and shoots has two components, one is a function of the time of the year ($\phi_{\oslash}$), which sets a different allocation strategy during the fall, sending most of the NPP to the roots at that time, and one that controls the allocation as a function of the vegetation cover, which allocates most of the NPP to the shoots when the vegetation cover is low. During the fall, the above ground biomass has already developed, and thus all the biomass produced is allocated to be stored in the roots. The phenology factor is expressed mathematically as:

$$\phi_{\oslash} = \begin{cases} 1 & \text{for } 0.05 \leq y_{\oslash} \leq 0.75 \\ 1 - (y_{\oslash} - 0.75)\left[\frac{1-0.1}{0.8-0.75}\right] & \text{for } 0.75 < y_{\oslash} < 0.8 \\ 0.1 & \text{for } y_{\oslash} \geq 0.8 \text{ or } y_{\oslash} < 0.05 \end{cases} \tag{3.53}$$

where $y_{\oslash}$ is the fraction of the year when the vegetation change is being calculated.

The above equation limits above ground biomass growth during the last three months of the year (October, November and December), when any NPP produced is stored in the root pool.

An equation of the dynamics of the dead standing biomass above ground , B_d, is also provided here for reference:

$$\frac{dB_d}{dt} = d_r B_r - d_d B_d \tag{3.54}$$

where d_d is the rate of disintegration of the death standing biomass.

The equations representing the change in biomass can be solved directly by numerical integration, however, their analytical solution is used. Biomass changes are computed for each interstorm period or every two weeks, whatever occurs first, in synchrony with the soil moisture calculations. The value of transpiration, T, used to estimate NPP, is the mean transpiration of the corresponding time interval (see section 3.4.2). The soil moisture dynamics calculations assume a constant vegetation cover for each time interval, equal to the vegetation cover estimated for the end of the previous time interval. Below are the analytical solutions to equations (3.51), (3.52)

and (3.54).

$$B_g = \frac{1}{X} + \left(B_{go} - \frac{1}{X}\right) e^{-NPP\phi_{\oslash} X \Delta t} \tag{3.55}$$

$$\begin{aligned} B_r =& \frac{NPP\ M}{d_r} + \frac{NPP\phi_{\oslash}}{X d_r B_{gmax}} \\ &+ \left[B_{ro} - \frac{NPP\ M}{d_r} - \frac{NPP\phi_{\oslash}}{B_{gmax}} \left(\frac{1}{X d_r} + \frac{B_{go} - \frac{1}{X}}{d_r - NPP\phi_{\oslash} X}\right)\right] e^{-d_r \Delta t} \\ &+ \frac{NPP\phi_{\oslash}}{B_{gmax}} \left(\frac{B_{go} - \frac{1}{X}}{d_r - NPP\phi_{\oslash} X}\right) e^{-NPP\phi_{\oslash} X \Delta t} \end{aligned} \tag{3.56}$$

$$\begin{aligned} B_d =& B_{do} e^{-d_d \Delta t} + \frac{d_g X}{d_d}(1 - e^{d_d \Delta t}) \\ &+ \frac{d_g B_{go} - d_g X}{d_d - d_g} \left(e^{d_g \Delta t} - e^{d_d \Delta t}\right) \end{aligned} \tag{3.57}$$

with

$$X = \frac{1}{B_{gmax}} + \frac{d_g}{NPP\phi_{\oslash}} \tag{3.58}$$

and

$$M = 1 - \phi_{\oslash} \tag{3.59}$$

The initial green leaves, root and death standing biomass are represented by B_{go}, B_{ro} and B_{do} respectively.

In addition to the previous formulation for growth and death of the plants, the following processes are considered.

1. Respiration. Grass respiration rate, R [$\frac{gDM}{m^2 yr}$], is proportional to the amount of vegetation and temperature. It is represented in the following way, after *Sitch et al.* [2003]

$$R = R_{10} \frac{B_g}{cn} g_{T_a} \tag{3.60}$$

where R_{10} is a factor that relates respiration to biomass and the carbon to nitrogen ratio cn at 10^oC, and g_{T_a} is a function that takes into account the variability of respiration due to air temperature, and is given by

$$g_{T_a} = e^{308.56\left(\frac{1}{56.02} - \frac{1}{T_a + 46.02}\right)} \tag{3.61}$$

where T_a is air temperature in degrees celsius. If $T_a = 10$, then $g_{T_a} = 1$.

In this work daily air temperature is assumed to follow the yearly cycle of the solar forcing, similar to the way in which PET is calculated with equations (3.1) and (3.2). First, air temperature above a flat surface T_{ao} is estimated as

$$T_{ao} = \left(\frac{T_{amax} - T_{amin}}{2}\right) \cos\left[2\pi\left(\frac{JDay - L_{T_a} - 365/2}{365}\right)\right] + \overline{T_a} \tag{3.62}$$

where T_{amax}, T_{amin} and $\overline{T_a}$ are the maximum, minimum and mean daily air temperatures throughout a year. Once T_{ao} is known, T_a above each inclined surface element is calculated by

$$T_a = T_{ao}\frac{inso_i}{inso_o} \tag{3.63}$$

The carbon equivalent of the biomass consumed by respiration is subtracted from the NPP, at each vegetation update calculation, before that NPP is allocated to the grass biomass pools.

2. Stress due to soil moisture. Vegetation is stressed when the available water does not supply their needs because they begin to lose turgor, close their stomata to prevent further loss of water, and lose their ability to photosynthesize. In the present modeling approach, after a prolonged period of stress (following *Williams and Albertson* [2005]) the death rate of green biomass d_g doubles. A 30 day average of the instantaneous water stress $\langle\xi\rangle_{30}$ is computed and compared to a threshold 30 day averaged stress $\langle\xi\rangle^*_{30}$. If the threshold is exceeded, d_g doubles, until $\langle\xi\rangle_{30}$ becomes smaller than $\langle\xi\rangle^*_{30}$. The instantaneous water stress ξ is computed as follows [*Laio et al.*, 2001a]

$$\xi(s) = \begin{cases} 0 & \text{for } s \geq s_* \\ \left[\frac{s_* - s}{s_* - s_w}\right]^2 & \text{for } s_w < s < s_* \\ 1 & \text{for } s \leq s_w \end{cases} \tag{3.64}$$

The link between water stress $\langle\xi\rangle_{30}$ and d_g is mathematically expressed by

$$d_g = \begin{cases} d_{go} & \text{for } \langle\xi_{30}\rangle \leq \langle\xi\rangle^*_{30} \\ 2d_{go} & \text{for } \langle\xi\rangle_{30} > \langle\xi\rangle^*_{30} \end{cases} \tag{3.65}$$

where d_{go} is the original death rate or rate of senescence of the green leaves.

The death rate for roots d_r is assumed to remain constant.

3. Leave "flush". Grass grows very rapidly when the first rains fall after a long period of drought. Given that at the arrival of those first rains the green biomass is negligible, the growth is only possible due to the "flush" of stored carbon from the roots to the leaves. Adopting a mechanism of flush from the carbon pool to

the green leaves pool is required to represent such rapid growth with the arrival of the first rainfalls. In the study sites these rainfalls correspond to the North American Monsoon, which brings convective type rain to the whole American Southwest in the summer, usually beginning in July and lasting roughly three months. In some years, flush also takes place during the spring if the amount of moisture stored in the soil is significant. Spring flush, however, is of a lower magnitude than that taking place during the monsoon.

The leave flush, LF, is allowed to occur only when the following four conditions are met, following *Williams and Albertson* [2005]

$$\begin{aligned} &\beta_{wp} > \beta^*_{wp} \\ &B_g > 0.5 B_{gmax} \\ &0.2 < y_{\oslash} < 0.75 \\ &\frac{B_r}{B_g} > 1 \end{aligned} \tag{3.66}$$

The first condition makes sure that enough water is available to the plant. β_{wp} is a parameter used to describe the water available to plants in the ecohydrology literature. β^*_{wp} is a threshold value below of which the plant is water stressed. The mathematical expression for β_{wp} is

$$\beta_{wp}(s) = \begin{cases} 1 & \text{for } s \geq s_* \\ \frac{s - s_w}{s_* - s_w} & \text{for } s_w < s < s_* \\ 0 & \text{for } s \leq s_w \end{cases} \tag{3.67}$$

The second condition limits the leaf flush to 50% of B_{gmax}. The third condition limits the time when leaf flush is possible. The fourth condition limits the leaf flush to the ratio between root biomass and green leaves biomass. Leaf flush only occurs as long as the pool of carbon in the roots is larger than that in the leaves. Furthermore, leaf flush is limited by the amount of root biomass, it is actually proportional to root biomass, and temperature [*Nouvellon et al.*, 2000]. In the simulations presented in Chapter 4, the root biomass and temperature dependence are represent with

$$LF = lff \; B_r \left(\frac{T_{ao} - T_{amin}}{T_{max} - T_{amin}} \right)^2 \tag{3.68}$$

where lff is the leaf flush factor, and the term in the parenthesis is a factor that makes leaf flush maximum during the summer and minimum in spring. In Chapter 5, translocation is assumed temperature dependent with $Q_{10} = 3$ [*Nouvellon et al.*, 2000], so that

$$LF = lff \; B_r \; 3^{\frac{T-25}{10}} \tag{3.69}$$

In both equations, leaf flush increases with temperature. Several sources have proposed values for the leaf flush factor and some examples are provided in Table 3.6 (e.g, *Montaldo et al.* [2005]; *Williams and Albertson* [2005]; *Nouvellon et al.* [2000]).

Table 3.6: Parameters for the vegetation model from various sources

Variable		A	B	C	D	E	Notes
d_g	$[1/year]$	8.76	2.336	2.71 - 51.1		8.76	a
d_r	$[1/year]$	0.63875	1.825	0.2847		0.63875* 0.2847**	
d_d	$[1/year]$		36.5			36.5	
lff	$[1/year]$	18.25	1.825	1.825		18.25* 1.825**	b
B_{max}	$[kgDM/m^2]$	0.2				0.2	
WUE	$[kgDM/kgH_2O]$			0.00393-0.00437		0.00275* 0.005**	c
$\langle\xi\rangle_{30}^*$		0.8				0.8	
β_{wp}^*		0.7				0.7	
R_{10}	$[\frac{gC}{gNyear}]$				24.09	24.09	
cn					29	29	
T_{vmin}	$[°C]$		-2	7		-2	d
T_{vmax}	$[°C]$		30	n/a		30	d
T_{vopt}	$[°C]$		18	38		18	d

References: A. *Williams and Albertson* [2005]; B. *Montaldo et al.* [2005]; C. *Nouvellon et al.* [2000]; D. *Sitch et al.* [2003]; E. This work

Notes: a) the values of d_g vary from old grass leaves to younger grass leaves; b) in *Montaldo et al.* [2005], different values of lff are used without any explanation, once 1.825 and another time 18.25; c) the lower value correspond to an estimation on an annual basis, the higher value to an estimation on a growing season basis. Values of 0.013 to 0.015 have been measured in the field, and values of 0.016-0.017 on single leaves, according to *Scholes and Walker* [1993]; d) *Montaldo et al.* [2005] and *Nouvellon et al.* [2000] use different models for temperature stress. * Chapter 4; ** Chapter 5.

4. Translocation of carbon from leaves to roots Grasses require certain amount of root biomass to support the above ground biomass. This requirement can be expressed as the root to shoot ratio, r_x. It is higher in water and nutrient limited environments. When the r_x is not satisfied, that is, $R_x > \frac{B_r}{B}$, translocation from the leaves to the roots takes place at each modeling time step [*Nouvellon et al.*, 2000]. This is expressed mathematically as

$$r_f = \frac{r_x B - B_r}{1 + r_x} \tag{3.70}$$

In this work r_x is assumed 1.

5. Stress due to temperature. Plants have adapted to function optimally at certain temperature ranges. Higher or lower temperatures can decrease their functionality and even damage and kill them. Several functions to capture stress have been proposed (e.g., *Montaldo et al.* [2005]; *Nouvellon et al.* [2000]). In this work a temperature stress function similar to the instantaneous water stress (3.64) is used. Temperature stress is induced in proportion to a temperature stress factor, Υ, given by

$$\Upsilon = \begin{cases} 0 & \text{for } T_a \leq T_{vmin} \text{ or } T_a > T_{vmax} \\ 1 - \frac{T_{vopt} - T_a}{T_{vopt} - T_{vmin}} & \text{for } T_{vmin} < T_a < T_{vopt} \\ 1 & \text{for } T_{vopt} \leq T_a \leq T_{vmax} \end{cases} \tag{3.71}$$

where T_{vmin}, T_{vmax} and T_{vopt} are the minimum, maximum and optimal temperature thresholds for grass functioning. Examples of proposed values for these parameters are given in Table 3.6

Equation (3.71) sets thresholds of optimum, maximum and minimum "operational" temperatures for the grass represented in CHILD. These thresholds are seldom exceeded by the daily air temperature T_a. However, they are often exceeded by the hourly air temperatures. Furthermore, by simulating the evolution of vegetation in CHILD at an hourly scale, with observed hourly temperatures, we observed that the temperature stress described by (3.71) affects the distribution of grass in space. Less grass biomass grows on south-facing terrain due to the effect of the temperature stress than in north-facing terrain. Such effect in the spatial distribution of grass does is not visible when simulations are carried out at a daily time step with observed daily temperatures or simulated temperatures (i.e., using equation (3.62)).

In order to capture hourly effects using mean daily temperatures, a relationship is needed between daily values of Υ, Υ_d, and hourly values, Υ_h. Such relationship was found by ploting for each day during a period of nine years, the daily average of Υ_h, estimated with hourly temperature observations (the daily average of Υ_h is Υ_d), against the daily temperature, as shown in Figure 3-6. The temperature data corresponds to the Kendall site, between 1997 and 2006.

From the plot, a relationship between daily temperature and Υ_d was defined as follows:

$$\Upsilon_d = \begin{cases} 0 & \text{for } T_a \leq -2° \\ (T_a + 2)\frac{0.8}{16} & \text{for } -2° < T_a \leq 14° \\ (T_a - 14)\frac{0.2}{7} & \text{for } 14° < T_a \leq 21° \\ 1 & \text{for } 21° < T_a \leq 23° \\ (T_a - 23)\frac{-0.5}{7} + 1 & \text{for } 23° < T_a \end{cases} \tag{3.72}$$

We use this expression in CHILD.

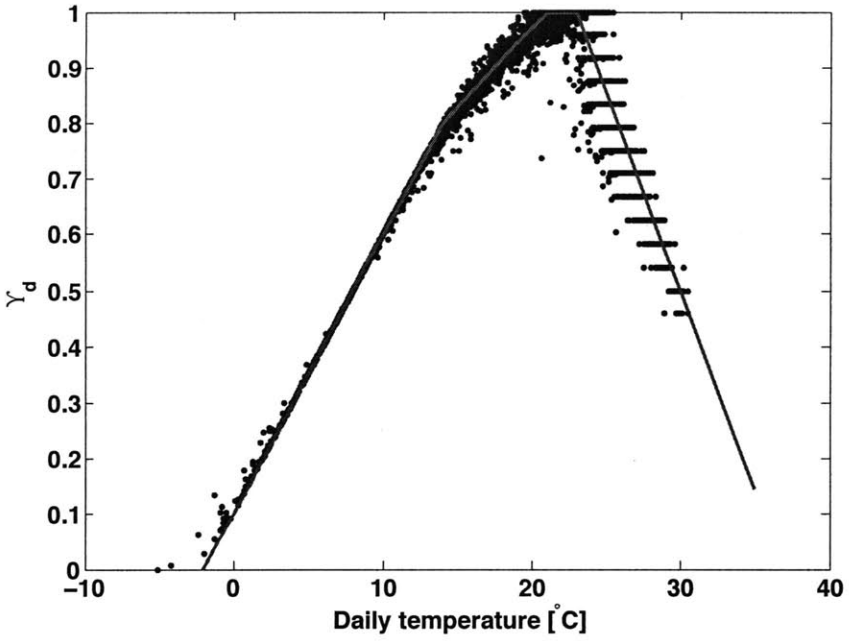

Figure 3-6: Daily average of Υ_h, Υ_d, as a function of daily temperature. Hourly temperature data used corresponds to the Kendall site, between 1997 and 2007.

Given the above five modifications, the equation for NPP (3.50) maybe rewritten as

$$NPP = T\Delta t\ WUE\rho_w\Upsilon_d - R \tag{3.73}$$

The leaf flush factor and leaves to roots translocation are accounted for calculated after the vegetation has been updated based on the NPP alone, using equations (3.55), (3.56), (3.65) and (3.73).

3.5.4 A coupled model

The coupling among the system elements represented in the model represent the dynamic interaction between vegetation and soil moisture. In addition to providing a tool for the study of the bi-directional interactions between topography and vegetation, this coupled model addresses the importance of linking of vegetation dynamics, soil water storage, and precipitation, which can have large implications in both, water recharge and vegetation productivity, as *Newman et al.* [2006] suggest. The next Chapter shows how the vegetation and soil moisture dynamics components of the model compare to observations.

CHAPTER 4 | TEMPORAL AND SPATIAL DYNAMICS OF GRASS IN SEMIARID ENVIRONMENTS

4.1 Introduction

Grasslands generally have mean annual precipitation between 150 to 1200 mm, have a wet and a dry season, usually with rains coinciding with the warmest time of the year, and mean annual temperatures between 0 and 25 °C. In this type of landscape, disturbances to the vegetation, mainly by fire or grazing, in addition to drought, prevent woody vegetation establishment. The distribution of grasslands in the planet is dictated mainly by climate. Along a precipitation gradient, grasslands are located between forests and deserts. Temperature indirectly modulates water demand and consequently water availability. Increases in temperature result in increases in evaporation and transpiration; as a result, for a similar precipitation regime, water availability for vegetation consumption decreases [*Sala et al.*, 2001].

Grasslands are water limited ecosystems where productivity and biodiversity generally increase with water availability. In grasslands where precipitation exceeds 500 mm per year, nutrients and light become limiting factors for productivity [*Gibson*, 2009]. Given that water is the main limiting factor in the grasslands studied in this work (rainfall is between 250 and 350 mm per year), the link between moisture availability, biomass productivity, and the dynamics of these two variables in the landscape system are discussed in this chapter.

4.1.1 Factors affecting the moisture and vegetation dynamics of grasslands

Climate

The interplay between rainfall and evaporative demand determine the available moisture on a grassland system, and consequently its productivity. These two weather

characteristics are variable in time. Evaporative demand follows the solar forcing, is relatively constant from year to year, is maximum during summer and minimum in winter. Rainfall is significantly different across seasons and from year to year. The superposition of maximum rain and evaporative demand, which is frequently observed at grasslands, is advantageous for grass growth for two reasons. First, grasses are able to have a dormant and active state that allows them to assimilate carbon from the onset of the rainy hot season, and remain inactive the rest of the year. Second, they have extensive shallow root systems that allow them to absorb moisture in the top most soil layers. Other plant functional types (PFT) with root systems in deeper layers usually do not do well in the hot rainy season because most of the water remains close to the surface where it quickly evaporates, if not absorbed by grass roots. Precipitation that occurs during the period of minimum evaporative demand infiltrates deeper into the ground. This creates a source of moisture for deeper rooted plant functional types such as woody species.

In grasslands inter-annual variations of rainfall often lead to sequences of dry or wet years, periods in which vegetation productivity decreases or increases accordingly. Annual variability increases with decreasing mean annual precipitation (MAP) [*Knapp and Seastedt*, 1998]; the regional amplitude of the variability of productivity decreases with increasing MAP.

Soils

The interplay between soil texture and climate control moisture available to plants by controlling how much and how deep moisture infiltrates, and by setting the percentage of soil moisture losses from the root zone due to leakage, evaporation, and transpiration.

In grasslands with more than 370 mm or rainfall per year, the mayor losses of water are due to leakage and the magnitude of the loss decreases with water-holding capacity. In drier grasslands, however, precipitation rarely penetrates deep into the ground and the mayor losses of water are due to evaporation, which increases with increasing water holding capacity. As a consequence, productivity increases with water-holding capacity (or finer textured soils) in 'wet' grasslands, and decreases with water-holding capacity (or finer textured soils) in drier grasslands [*Sala*, 2001].

Water penetrates deeper into coarse-textured soils than in fine-textured soils, and when rain falls in the cool season of the year. Deeper penetration of the moisture reduces losses by evaporation. This is convenient for vegetation in semi-arid regions, including grasslands. However, if soil's texture is too coarse, water may be lost to leakage or may be available only to deep rooted woody vegetation. When soil is fine-textured or when rain falls in the hottest time of the year, moisture remains close to the surface, and is thus available only to shallow rooted vegetation such as grasses before it evaporates. Because of this, fine textured soil, together with a rainy season that overlaps with the hottest time of the year, favors grasses over woody vegetation [*Sala et al.*, 2001].

Another characteristic of the soil that affects water storage is the soil depth, because it sets the size of the store of moisture. This results in limited productivity in regions of shallow soils. These regions are generally close to watershed divides, or in zones of frequent erosion such as steep terrain or channels.

One last soil characteristic related to moisture and vegetation dynamic in the soil is its organic content, because soil hydrologic properties are modified by organic material. Usually more organic material results in higher infiltration rates and porosity, augmenting moisture availability to plants.

Vegetation

Grasslands are communities of vegetation composed of several PFTs (grasses, shrubs, herbs, and succulents) and different species adapted to a diverse set of environmental conditions including light, temperature, nutrients, and moisture. Growing rates, death rates, and sensitivity to environmental factors differ among PFTs and species, and so do the associated biomass dynamics. Significant differences in species compositions are observed as environmental conditions change in space and in time. An example of spatial differences is that observed along a latitudinal gradient in the USA central plains. C3 grass species dominate the colder northern part of the great plains, where as C4 grass species, adapted to warmer temperatures, dominate the southwestern region of the plains. Temporal differentiation in species is more subtle. An example is the increase in the percentage of drought tolerant species in a grassland community after several years of drought, and its decrease after a sequence of wet years [*Gibson*, 2009].

Grasses may be annual, biennial, perennial or other. These differences affect their dynamics. Perennial species current state has an effect on the next year's carbon assimilation of the individual, in contrast to the ephemeral nature of annuals. Perennial grasses develop significant root components (or below ground biomass (BG)) that store carbohydrates often used as building material for the above ground (AG) biomass (or shoots and leaves) in subsequent years. They may also simply facilitate effective moisture absortion [*Oesterheld et al.*, 2001]. The above makes the AG biomass dependent on the BG biomass state. At the same time, BG biomass is dependent on the AG state, given that all carbon assimilation through photosynthesis is a function of the AG biomass. The growth and death rates of the AG biomass are larger than those of the BG biomass. This difference in dynamics, plus the interplay between roots and shoots in their dynamics, warrant a differentiation between the two in the study of vegetation dynamics.

Often, the BG biomass is neglected in vegetation dynamics studies. However it is a very important component of the system in grasslands, and more so the more arid the grassland. BG biomass is generally more than twice the AG biomass, and allocation of assimilated carbon to the roots increases with dry and cold conditions [*Gibson*, 2009].

Other factors

Two factors that are often overlooked when considering the distribution of grasslands as a function of climatic variables are fires and grazing. These two disturbances often contribute to the predominance of grasses over woody vegetation (particularly for mean annual rainfall above 650 mm per year [*Gibson*, 2009]). Long-term experiments in the Konza Prairie where fire and grazing have been suppressed illustrate such woody encroachment [*Briggs et al.*, 1998]. Many grasslands are maintained without the intervention of humans by fires that result from dry and hot conditions prior to the arrival of summer rainfall, and to grazing of wild roamers. Other grasslands are maintained by agricultural activities.

The form of the land surface is another factor that can change the local conditions enough to be reflected in the composition of species or in vegetation productivity. Generally higher elevations are cooler and have more precipitation due to the orographic effect on rainfall, resulting in more moisture available for vegetation. Valley bottoms and hollows hold deeper soils and more moisture, favoring ecosystem productivity, and sometimes resulting in woody vegetation establishment. Aspect also plays a role in grassland productivity, having an effect similar to that of elevation changes: southfacing terrain receives more solar radiation than northfacing terrain, resulting in less moisture availability in terrain facing south, and more moisture availability in terrain facing north.

Light and nutrients may become limiting factors for grassland productivity in regions where mean annual precipitation is above 500 mm per year [*Gibson*, 2009]. *Knapp et al.* [1998] illustrate how light becomes a limiting factor in a tall grass prairie (Konza, with 800 mm of rainfall per year); after a long period without a fire, old long blades of grasses prevent light from reaching young productive leaves. Following the removal of old grass blades during a fire, light is no longer a limiting factor and grass grows substantially. But then, due to the intake of nitrogen by the grass during the period of fast growth, the soil is depleted of nitrogen and nitrogen becomes the limiting factor for growth. In this example, if fires occur on an annual basis, the grassland is nitrogen limited; instead, if fires occur once every several years, the system is light limited. Such limitations do not apply to our study area.

4.1.2 Grassland dynamics under the semi-arid American Southwest climate

Grasslands in the American Southwest share a common climate. Mean annual precipitation is below 370 mm per year, and is characterized by light rain during the fall and winter, resulting from cold fronts that bring moisture from the Pacific, a dry season during the spring, and the North American Monsoon in the summer, which begins in July and lasts until September, and produces more than 50 percent of the yearly precipitation. Inter-annual winter and monsoon precipitation variability are large and independent of each other. Winter precipitation increases during El Niño

years, and decreases during La Niña years. These fluctuations contribute to the total inter-annual precipitation variability, however, given the significant portion of the annual rainfall contributed by the monsoon rains, annual rainfall is not determined by the El Niño/La Niña phenomenon.

Winter/Fall rainfall is uniform in space, resulting in a uniform growth during spring if sufficient moisture is available when the spring growing season begins. During spring, rainfall is rare, thus, a dry down and biomass reduction follows the spring growth. By the end of the spring, prior to the monsoon rains, temperature is high and conditions very dry. With the onset of the monsoon rains in July, AG biomass rapidly increases. This second growing period leads to a second vegetation peak (or the only vegetation peak in years with little winter precipitation). Monsoon rainfall consists of small-scale convective storms with high-intensity short-duration characteristics that distribute unevenly water across the landscape. This uneven distribution is reflected in the vegetation growth. Various researchers have reported the dynamics discussed above. They have based their studies on NDVI calculations derived from various satellite images [*Pennington and Collins*, 2007; *Weiss et al.*, 2004]. The following section discusses measurements and remotely sensed data from the Kendall site (described in Chapter 2) that sheds light on its vegetation and moisture dynamics.

4.2 Meteorological, soil moisture, soil properties, and NDVI data

Metereological observations betweeen 1997 and 2005, including rainfall, temperature and evapotranspiration; soil moisture measurements between 1990 and 2007 at various depths; runoff measurements of a small subwatershed at Kendall between 1999 and 2008 [*Keefer et al.*, 2008; *Stone et al.*, 2008]; and NDVI data from MODIS between 2000 and 2006 (USGS' Land Processes Distributed Active Archive Center(https://lpdaac.usgs.gov/)) are analyzed to study the moisture and vegetation dynamics of the Kendall site. The NDVI data corresponds to the averaged NDVI inside a square area of approximately 4 km to the side that surrounds the Kendall site (Figure 4-1). This average is assumed representative of the mean NDVI of the vegetation dynamics at Kendall. This wealth of information is synthesized in Table 4.1 and presented graphically in Figures 4-2, 4-3, 4-4, and 4-5.

These images show the information averaged to 1 day intervals except for the NDVI. Moisture data is only presented for the 5 cm depth. Figure 4-2 clearly shows the yearly fluctuation of temperature, the peak of precipitation during the monsoon every year, and the synchrony between rainfall, temperature, and evapotranspiration during the summer. By comparing the evapotranspiration data and NDVI data (Fig. 4-5), a correlation between the two becomes apparent, indicating high photosynthetic activity resulting from the monsoon rains, which is a combination not only of the available mositure, but also of the solar forcing (reflected in temperature).

Table 4.1: Meteorological, soil moisture and NDVI data sets

	Time period	Resolution	Location	Instrument	Measurement depth [cm]
Temperature	1997-2005	20 min	KENMet		
Precipitation	1997-2005	20 min	KENMet	rain gage	
Evapotranspiration	1997-2005	20 min	KENMet		
Moisture 1	1996-2001	20 min	KENMet	electric resistance	5
Moisture 2	2001-2007	20 min	KENMet	delta T theta probe	5, 15
Moisture 3	1990-1998	various (days)	KSTrench	TDR	5, 10, 15, 20, 30, 50
Moisture 4	1990-1998	various (days)	KNTrench	TDR	5, 10, 15, 20, 30, 50
Moisture 5	2004-2007	20 min	TDRK1	TDR	5, 15, 30, 50, 75, 100, 200
Runoff	1999-2008	daily	Flume 112	V notch weir	
NDVI	2000-2006	16 days, 250 m	Kendall	MODIS Terra	

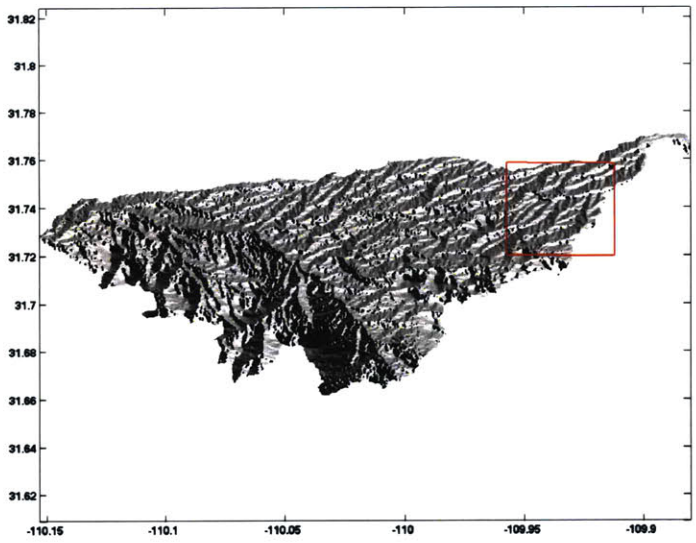

Figure 4-1: The red square is the area within the WGEW considered in the estimation of the NDVI time series presented in Figure 4-5.

In most years moisture is available during the late fall and winter, however, evapotranspiration and NDVI are low probably due to the dormancy of vegetation and low solar forcing (thus low evaporative demand). The annual variability of the solar forcing, reflected in temperature in this semiarid setting, is shown in detail for 1999 in Figure 4-6, that shows the minimum and maximum temperatures observed each day during that year (this figure also shows how the representation of temperature in our model compares to measurements; our model is described in Chapter 3). The coincidence of the largest proportion of annual rainfall, photosynthetic activity, and peak temperatures is characteristic of grassland ecosystems.

In the Kendall grassland some species exhibit spring growth. The signal of the spring growth is not as clear as the monsoon growth every year, but it is significant in years with particular high winter moisture (due to late fall/winter precipitation higher than average), such as 2001 and 2004, as the rainfall records and NDVI signal show (See red ellipses in Figs. 4-2 and 4-5).

Differences in rainfall are difficult to distinguish in Figure 4-2, nevertheless less precipitation in 2002 and more precipitation in 2000 is evident. This is clearer in Figure 4-7 that shows the annual precipitation for the Kendall site and at another research station within the WGEW a few kilometers east of Kendall. The differences in annual precipitation from year to year, and between the two locations just 5 km away, are significant.

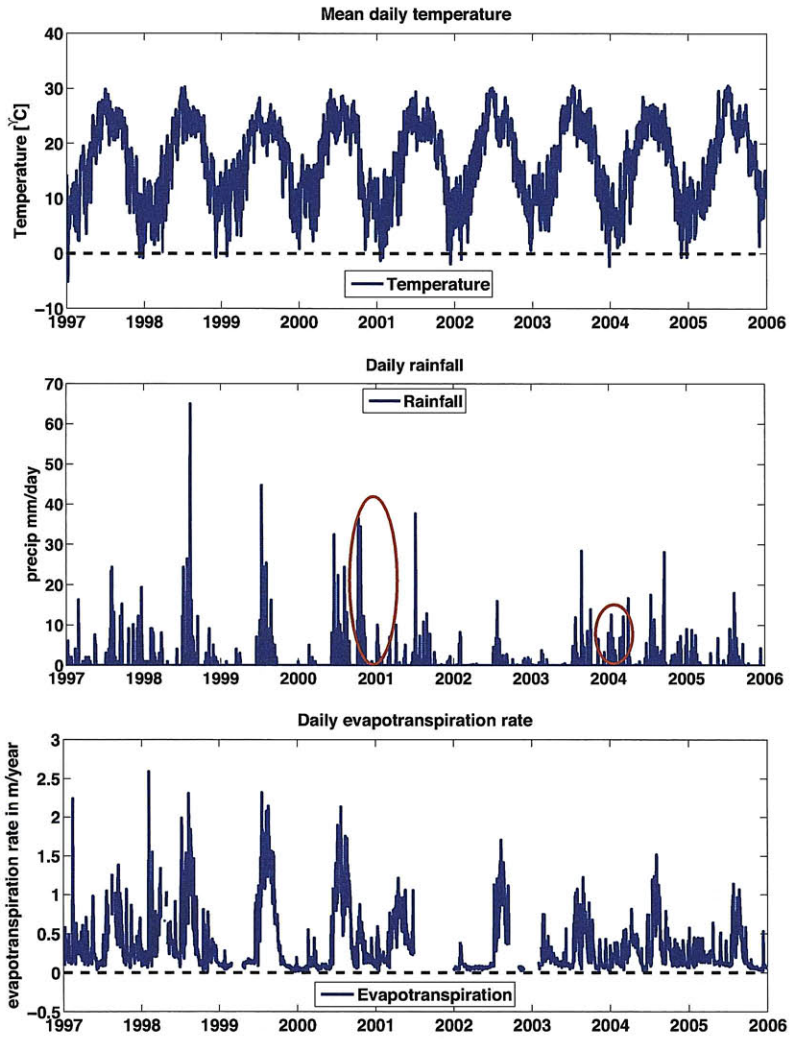

Figure 4-2: Measurements at the Kendall meteorological station, 1997-2006

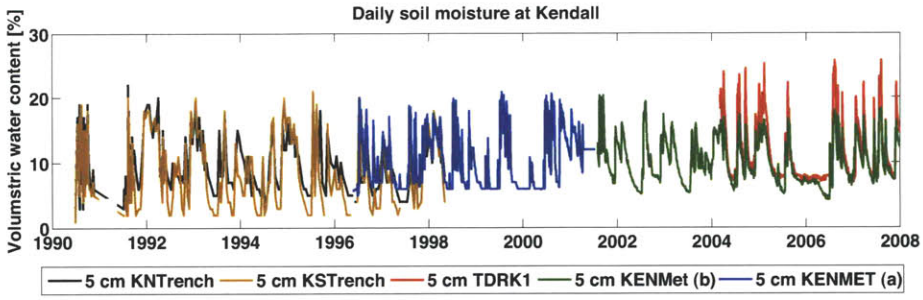

Figure 4-3: Moisture measurements at 5 cm, 1990-2007

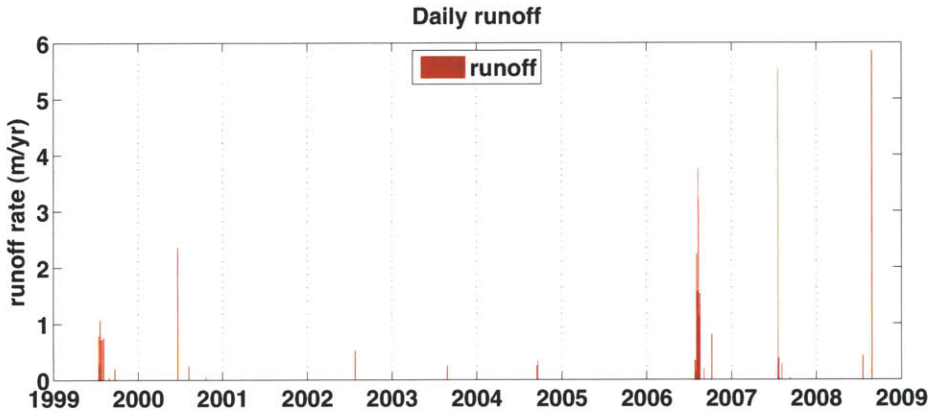

Figure 4-4: Runoff at subwatershed 112 of WGEW, 1999-2008

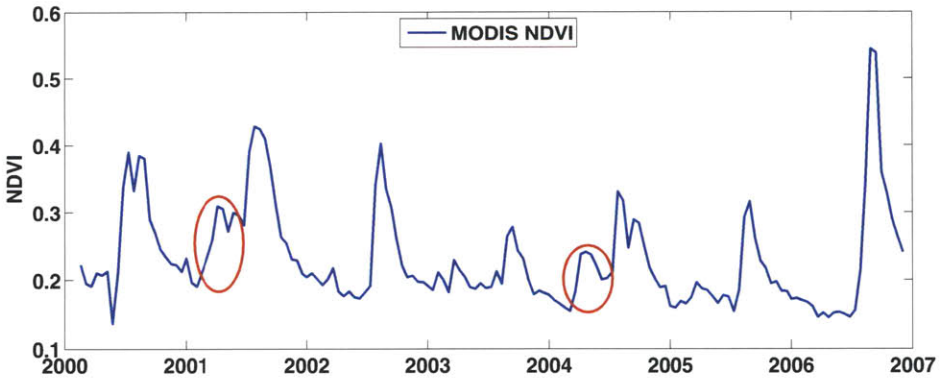

Figure 4-5: NDVI from MODIS Terra, 2000-2006

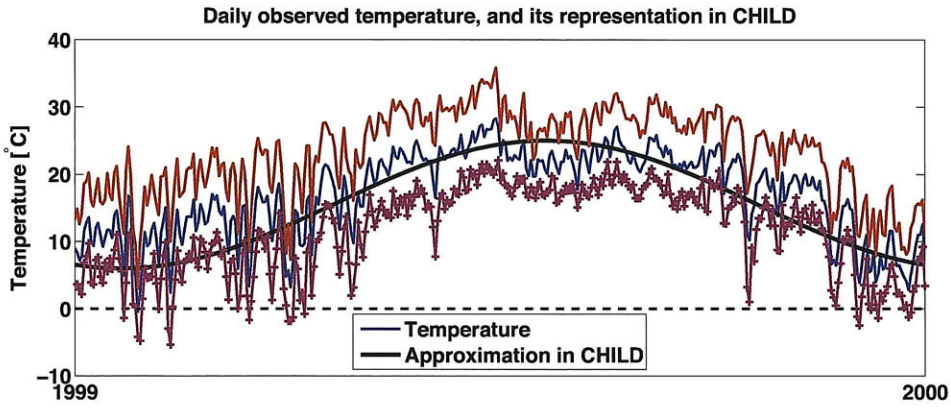

Figure 4-6: Minimum (pink) and maximum (red) temperatures during each day of 1999 at Kendall. A blue line represents the mean daily temperature, and a black line the representation of daily temperature used in CHILD.

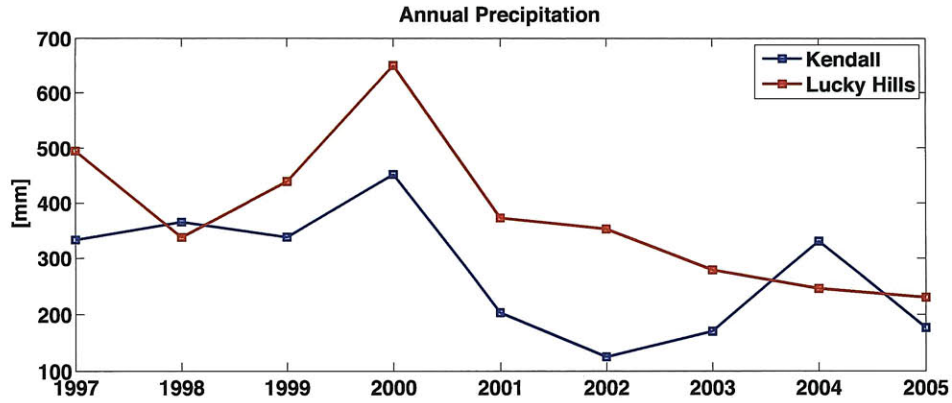

Figure 4-7: Annual precipitation at Kendall and Lucky Hills, WGEW, 1997-2005

Moisture dynamics and soil texture

Moisture dynamics are not uniform in space. They are affected by the form of the terrain and soil texture (and other soil properties): variations in the solar incidence angle make evapotranspiration rates faster where the terrain faces more directly the sun; lateral fluxes increase with terrain steepness, thus gently sloping terrain retains moisture longer; water flows from ridges to hollows and valleys, making the latter moister than ridges; and finally texture (and other soil properties) in combination with climate modulate the fluxes of moisture along the soil column as discussed in Section 4.1.1.

Soil properties are not uniform in space either, and they change with depth and relative to the location within a catchment. Hydrologic properties are tightly linked to soil texture [*Cosby et al.*, 1984]. The variability of texture with depth, from two locations at the Kendall site, are used to infer the effect of soil texture properties and their variability with depth on moisture dynamics. Two soil pits were dug at the Kendall site in a north facing hillslope [*Scott et al.*, 2000] and at a ridge [*Emmerich*, 2008], next to the location of the moisture measurements KNTrench and KENMet, respectively, as shown schematically in Figure 4-8. This figure also shows location of the other soil moisture measurements discussed in this section along a cross section of a small catchment in the Kendall site. The texture and gravel content (or coarse fraction by weight) for various soil layers in these pits were estimated. The data is given in Table 4.2, and the texture classification for each layer is presented graphically in Figure 4-9.

Figure 4-9 shows the changes in texture with depth, as well as the position with depth of moisture measurements at KNTrench, KSTrench and KENMet. The differences in texture with depth are reflected in the moisture measurements at various depths, as is discussed below. Figure 4-9 also shows the position within a texture classification triangle of each soil layer in each of the two soil pits. In the texture triangles the color of the points indicates the soil layer it represents. This shows that the soil at Kendall is more than 40 percent sand, with some clay content varying between 10 and 35 percent clay, and between 10 and 35 percent silt. Moreover, it shows how clay content peaks at about 15 cm in depth, making soil at that depth less permeable and more absorbent of water. High clay content layers are colored pink in the figure.

Some of the effects of land surface form are reflected in the measurements of moisture at Kendall. First, soil losses, most likely due to evapotranspiration, are faster in the south facing terrain where solar radiation is higher than in the north facing terrain. This is evident in the moisture measurements presented in Figure 4-3 (5 cm KNTrench (north facing) vs 5 cm KSTrench (south facing)). Second, a hillslope probably captures flow from the ridge, thus, this might explain the slightly higher moisture measured at the hillslope in (TDRK1) than at the ridge (KENMet (b)), as Figure 4-10 shows. In this figure a faster decrease in moisture in the southfacing hillslope (TDRK1) becomes apparent. This can be due to the steeper slope, or higher solar incidence at the hillslope (TDRK1) than at the ridge (KENMet).

Table 4.2: Summary of soil properties from two soil pits at Kendall

Horizon	Depth [cm]	Clay [%]	Silt [%]	Sand [%]	Coarse fraction by weight [%]
			Pit next to KNTrench		
A	0-4	15.8	16.9	67.3	64
BT1	4-9	28.7	10	61.3	43
BT2	9-16	44.2	13.2	42.6	44
BT3	16-35	45.9	10.8	43.3	53
BT4	35-62	28.8	14.5	56.7	32
2CK	62-150	11	21.8	67.2	45
			Pit next to KENMet		
A	0-5	23.5	9.3	67.2	37
BW1	5-13	32.1	12.7	55.2	56
BW2	13-25	36.1	13.3	50.5	40
2BK1	25-43	26.8	17.3	55.9	24
2BK2	43-56	19.5	21.3	59.2	5
2CK1	56-75	18.8	26.0	55.2	17
2CK	75-102	16.8	27.3	55.9	10
2C1	100-145	10.8	21.3	67.9	12
2C2	145-225	10.1	17.3	72.5	36
2C3	225-255	8.8	12.7	78.5	38

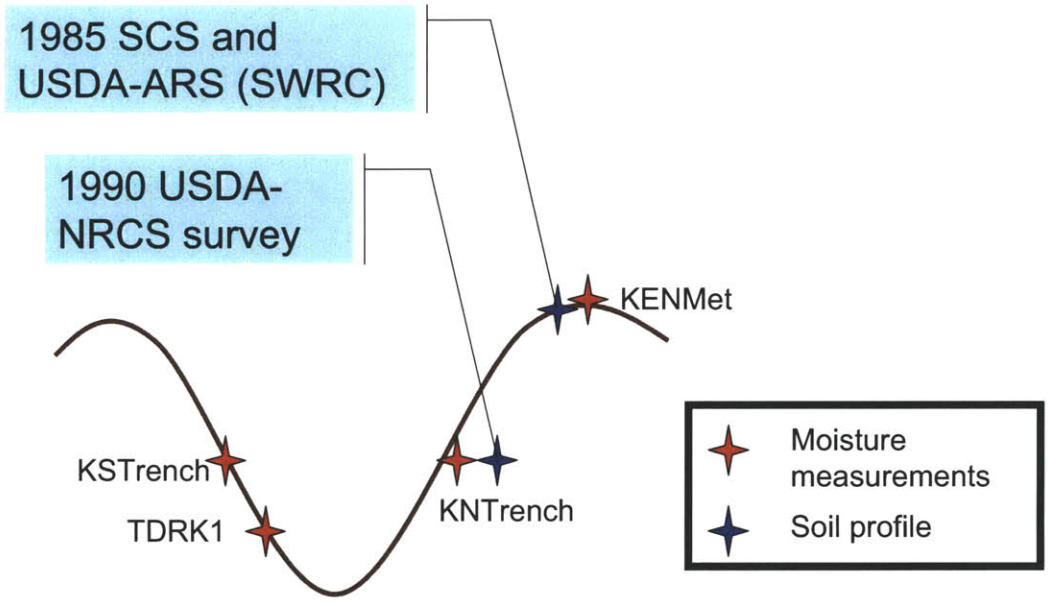

Figure 4-8: Location of the moisture measurements and soil sampling sites at Kendall. The figure schematically represents a cross section of a small catchment in the Kendall site, with the north facing hillslope on the right side of the figure and the south facing hillslope on the left.

Soil measurements at different depths (as an example, measurements for the KN-Trench and KSTrench are provided in Figure 4-11) show the effects of soil texture in the moisture holding capacity. The maximum and minimum volumetric soil moisture measurements consistently increase with depth, between 0 and 20 cm, in agreement with the increase in clay and decrease in coarse fraction by weight. This figure also shows how rainfall rarely reaches the 30 and 50 cm depths during the monsoon, and how moisture reaches these layers more frequently during the winter.

From the moisture measurements and soil information the following can be concluded: a) the high coarse fraction percentage in the soil reduces the pore space in the soil, given that gravel is non-porous, thus the soil's water store capacity is reduced; b) the top layer of sandy loam, with a high saturated hydraulic conductivity (K_s), allows the easy infiltration of rain; c) the clayey layer beneath the sandy loam reduces leakage; and d) less moisture evaporates from the sandy loam layer than it would if it were a clayey layer. The latter three conclusions (b, c and d) indicate that the top 15 cm of soil at Kendall are a favorable soil layer for root development, where moisture availability for vegetation is high relatively to other layers. Measurements show that about 80 percent of the grass roots are in this layer (Figure 4-12).

Despite the decrease in hydraulic conductivity associated with the increase in clay content, moisture infiltrates through the clayey layers in wet winters and occasionally in during extremely wet monsoons, reaching depths larger than 50 cm. Figures 4-

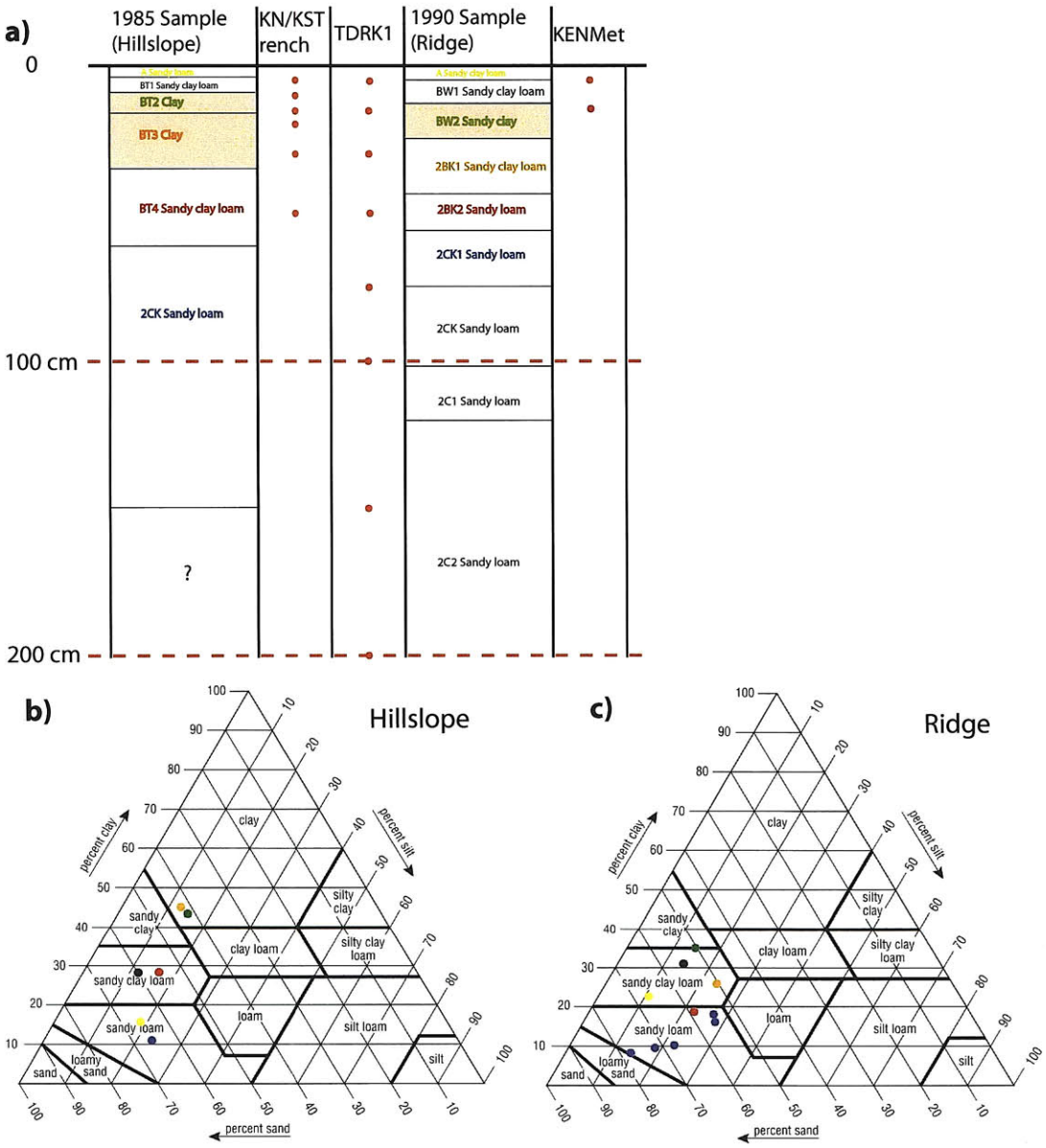

Figure 4-9: Vertical profile of soil at the Kendall site: a) vertical profile of soil texture measured at two soil sampling pits, and location of soil moisture measurements; soil texture corresponding to different depths of the pits in b) the hillslope and c) the ridge is indicated with colored dots in a soil texture classification triangle. Dot colors correspond to colors of layers in a).

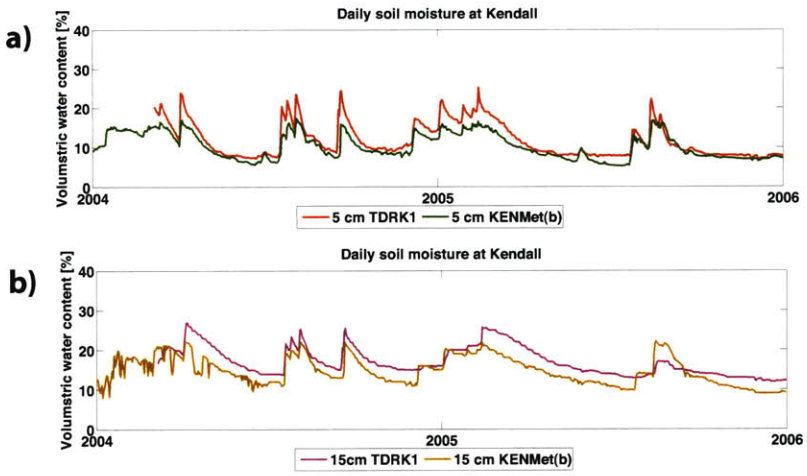

Figure 4-10: Moisture measurements at KENMet and TDRK1 between 2004 and 2005 at (a) 5 and (b) 15 cm depths.

11b and 4-11c show that in the winters 1991/1992, 1992/1993, and 1994/1995, this happened. Moisture in these wet winters is uniform in depth, in both the wetting and drying periods. During the drying period, in early spring, moisture from the clayey layers is likely extracted by roots. Even though the majority of the roots establish at the top of the sandy loam layer, some roots extend up to 90 cm depths (Figure 4-12).

Transpiration is proportional to the amount of above ground biomass cover, and so is the infiltration capacity of the soil. Therefore, the distribution of biomass affects the moisture dynamics, and because the amount of biomass is a function of moisture, a feedback loop between moisture and vegetation is established. The effect of such feedback on the moisture measurements discussed above is not known. If, for example, transpiration is the dominant effect of vegetation in moisture, then vegetation would reduce moisture in the places with more moisture, because more vegetation would establish there. As a consequence, the differences in moisture resulting from the form of the terrain (insolation, slope, drainage area) and soil texture would be reduced. If instead infiltration is the dominant effect, then vegetation would increase moisture in places already moist, amplifying the differences in moisture resulting from the form of the terrain and soil texture. A modeling study by *Caylor et al.* [2006] supports the idea that vegetation reduces moisture, particularly in wetter climates. At Kendall however, correlation between moisture and vegetation is more likely. Vegetation is higher where moisture is expected to be higher, both in north facing hillslopes (that have less exposure to the sun) and in valley bottoms where contributing areas are large and slopes gentle (see Chapter 2 for reference).

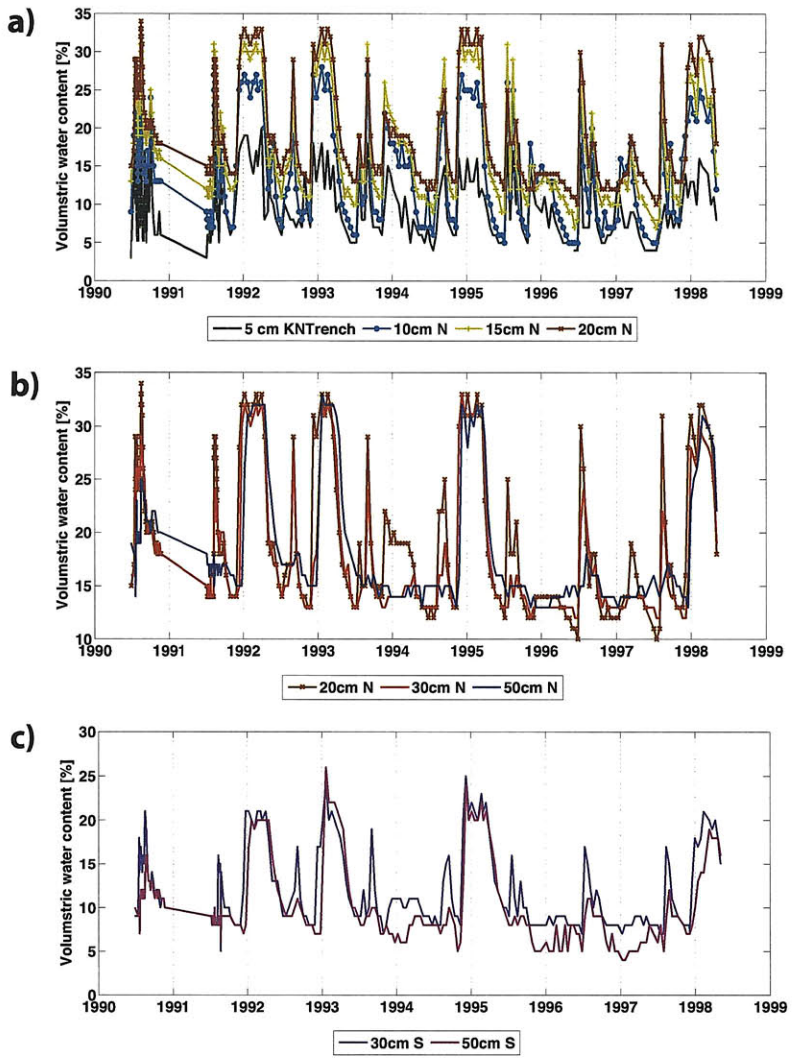

Figure 4-11: Moisture measurements at KNTrench (a and b) and KSTrench (c) at various depths (1991-1999).

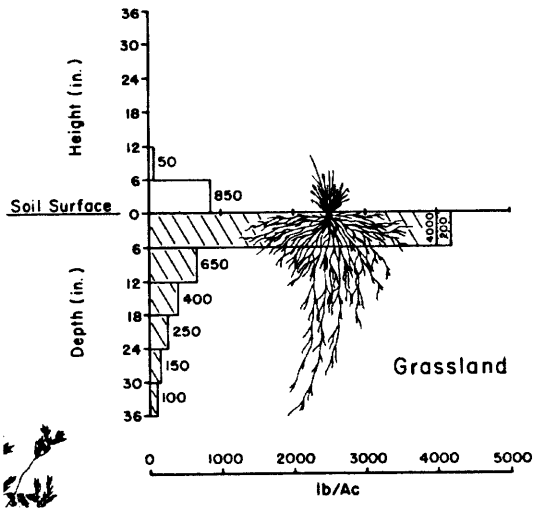

Figure 4-12: Root distribution of grasses measured in the region of study, extracted from *Cox et al.* [1986].

4.3 Simulated time series of soil moisture, grass cover, evaporation and transpiration

With the purpose of evaluating the vegetation and water fluxes dynamics of the model described in Chapter 3, water fluxes and vegetation dynamics are simulated with CHILD over the course of 11 years (1997-2007) at the Kendall site, using daily rainfall observations. In the model the storm duration is set to one hour, the interstorm duration to 23 hours, and the rainfall depth is equal to the total daily precipitation. In this simulation the Barlett-Lewis algorithm is 'turned off'.

The initial topographic template in the simulation is a DEM of the Kendall site with a 30 m resolution *(also used in Chapter 2)* [*Heilman et al.*, 2008], and because in this case the objective of the simulation are not the fluxes of sediments or elevation changes, sediment fluxes, weathering and uplift are 'turned off' by increasing the threshold for erosion to very high values, reducing the weathering rate to a very low value, and setting uplift to zero. In the simulation the root zone is assumed equal to the soil depth, and is equal to 15 cm. As discussed above, about 80 percent of the grass roots at the study site have been measured in the top 15 cm of soil. The rest of the parameters used in this simulation are provided in Tables A.1, A.3, A.4, and A.6.

4.3.1 Estimation of biomass from NDVI

In order to compare the vegetation dynamics of the simulation to the information captured by satellite in the form of the NDVI time series, biomass was estimated assuming that vegetation fractional cover is proportional to the square of NDVI as

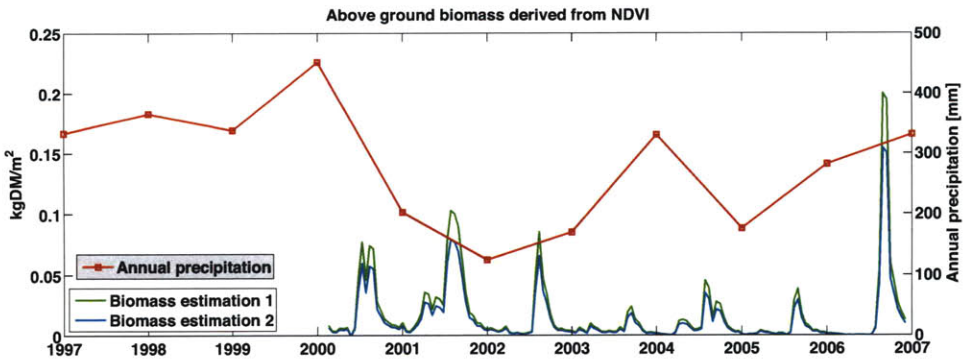

Figure 4-13: Biomass estimated from NDVI at Kendall (2000-2006). The first estimation assumes that the maximum NDVI observed in the period of record corresponds to a full vegetation cover, which is assumed to be 0.2 $kgDM/m^2$. The second estimation assumes that an NDVI of 0.6 corresponds to a full vegetation cover. This figure also shows the total precipitation of each year illustrating that biomass is not directly correlated to annual precipitation.

follows,

$$V = \left(\frac{NDVI - NDVI_0}{NDVI_\infty - NDVI_0} \right)^2 \tag{4.1}$$

and that vegetation fractional cover is proportional to biomass. In the equation above, $NDVI_0$ and $NDVI_\infty$ correspond to the NDVI of bare vegetation and full vegetation respectively [*Montandon and Small*, 2008]. The minimum and maximum values of NDVI registered in the time series maybe assumed $NDVI_0$ and $NDVI_\infty$, respectively. Because NDVI is know to saturate at around 0.6, often $NDVI_\infty$ is assumed to correspond to this value. Calculations assuming both criteria for the NDVI time series at the field site are presented in Figure 4-13 for comparison. Notice how above ground biomass has little correlation with annual rainfall.

4.3.2 Model outputs

Spatially averaged above ground vegetation biomass, evapotranspiration (and each of its components, transpiration and evaporation from bare soil), leakage, runoff, infiltration, and soil moisture of the model for each day of the simulation, and root biomass every 3 months, are provided in Figures 4-14, 4-15 and 4-16. A relatively good agreement between NDVI-derived biomass and the model is observed (Figure 4-14), except in 2006. The model captures the spring growth reflected in the NDVI in 2001 and in 2004, when spring was preceded by fairly wet winters (Figure 4-15). In the model, "spring flush", or the use of carbon stored in the roots for shoot production at the beginning of the growing season, either in spring or during the monsoon, is

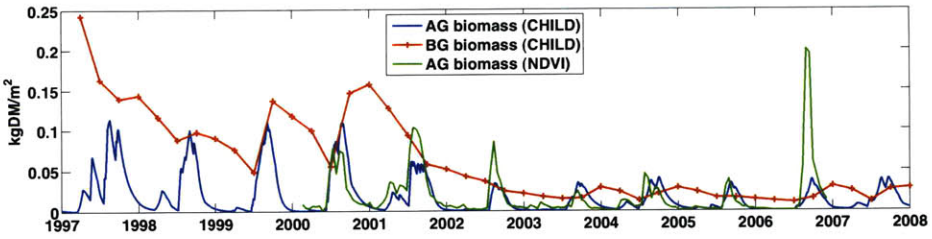

Figure 4-14: Above ground and below ground biomass estimated with the model and that estimated from NDVI.

limited by the root carbon pool, which is low from 2002 on (Figure 4-14). This low value of root carbon, and its effects on leaf flush, are consequence of the parameters used in the simulation which are taken from *Williams and Albertson* [2005]. However, it is likely that those low estimates of the root carbon pool are underestimating the actual amounts, which according to the observations of *Cox et al.* [1986] (Figure 4-12), are more than an order of magnitude higher. Yet, more information about the dynamics of the root carbon pool not available at the moment are required to have a better understanding of their actual dynamics.

Two hypotheses that explain why the model does not capture the spike in vegetation in 2006 are the following. One is that the spike is related to an accumulation of nutrients that took place during the low vegetation growth years between 2003 through 2005, such that during the moist conditions of 2006 vegetation grows at a faster rate than in other years. The second is that the root carbon pool is larger than what the model estimates, and that the leaf flush magnitude is proportional to moisture. During the monsoon of 2006, the soil held more moisture than in the previous 6 monsoons, according to our simulations and observations (Figure 4-15b), and thus it is plausible that the rapid shoot growth in that year at the beginning of the monsoon was related to a particular vigorous leaf flush triggered by extremely moist conditions.

The second hypothesis can be further explored with the help of the current model by making leaf flush proportional to the degree of soil saturation, and by further investigating root carbon dynamics. Exploring this hypothesis is nevertheless outside the scope of this effort.

CHILD represents in a very simple way the soil moisture dynamics. The soil moisture formulation was devised with the objective of incorporating a more realistic representation of vegetation and moisture dynamics into a landscape evolution model, where simulations would evolve the landscape in hundreds or thousands of years. The hydrologic fluxes such as rainfall, infiltration and runoff had been purposely incorporated in simple ways. The current model seems to do well given those objectives and limitations.

CHILD assumes a homogeneous soil up to a depth of 15 cm (assumed the root zone), and it only keeps track of moisture in those 15 cm where moisture, in addition,

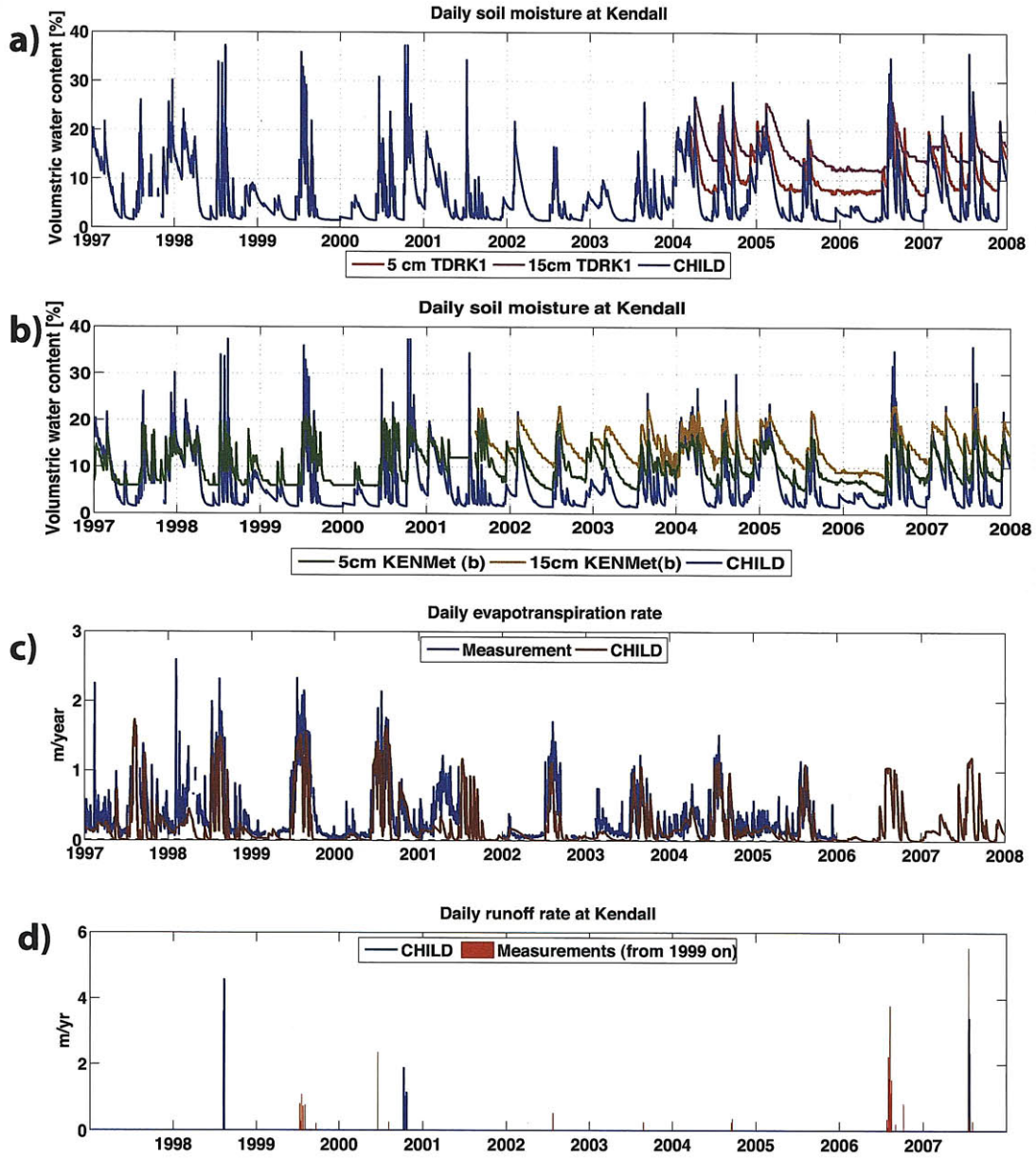

Figure 4-15: Comparison of simulated and measured moisture (measurements at 5 and 15 cm depths from a) TDRK1 (2004-2007) and b) KENMet (1997-2007)), c) evapotranspiration (measurements between 1997 and 2005), and d) runoff (measurements between 1999 and 2007).

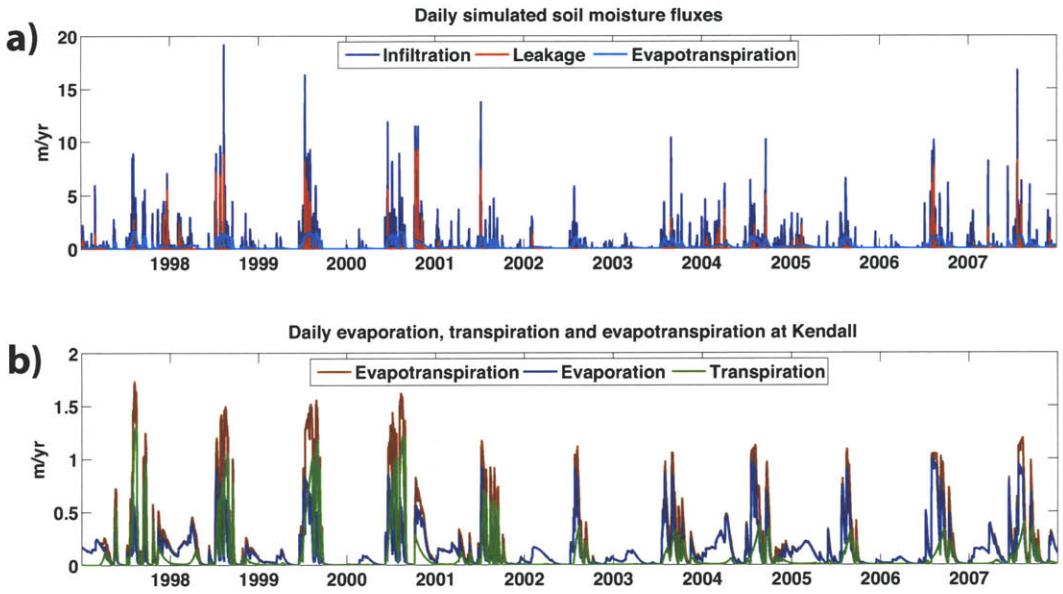

Figure 4-16: Simulated soil moisture fluxes: a) shows infiltration, leakage and evapotranspiration; and b) the two components of evapotranspiration, namely evaporation and transpiration.

is assumed homogeneous throughout its depth. Moisture inputs to the soil are due to infiltration, and outputs due to leakage, evaporation from bare soil, and transpiration. In the model leakage is a function of moisture, and evaporation and transpiration are functions of the atmospheric forcing, above ground vegetation cover, and soil moisture.

CHILD does not capture all the dynamics that occur at different rates along the vertically heterogeneous soil layer, yet it captures relatively well the moisture available for vegetation in the first 15 cm, where most of the grass roots are located (Figure 4-12), and reproduces well the evapotranspiration rates. Figures 4-17 and 4-18 show in greater detail the moisture and transpiration dynamics in 2003 and 2004-2005 respectively.

Modeled evapotranspiration rates are in better agreement with measurements than soil moisture. Differences between measured and simulated moisture are partly attributed to the limitations of the vertically homogeneous moisture model assumed. While the model assumes uniform moisture and moisture losses as depth increases, in reality moisture and losses change with depth: rainfall always reaches the top few centimeters of soil, but as depth increases, the number of rainfall events that reach those depths decreases. This leads to high moisture close to the surface even during small rainfall events, and high evapotranspiration rates, which are of short duration. This is illustrated in Figures 4-18a and 4-18b. In these figures green circles indicate a rainfall events that were so small that did not even reach the 5 cm depth, but did produce high evapotransiration rate periods of short duration. During such small rainfall events, the model assumed a slight uniform increase in moisture through out the root

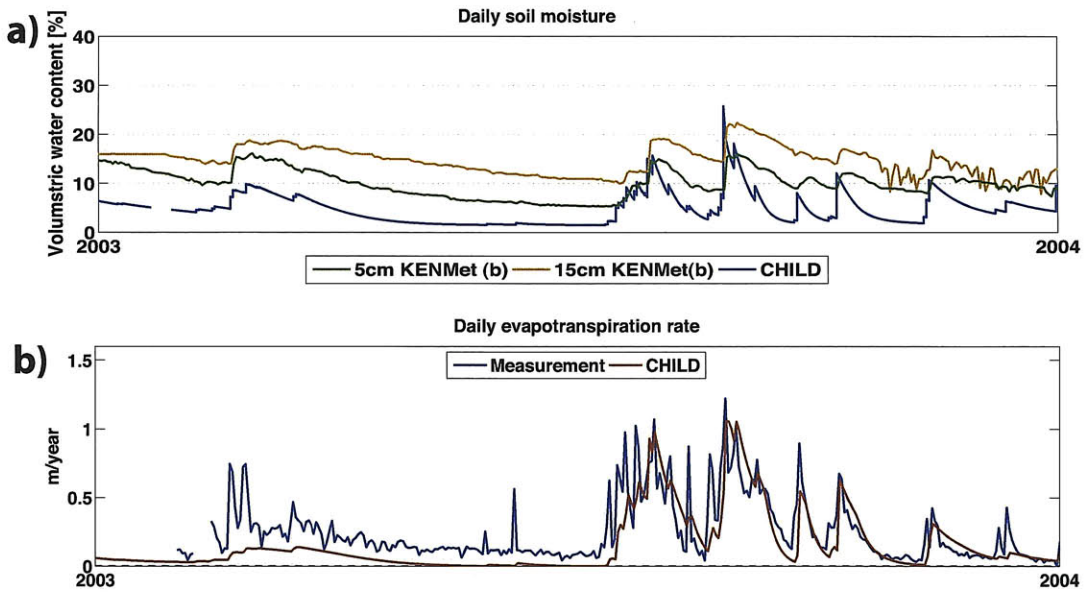

Figure 4-17: Comparison of simulated and measured a) moisture (at 5 and 15 cm depths from KENMet) and b) evapotranspiration, at Kendall (2003).

zone, and then evapotranspiration rates proportional to depth averaged moisture.

A second reason why modeled and measured moisture do not converge is due to the parametrization of the soil hydrologic properties. Currently, the model was specified with soil parameters corresponding to a sandy texture [*Laio et al.*, 2001b]. New parameters corresponding to textures and effective porosity closer to those observed in the field can bring the moisture values closer to those observed in the field. However, when a more clayey soil like the one observed at Kendall in the top 15 cm is used, vegetation productivity is reduced mainly due to a reduction in infiltration. Because of this, the sand parameters are left in place.

The detailed moisture time series presented in Figures 4-17a and 4-18a shows that moisture decreases faster in the model than at the 5 and 15 cm depths in KENMet and TDRK1, respectively. This is particularly so when the modeled volumetric water content is above 16 %. Above this water content, the model assumes leakage losses. Yet, simulated evapotransiration rates are in relatively good agreement with measurements, particularly during the monsoon. This is likely due to high evapotranspiration rates from the top 4 cm of the soil, and transpiration that draws water from deeper layers, that the measurements of moisture at 5 and 15 cm of depth do not capture.

The model does not capture the moisture dynamics occuring at deeper depths. Moisture is probably extracted by vegetation from depths of up to 90 cm, and moisture measurements, as discussed previously, reach depths of 50 cm during wet winters only, and occasionally during wet monsoons. These deeper layers, however, are not frequently reached by rainfall water, and are not the main source of moisture in

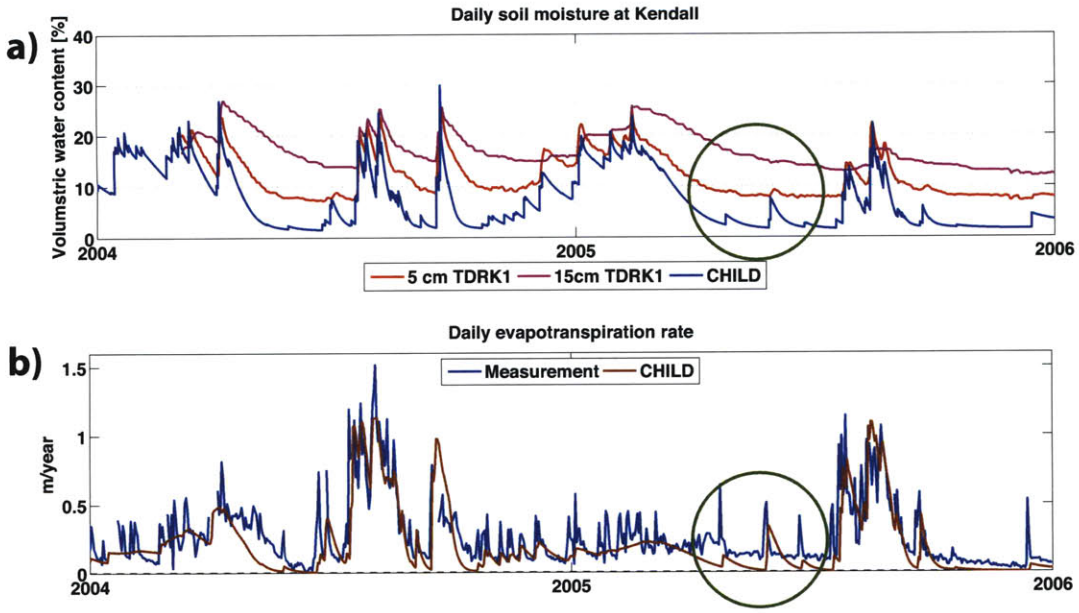

Figure 4-18: Comparison of simulated and measured a) moisture (at 5 and 15 cm depths from TDRK1) and b) evapotranspiration, at Kendall (2004-2005).

grasslands.

Improvements in the model, such as the use of a Richards equation and multiple soil layers are likely to improve the representation of the moisture dynamics of a model, with the cost of more computational time, and complexity in the already elaborated modeling framework. A more detailed representation of moisture dynamics, for example, would increase the number of parameters that need to be specified in the model.

In the model the components of the evapotranspiration, transpiration and evaporation from bare ground, are accounted for separately, as indicated in Figure 4-16b. They provide an idea of the usage of stored moisture by vegetation. This figure shows that moisture in this upper 15 cm layer is mainly utilized by the plants during the monsoon, and little of it is used during winter, when most losses, smaller than those of the monsoon, occur by evaporation. The figure also shows that during 1997 through 2001, moisture was mostly transpired, but that in the following years, when vegetation growth was limited, moisture mostly evaporated.

Runoff is currently underestimated by the CHILD. Runoff only occurred in the simulations of the 1998, 2000 and 2007 monsoons (Figure 4-15d), where as field measured runoff occurred a few times in the 1999 through 2008 period, but was particularly significant in 1999 and 2006, not registered by the model. Two reasons for such underestimation are the following. One is that rainfall interstorm variability is not considered in the simulation. Often, interstorm variability in the region during the monsoon is high, with peaks of high intensity that last only a few minutes but

that result in runoff. A second reason is the underlying clayey layer that is likely to act as an impervious layer, resulting in significant lateral flow that results in runoff at the outlet of even a small basin, instead of the mostly vertical leakage currently assumed by the model. Because of that, a higher anisotropy ratio in the model may improve the runoff representation.

4.3.3 Spatial analysis

Following the spatial analysis presented in Chapter 2, a similar analysis of the spatial relationships between topography and vegetation of the simulation is presented in this section to inspect whether or not the model reproduces those relationships. The relationships between vegetation cover and drainage area, aspect and slope, for four different times of the year, January 1, April 1, July 1 and October 1 throughout the 11 years simulated, shown in Figures 4-19, 4-20 and 4-21, are in agreement with what is presented in Chapter 2. July 1 and October 1 correspond approximately to the onset and end of the monsoon rains, respectively. In this period of time the time averaged vegetation and moisture are high and low, respectively. During January 1 and April 1, vegetation cover is generally dormant. In this period of time moisture is relatively high due to the small potential evapotransipiration and winter rains.

Biomass as a function of drainage area

The 11 years averaged relative biomass as a function of drainage area at different times of the year are shown in Figure 4-19. The figure also shows with error bars the standard deviation of the data. Little change in biomass as drainage area increases is apparent in the simulations, in contrast to the increase in NDVI/biomass observed in the data corresponding to the field site. This difference is attributed to the uniform root zone prescribed in the simulations. The increase in grass growth in the field as a function of drainage area is attributed to the accumulation of more moisture as drainage area increases in the direction of the catchment output, but also to the accumulation of sediments which makes the water storing capacity larger, and allows the soil to store the higher amounts of moisture that flow towards these regions. Nevertheless, a slight increase in biomass is observed, for any time of the year sampled, as drainage area increases past 80 000 m^2. This drainage area corresponds to channels, where moisture converges, as clearly visible in the drainage area map of the catchment (Figure 4-22).

The error bars in the figure also show that the spatial variability of biomass decreases with drainage area, probably because in the channels (high drainage area) there is little variability of slope and aspect, where as in the hillslopes (low drainage area), variability of aspect and slope is higher (see aspect and slope maps in Figures 4-23 and 4-24). The figure also shows that the spatial variability of biomass is highest in April 1 and lowest in July 1. This maybe explained by the redistribution of moisture after wet winters, and prior to April, that affect vegetation distribution in April, and

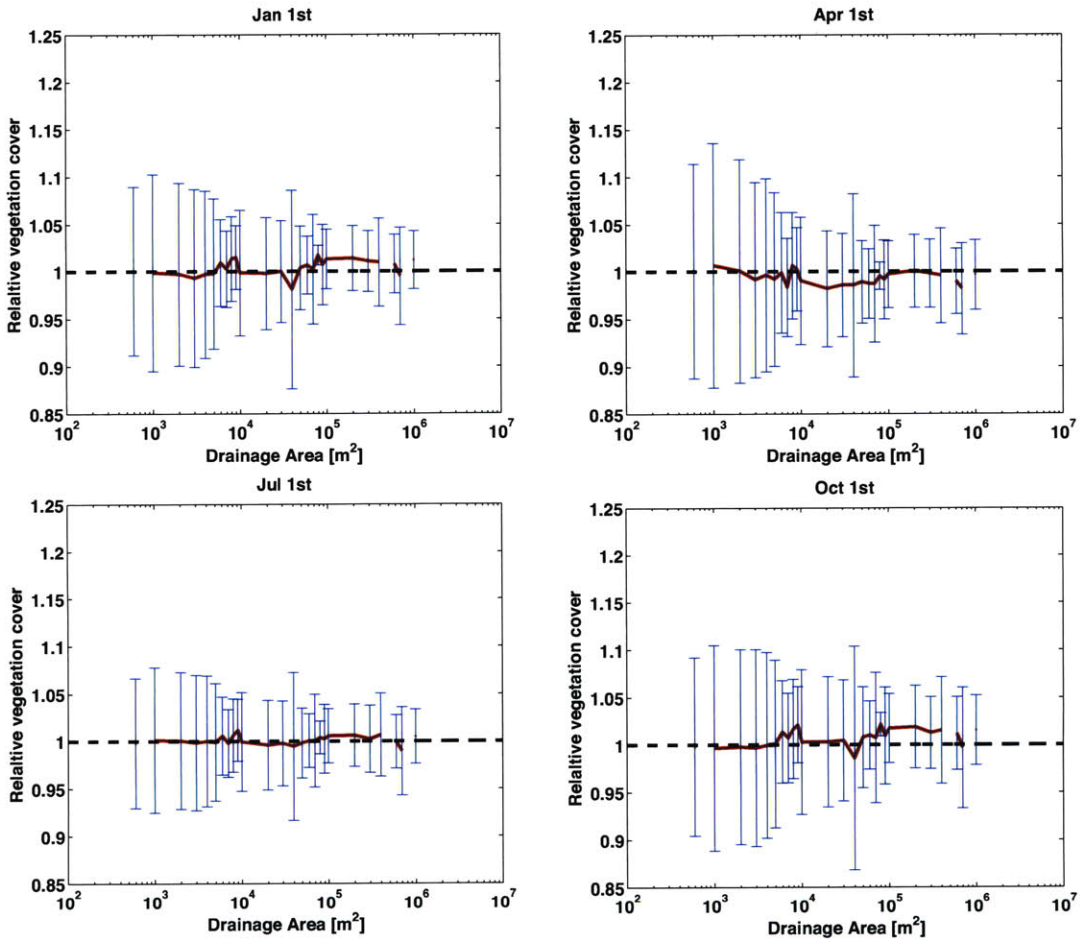

Figure 4-19: 11 years time averaged relative biomass as a function of drainage area, for the modeling results. Four different times of the year were sampled for this analysis: January 1, April 1, July 1 and October 1.

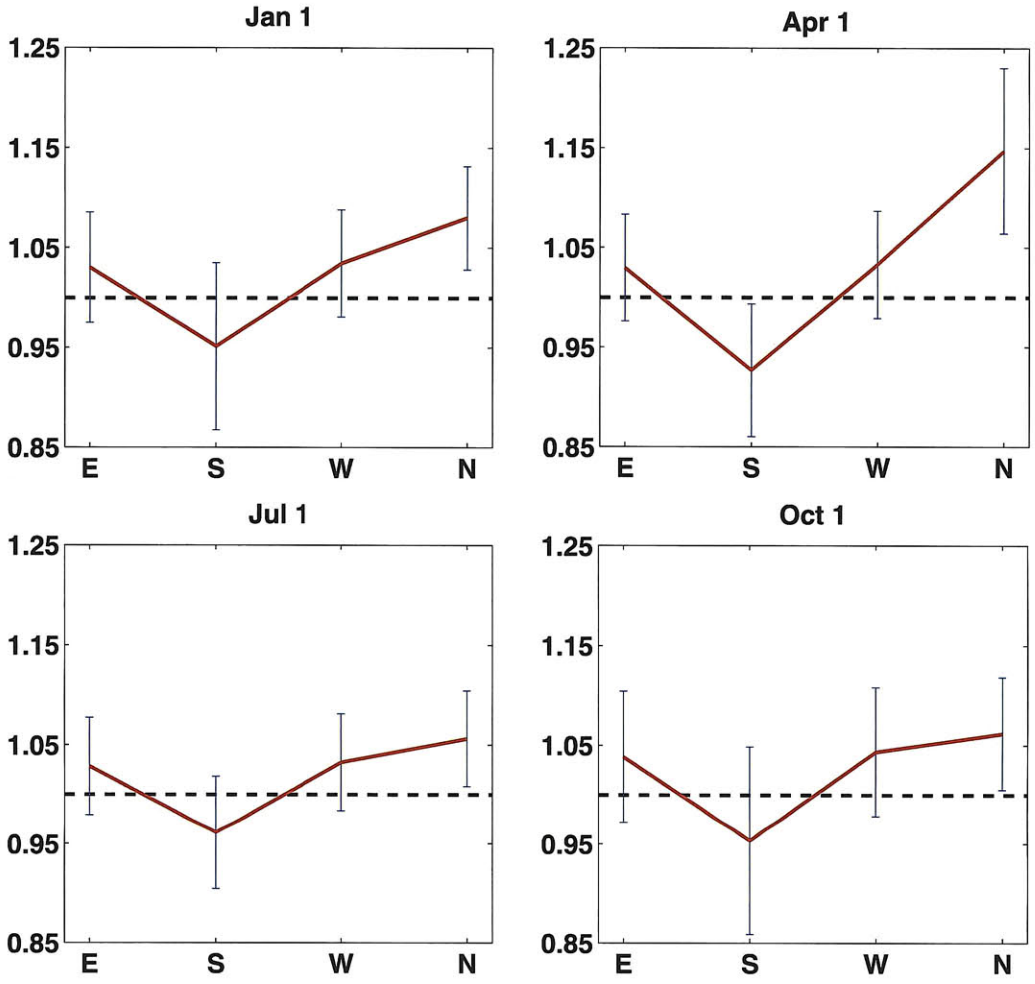

Figure 4-20: 11 years time averaged relative biomass as a function of aspect, for the modeling results. Four different times of the year were sampled for this analysis: January 1, April 1, July 1 and October 1.

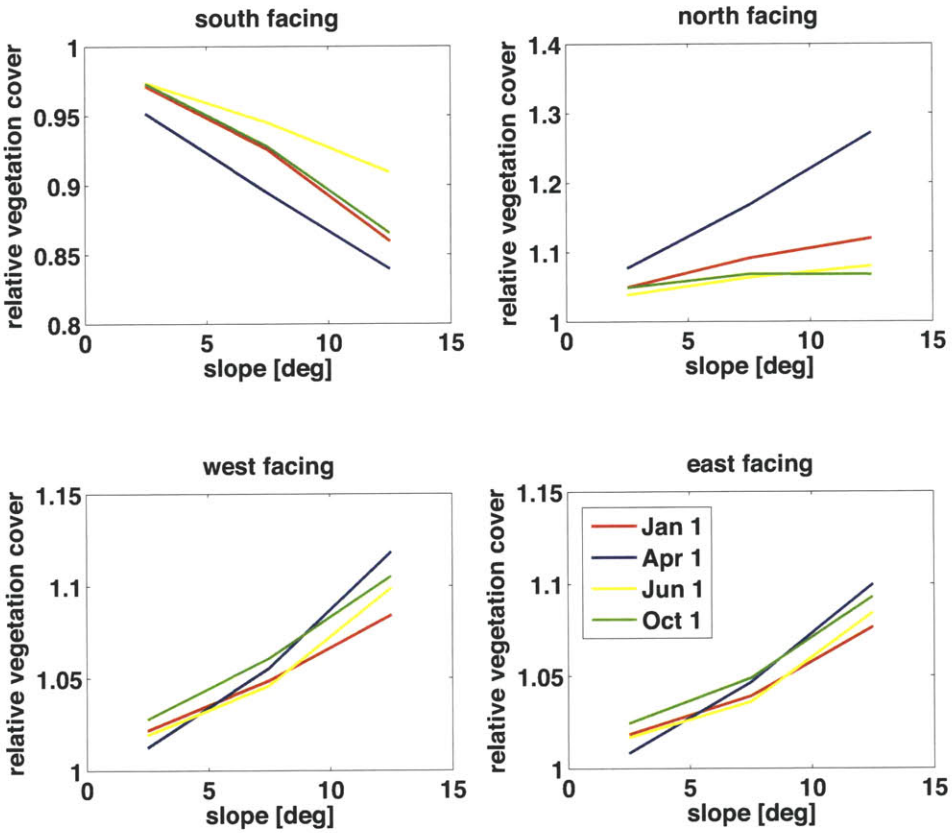

Figure 4-21: 11 years time averaged relative biomass as a function of slope, for terrain facing south, west, north and east, corresponding to the modeling output. Four different times of the year were sampled for this analysis: January 1, April 1, July 1 and October 1.

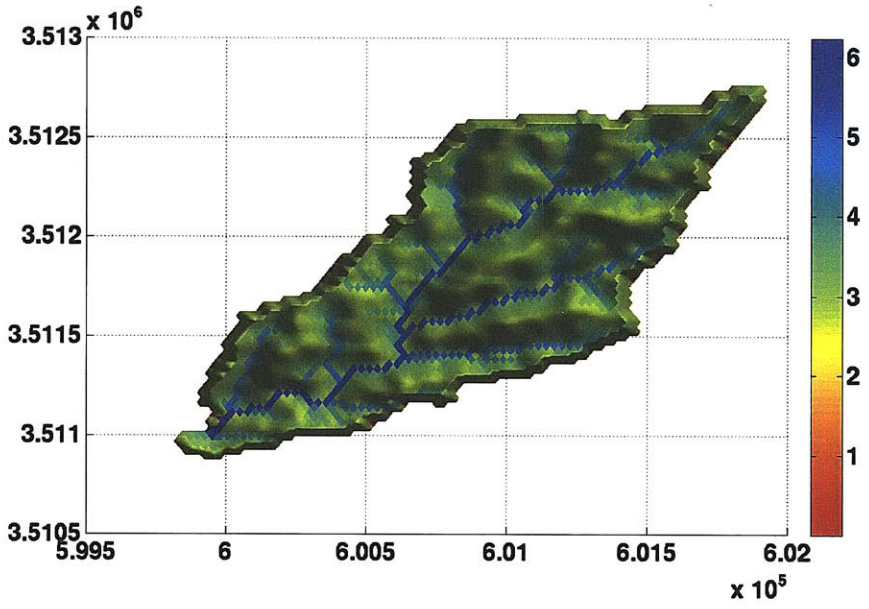

Figure 4-22: Map of drainage area of the watershed used in the simulation. The values are of the log_{10} of the drainage area, so that dark blue represents approximately 1000 000 m^2 and green 1000 m^2.

the lack of moisture on July 1, and thus of a more uniform lack of vegetation cover in July 1st that follows three months of no rain and high potential evapotranspiration.

Biomass as a function of aspect

The 11 year time averaged relative biomass as a function of aspect for different times of the year (Figure 4-20) show that less vegetation grows on terrain facing south than in any other direction, and that more grass grows on north facing terrain than in any other direction. This reflects the inverse relationship between solar radiation and vegetation growth discerned in the field through remotely sensed information as discussed in Chapter 2. The greatest differences in relative biomass amongst aspects occur in April 1, after the long period where moisture differences between different aspect may become significant (if April is preceded by a wet winter) and be reflected in the vegetation. During such period moisture remains for a long time in the soil given the small potential evapotranspiration, and the highest differences in insolation between north and south aspects and between different slopes take place.

Figure 4-20 also shows that the largest spatial variability is on the south facing terrain through most of the year, except in April. Such variability probably results from the larger percentage of terrain facing south in the domain (Figure 4-23) with a large spectrum of drainage areas and slopes (Figures 4-22 and 4-24). In April 1 the largest variability is observed in the north facing terrain, likely due to a more significant sensitivity of moisture fluxes to the incident solar radiation in terrain facing

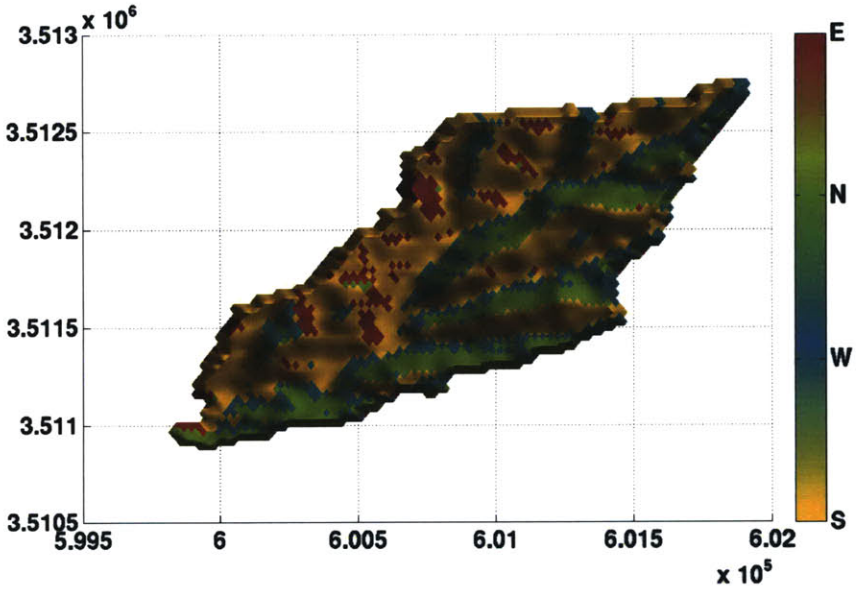

Figure 4-23: Map of aspect of the watershed used in the simulation.

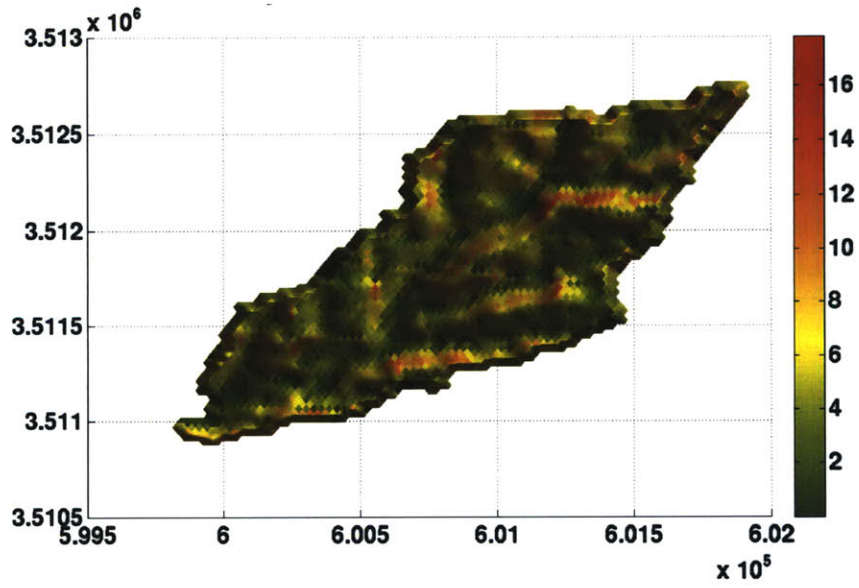

Figure 4-24: Map of slopes of the watershed used in the simulation, the slope is in degrees.

this direction at this time of the year. As Figure 4-21 shows, this indeed seems to be the case, as the highest sensitivity of biomass to slope in the north facing terrain corresponds to April 1.

Biomass as a function of slope

The 11 year averaged relative biomass as a function of slope for each aspect, for four different times of the year (Figure 4-21), shows that biomass changes with slope in the opposite direction to the incident annual radiation, as expected. The time of the year when slope has the largest impact on biomass distribution is in April. The reason for this was discussed in the previous paragraph.

4.4 Discussion

4.4.1 Representation of the vegetation dynamics implemented in CHILD

The main goal of this work is to have an adequate representation of the vegetation dynamics. The NDVI data presented in this section was continuously used in the development of the vegetation dynamics module. Two important components of the module resulting from this exercise are the addition of a leaf flush algorithm that produces a rapid increase of biomass with the onset of monsoon rains, or with the increase in temperature during spring after wet winters, and the addition of a phenology algorithm that results in allocation of all the assimilated carbon to the roots during the fall (instead of partitioning it between the shoots and roots as during the spring and summer). The first addition reproduces better the rapid increase in NDVI observed with the onset of monsoon rains, where as the second, the decrease in NDVI during the fall.

The resulting version of CHILD is satisfactory. The comparison between the simulated vegetation, moisture, and evapotranspiration and measurements suggests a reasonable representation of the landscape system.

4.4.2 Controls on vegetation dynamics

Drawing from these simulations, observations, and past work, it is possible to propose a set of controls on vegetation dynamics in semiarid grasslands that can be grouped in three categories: climatic controls, initial conditions, and local conditions.

Climatic controls

The timing, type and amount of rainfall during a year and its inter-annual variability control the amount of moisture entering the root zone and the distribution in time and space of such moisture input. Temperature, light and potential evaporation at different times of the year control the rates of evapotranspiration, photosynthetic efficiency, and plant stress.

These climatic characteristics drive the timing of the onset of vegetation growth and dormancy, and make the environment more suitable to grasslands, rather than to forests or deserts. The timing of the onset of vegetation growth and dormancy is well represented by CHILD using the water use efficiency (WUE) approach described in Chapter 3. This correct representation of the timing is due in large part to taking into account leaf flush at the onset of the growing season, and the allocation of all the assimilated carbon to the roots during the fall. CHILD also captures well the 'spring growth' conditional on winter moisture, which only occurs after 'wet' winters. A decline in vegetation usually following the spring growth during a dry and hot period that separates the spring growth from the monsoon rains is also captured by CHILD. This decline in between the growing seasons leads to two vegetation peaks in a year, such as 2001 and 2004 (Figure 4-14). The vegetation peak lags behind a moisture peak. The lag is generally of a few months in spring, and a few weeks during the monsoon. This difference in lag times reflects the differences in transpiration and vegetation growth rates, which are higher during the monsoon.

Spring growth is likely to be more sensitive to moisture stored beneath the 15 cm of soil than monsoon growth, because, as the moisture measurements indicate, moisture is stored and then depleted from those regions mainly during wet winters. The usage of that moisture, however, is not accounted for in the current version of CHILD and can be explored in future work. Yet, given that the majority of the photosynthetic activity occurs during the monsoon, and that the majority of the roots are in the top 15 cm, this is not a big concern.

The nature of the precipitation events results in a uniform distribution of moisture during winter, and thus a uniform growth of vegetation in spring (when it does occur), and a more heterogeneous distribution of moisture during summer, which is reflected in a heterogeneous vegetation growth in space (as pointed out during the introduction to this chapter).

The annual variability in precipitation, which is reflected in rain of less than half the mean annual in 2002 (see Figure 4-7), affects significantly biomass productivity, but not in a linear fashion, as illustrated in Figure 4-13. Rather, the effects of the yearly rainfall variability are reflected in a cumulative manner. *Oesterheld et al.* [2001] showed that the previous year information, combined with the current year information, are much stronger predictors of the vegetation productivity in a given year than the current year information alone. The significant contrast in biomass between 2000-2002 and 2003-2005 reflected in NDVI measurements (Figure 4-13), and simulated biomass (Figure 4-14) are an example of the accumulative effects of

the annual variability in rainfall in grassland productivity in the field and in the model.

Initial conditions

The initial conditions of moisture, nutrients and carbon pools at the beginning of a year, at the beginning of spring, or at the beginning of the monsoon, have an effect on the moisture and vegetation dynamics. They can be considered the memory of the system, that reflect previous conditions. Some of these conditions, moisture and the above ground (AG) biomass in particular, change relatively rapidly in time, and thus might be considered short term memory components of the system. Below ground (BG) biomass, on the other hand, probably changes more slowly, given its larger biomass pool [*Cox et al.*, 1986; *Gibson*, 2009]. In the simulations the root biomass changes are slower than above ground biomass changes (Figure 4-14). This work did not investigate the role of nutrients, but previous investigations reveal that nutrient accumulation throughout several years in tall prairies may be consumed in one growing season and result in an increase in vegetation growth [*Knapp et al.*, 1998]

The "long term memory" component of the system, the root biomass, probably dampens the temporal and spatial fluctuations of precipitation and above ground biomass, by storing carbon assimilated during the high productivity years, and using it during the low productivity years.

The "short term memory" components of the system, soil moisture and AG biomass, interact among each other. The initial moisture represents a pool of stored moisture vegetation may use, regardless of the precipitation that may occur in the period of study, and has effects on the carbon assimilation in the near future. For example, an initial high moisture content in January 1st of a given year, will result in spring vegetation growth independently of whether it rains or not during the next six months. Above ground biomass at the beginning of the monsoon season, for example, is reflected in higher soil moisture losses in the season, due to higher transpiration rates at the onset of the monsoon rains. These higher moisture losses may actually reduce the length of the growing season if rainfall is not abundant. Vegetation also increases the infiltration capacity of the soil (see Introduction chapter). Thus, the amount of water that infiltrates from a high intensity rain at the beginning of the monsoon depends on the initial above ground biomass. The interplay described above affects the carbon assimilation in the grassland, and as a consequence, the root carbon pool, or "long term memory" component of the system.

Vegetation and moisture interact at a longer time scale (10, 100 or 1000 of years) as well. This is not considered in the simulation discussed in this chapter. Such interaction is well described by *Jenny* [1958] and consists on the evolution of vegetation and soil as one entity, as a function of parent material, time, climate, topography and existing vegetation species. Under such framework and time scales, moisture dynamics affect vegetation development, which in turn controls the evolution of the soil mantle. As the soil mantle evolves, so do its hydrologic properties, and thus the mois-

ture dynamics, closing a feedback loop between soil and vegetation characteristics. Two soil characteristics that affect the moisture dynamics, soil depth and texture, are discussed below as static elements of the system. The evolution of the soil depth is investigated in the following chapter.

Local conditions

Four local controls on moisture and vegetation dynamics have been identified: soil depth and texture, topographic position, and exposition to the sun. All of these are assumed constant in time. However under larger time scales of the order of tens, hundreds or thousands of years, they are expected to change. Those changes are discussed in the following chapter.

Moisture availability and soil depth and soil texture

The amount of water stored in the soil available for plants is that in the root zone, and that amount depends on the root zone's depth and hydrologic characteristics of the soil, characteristics which are often correlated with the soil texture. The effect of soil texture in vegetation dynamics is discussed below. Soil hydrologic properties may also be affected by soil organic matter, macropores resulting from animal or vegetation activity, gravel content, and mineral composition of clays, but these other factors are not accounted for in this work. The influence of groundwater in the root zone is not relevant in the area studied because the water table is tens of meters below the surface, however, in other regions the effects of groundwater on the moisture and vegetation dynamics is relevant. Some other processes, such as the transfer of moisture from deeper to shallower layers of soil by roots during the night (hydraulic uplift) are not considered either and their effect is assumed limited at the site of study.

Bucket model representation

In CHILD moisture is represented with a 'bucket' model, and as such, it does not represent in detail the vertical distribution of moisture or the layering of the soil with depth. Instead, it assumes a vertically homogeneous moisture and soil properties. Furthermore, it only computes moisture within the soil layer defined as the root zone, and moisture leaking the layer (in the vertical direction) is assumed lost. Under these assumptions, two things happen. First, moisture store is directly proportional to the soil depth, and second, any amount of infiltration is distributed along the whole depth of the root zone. In reality, moisture may infiltrate only down to a fraction of the root zone depth, sometimes it only reaches a couple of centimeters in depth. This is a limitation of the current version of CHILD, and the differences between model and observations resulting from it are discussed above, and shown in Figure 4-18. In that figure, differences between model and measurements in moisture and evapotranspiration rates during a rainfall event in the dry season are indicated

with a green circle. However, moisture and evapotranspiration are well represented by this bucket model in most of the year, and particularly well during the monsoon, when most of the carbon assimilation occurs.

Representation of the root zone

In these simulations the depth of the root zone is set to 15 cm. This value can be increased or decreased to test the effect of the root zone extent on the vegetation dynamics. A larger depth increases the capacity of the soil to store moisture, and this is only relevant when the store can be filled with rainfall, and when such store is essential for vegetation growth during periods of little or no rain. However, soil depth alone is not enough to quantify moisture available for plants, this also depends on the distribution of roots as a function of depth (see Figure 4-12) and on the stratification of soils (see Figure 4-9). In the case of Kendall, for example, soil depth goes beyond a meter, but most of the roots are in the top 15 cm, and a clayey soil layer that starts at that depth slows down considerably the infiltration of moisture beyond that layer during the monsoon, as soil measurements show (Figure 4-11). These conditions make the first 15 cm an 'active' root zone depth from where most transpired moisture is drawn from. If such active layer were deeper, less leakage from it would occur. In the field, the leakage from this zone is captured by deep roots. In the model it is assumed lost.

Soil texture effects on vegetation, moisture and runoff

Soil texture is related to the pore space in the soil, its infiltration capacity, and the force with which the soil retains water. Sandy soils have a high infiltration capacity and retain little amounts of water, as a consequence, most rainfall infiltrates and a significant percentage of it leaks. However, they retain some moisture which is easily absorbed by plants. Thus in sandy soils losses to evaporation are small, where as losses to leakage are high. These conditions are favorable in an environment such as Kendall, where the potential of evapotranspiration is high. Clayey soils on the other end of the texture spectrum have a low infiltration capacity and high moisture retention capacity. Clayey soils are generally impermeable, and runoff losses, and evaporation losses are significant in them, where as leakage is minimized.

To see the effects of texture in conditions representative of Kendall, simulations under three different soil textures were carried out. The soil parameters used are those provided by *Laio et al.* [2001b], and correspond to sand, clay and silt loam. Some of the hydrologic properties of these soils are summarized in Table 4.3. The data shows the contrast in infiltration capacity between sand and the other two soil types. It also shows that regardless of a higher porosities (n) and water holding capacities (θ_{sf}) of the clay and silty loam soils, the amount of moisture available for transpiration, if the soil is completely saturated as an initial condition ($\theta_{fc} - \theta^*$), is similar between the sand and silty loam, and about 40 percent smaller for the clay. Furthermore, it

shows that the clay retains more water ($s_h = 0.44$) than the silt loam (0.14) or the sand (0.04), and thus evaporation loss rates are highest in the clay. This leads to less moisture available for transpiration.

The differences in moisture fluxes resulting from differences in texture are shown in Figure 4-25. The figure clearly shows the reduction in infiltration for the clay and silty loam, as well as a reduction in leakage. However, the evapotranspiration rate does not change as much. A more detailed picture of the evapotranspiration changes is provided in Figure 4-26, which also shows differences in moisture. Clearly, even-though moisture is higher in the clay case, the evapotranspiration rates are very similar. However, the response of the carbon assimilation is large, as illustrated in Figure 4-27a. Vegetation is almost insignificant from 2002 onwards in the clay, and orders of magnitude smaller on the silty loam than on the sand, clearly indicating that sand is the most favorable texture for the conditions simulated, in agreement with *Sala* [2001]. Figure 4-27b also shows that runoff is much higher in the case of clay and silty loam than in the case of sand, which is likely to have consequences in erosion processes and lateral fluxes of water in the basin.

Differences in soil texture maybe beneficial for different plant functional types (PFT) [*Sala et al.*, 2001], however, given that in this work only one PTF (grasses) is used, this is not investigated with the model.

Moisture and topographic position

The topographic position and exposition to the sun of terrain based on aspect and slope were broadly discussed in Chapter 2. The topographic position dictates how much moisture from upstream areas flows into a given location within the catchment. Locations close to the ridge have little contribution by lateral redistribution from neighboring locations, where as terrain in the valleys of a catchment generally have a significant contribution of moisture from their neighboring upstream terrain. This results in more carbon assimilation in the valleys than in the ridges, as discussed in Chapter 2. An increase in biomass with drainage area in the simulations is in agreement with the satellite observations.

Moisture and exposition to the sun

The exposition of the sun to terrain dictates differences in evapotranspiration rates at different points in the landscape, and differences in temperature. Generally north facing terrain will lose less moisture to evaporation than south facing terrain, and will experience less heat, providing an advantage for vegetation growth, as discussed in Chapter 2. Higher biomass in the north facing terrain in the simulations is in agreement with the observations.

Table 4.3: Summary of soil properties for sand, clay and silty loam, used in the simulations

	n	s_h	s_w	s^*	s_{fc}	θ_r	θ_{fc}	$\theta_{fc}-\theta_r$	$\theta_{fc}-\theta_w$	$\theta_{fc}-\theta^*$	$K_s[cm/day]$
Sand	0.37	0.04	0.05	0.16	0.44	0.01	0.16	0.148	0.144	0.104	103
Clay	0.46	0.44	0.47	0.64	0.78	0.2	0.36	0.156	0.143	0.064	35
Silty loam	0.47	0.14	0.16	0.35	0.59	0.08	0.28	0.212	0.202	0.113	35

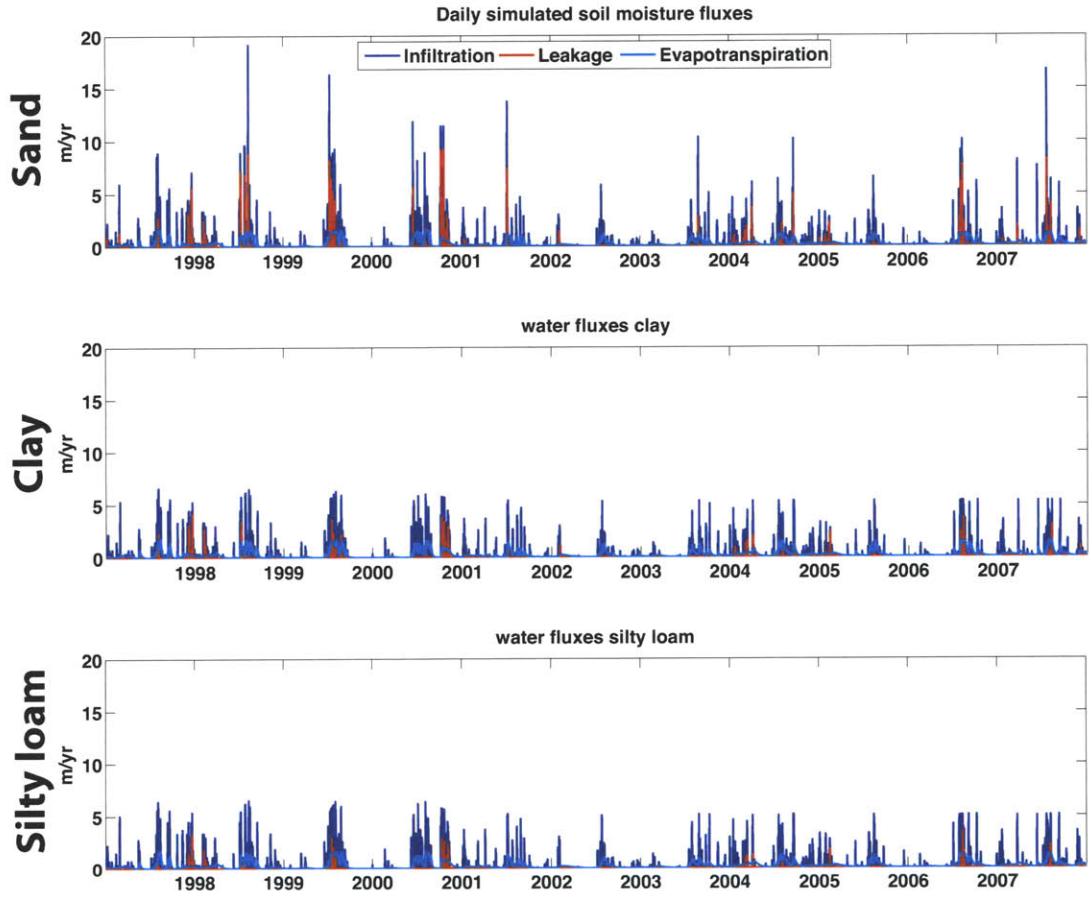

Figure 4-25: Moisture fluxes in and out of the soil in simulations of Kendall conditions (1997-2007) under different soil textures: sand, clay and silty loam.

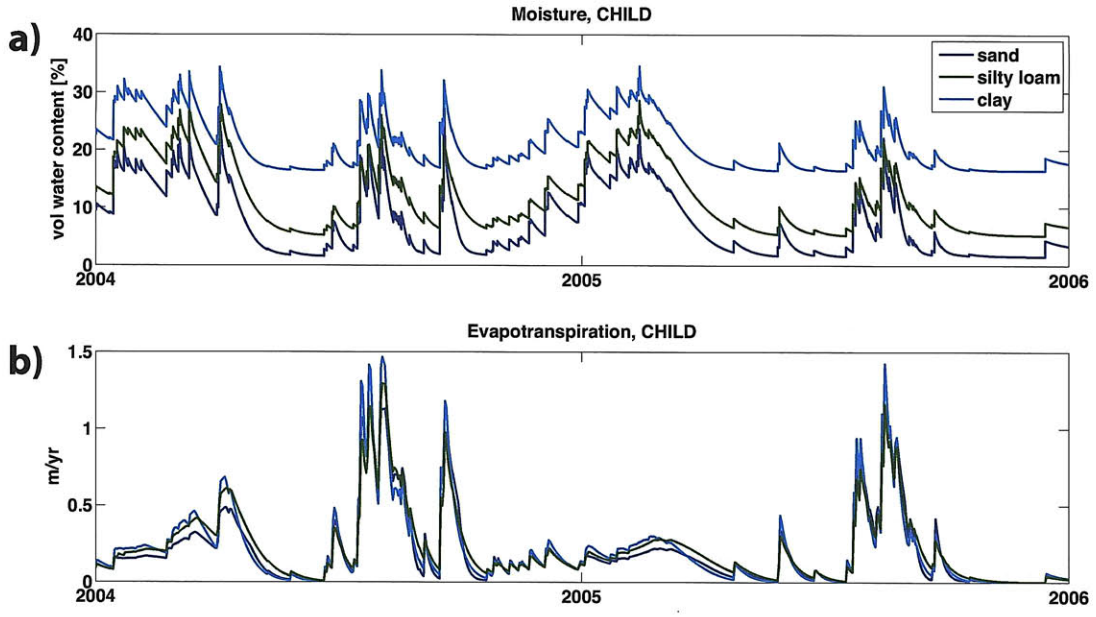

Figure 4-26: a) Moisture and b) evapotranspiration in simulations of Kendall conditions (1997-2007) under different soil textures: sand, clay and silty loam.

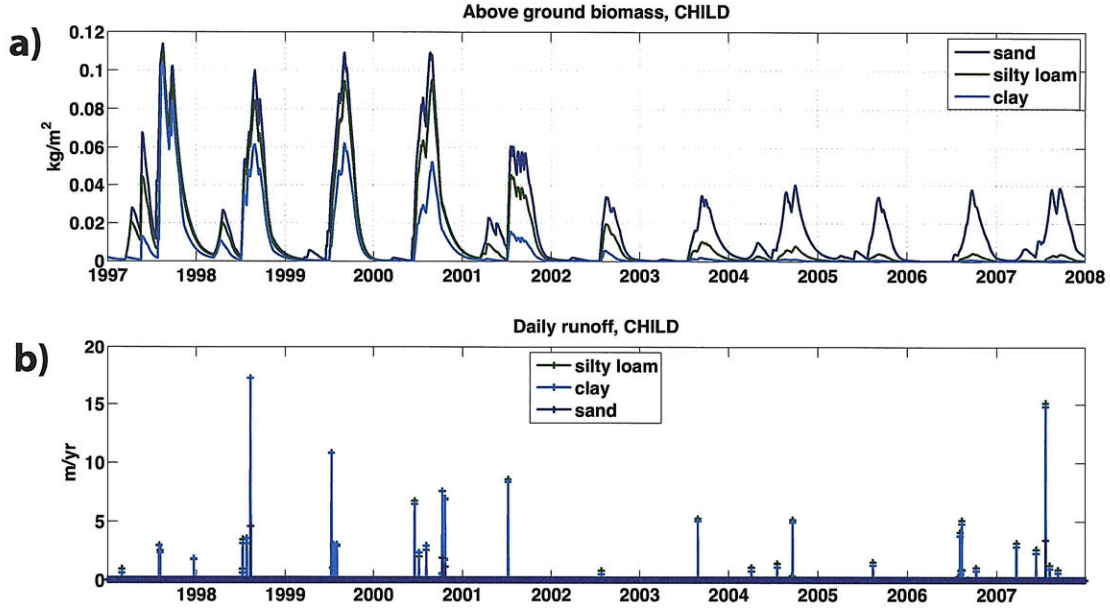

Figure 4-27: a) Above ground biomass and b) runoff in simulations of Kendall conditions (1997-2007) under different soil textures: sand, clay and silty loam.

CHAPTER 5

COUPLED EVOLUTION OF TERRAIN AND VEGETATION DISTRIBUTION

5.1 Introduction

Previous chapters have provided background about the vegetation-topography interactions, a data analysis that illustrates these interactions at two field sites, a description of the representation of these interactions with CHILD, and an evaluation of the vegetation and soil moisture dynamics represented with CHILD using measurements from the Kendall site (the site is described in Chapter 2). In this chapter CHILD is used to explore the interactions between topography and vegetation at time scales of thousands of years. The scheme of the landscape system represented in CHILD shown in Figure 5-1 provides a reference to what is being represented in these simulations. In the figure, ovals indicate the system states (topography and regolith, soil moisture, and vegetation), black rounded boxes the system processes (Hydrological, geomorphic and vegetation dynamics processes), and gray rounded boxes external forcings (rainfall, insolation and temperature, and tectonic uplift). The elements, processes and external forcings of the system are discussed in detail in Chapter 3. In the figure, arrows indicate interactions among the system components. Various feedback loops in the system are indicated with different colors. Red arrows indicate a loop of interactions among all of the system elements and processes. This loop is labeled $L100$. Blue lines indicate smaller feedback loops that involve more than two system components. For example, loop $L10$ (see figure) represents the feedback loop between geomorphology, topography and regolith, and hydrology. Green arrows indicate interactions among one element and one process of the system. For example, loop $L1$ (see figure) represents the feedback loop between geomorphology and topography and regolith. Table 5.1 provides a summary of the feedback loops represented in the figure. In the figure, a gray dashed line indicates the effect of topography on insolation and temperature. Insolation then interacts with hydrologic processes, and temperature affects vegetation dynamics, as described in Chapter 3.

For comparison, older generations of landscape evolution models represented only

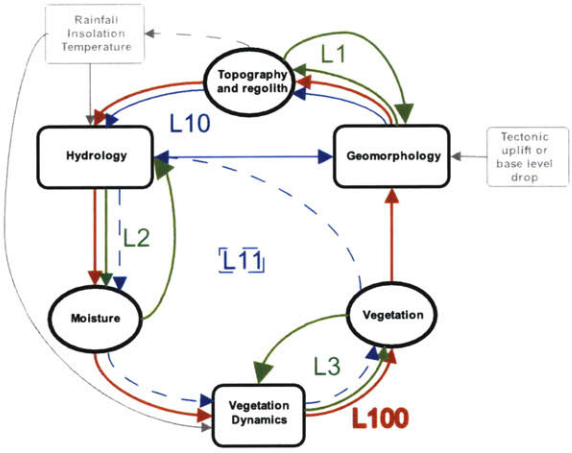

Figure 5-1: Scheme of the landscape system represented with CHILD. In the figure arrows indicate the direction of interaction among the various system components (elements and processes). Different colors indicate distinct feedback loops as labeled and described further in Table 5.1. Various arrows in one direction from one system component to another indicate that that connection forms part of more than one feedback loop, and not various connections.

Table 5.1: Feedback loops described in Figure 5-1

Name	Description	Other feed back loops included
L100	G→T+R→H→M→VD→V→G	L1, L2, L3, L10, L11
L10	G→T+R→H→G	L1
L11	H→M→VD→V→H	L1, L2
L1	G→T+R→G	
L2	H→M→H	
L3	VD→V→VD	

G = Geomorphology, H = Hydrology, VD = Vegetation dynamics, T+R = Topography and regolith, M = Moisture, and V = Vegetation.

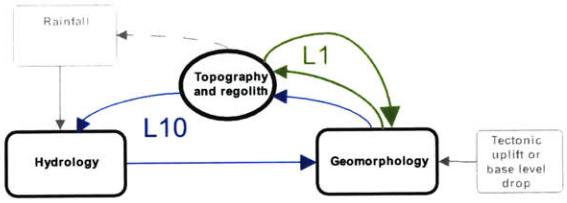

Figure 5-2: Scheme of the landscape system represented by former landscape evolution models.

a subset of the interactions represented with the current version of CHILD, as the scheme in Figure 5-2 shows.

The simulations presented in this chapter consists of five different scenarios, each representing a different subset of the landscape system interactions, and two different initial topographic settings. These sets of simulations are described in more detail in the Experimental setup section below. The vegetation-topography interactions described in Figure 5-1 result in: a) vegetation increase with moisture availability, b) more erosion in bare or lightly vegetated terrain, and c) a new organization of the elevation, regolith depth, and ecosystem productivity that results from the dynamic surface properties that follow the changes in vegetation cover in space and time. In addition to those results, bedrock erosion resulting from regolith erosion generated significant runoff and erosion heterogeneity in the landscape. That heterogeneity impacted significantly the topography and regolith, moisture and vegetation distribution of the system. In some circumstances, that surface heterogeneity lead to clear patterns of erosion, sedimentation, and vegetation.

5.2 Experimental setup

This chapter presents the simulation of two different initial topographic settings for 10 000 years. The first topographic setting, Topo1, is the same watershed used in the simulations of Chapter 4. It is a digital elevation model (DEM) of the Kendall site and has a 30 meters resolution. Its topographic properties (aspect, slope and drainage area) are provided in Figures 4-22, 4-23 and 4-24. Topo1 provides a wide range of realistic topographic conditions, a relatively large domain ($\sim 4km^2$) and a well defined drainage structure. The second topographic setting, Topo2, is a synthetic elevation domain that consists of two opposing and symmetric hillslopes, one facing north, and the other facing south, that converge in a valley, as Figures 5-3a, 5-3b and 5-3c show. This synthetic domain has a 5 meters resolution. The hillslopes follow a sinusoidal curve that reproduces the convex profile of the hillslopes near the ridges (characteristic of diffusion dominated erosion) and the concave up profile of the hillslopes close to the valley bottom (characteristic of fluvial dominated erosion). The dimensions of each hillslope are such that in a crossection of the hillslope, a straight line between its top and bottom would have a 20 % slope. The valley drains towards an outlet on the

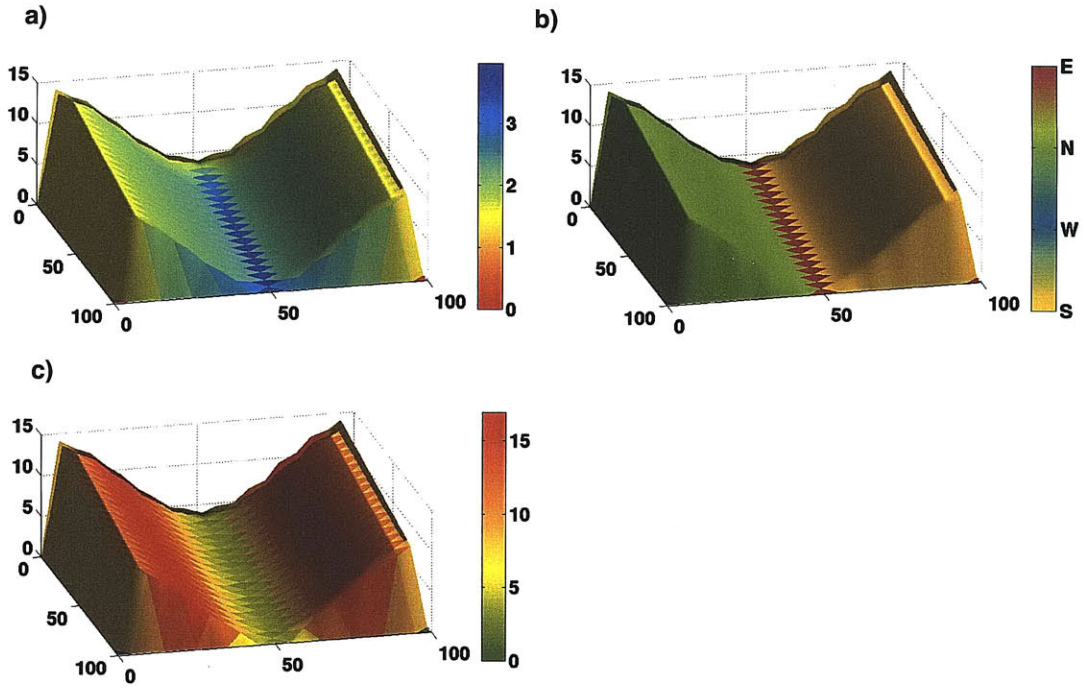

Figure 5-3: Maps of the properties of Topo2: a) drainage area (the values are of the log_10 of the drainage area, so that dark blue represents approximately 10 000 m^2 and yellow 25 m^2), b) aspect, and c) slope in degrees.

eastern edge of the domain with a 5 % slope. Topo2 provides uniform conditions and a high spatial resolution where the effects of vegetation differences between north and south facing terrain on geomorphic processes can be investigated with more clarity than in Topo1. Topo2 is a smaller domain than Topo1. It is $\sim 0.01 km^2$.

These simulations represent a semi-arid setting of the characteristics of the Kendall site. The climatic, hydrologic and vegetation dynamics parameters are provided in Tables A.1, 3.1, A.3 and A.5. The solar forcing, hydrologic processes and most of the vegetation dynamics processes parameters are the same that were used in the simulations presented in Chapter 4. Some differences in the vegetation parameters are due to the use of a different water use efficiency value (WUE) which is deemed more appropriate than the value used in the simulations presented in Chapter 4. Both values of WUE are within the range of values reported in literature for grasses. The differences in parameter values used in the simulations presented in Chapter 4 and this chapter are presented in Table 3.6. A range of values of WUE reported in literature are provided in Table 3.5. The parameters used in the representation of the geomorphic processes in the simulations presented in this chapter are summarized in Table A.2.

A difference between the simulations in Chapter 4 and the ones presented in this chapter is that the root zone depth (Z_r) is assumed to be at the most 15 cm, following the same reasoning than in Chapter 4 (that most of the roots are within the top 15

cm of soil). In this chapter the soil (or regolith) depth is allowed to change . This means that $Z_r = h_s$ only when $h_s \leq 0.15m$, and $Z_r = 0.15m$ otherwise.

Ten different simulations are presented and discussed in this chapter. They result from the combination of five different landscape scenarios, and two initial topographic settings, as summarized in Table 5.2. These different landscape scenarios were simulated to investigate the impact of vegetation dynamics on landscape evolution. The "dynamic vegetation" scenario consists of a landscape system where all the interactions described in Figure 5-1 take place. The "static vegetation" scenario, represented by Figure 5-4, assumes that vegetation does not change in time and is uniform in space. Vegetation cover is set to $0.07kgDM/m^2$. This value corresponds to the spatially and temporally averaged vegetation of the first 30 years of the dynamic vegetation scenario. In this scenario the feedback loops L11 and L3 are not present, and vegetation becomes an element that affects the hydrologic and geomorphic processes, but is not influenced back by the system. The "bare surface" scenario assumes no vegetation in the landscape and is represented by Figure 5-5. This scenario is similar to the static vegetation scenario, except that hydrologic and geomorphic processes are no longer under the influence of vegetation. This, as is shown below, has significant effects on landscape evolution. The "revegetation" and "degradation" scenarios combine the dynamic vegetation and bare surface scenarios. The objective of presenting these last two scenarios is to illustrate the effect of changes in the evolution of a landscape when vegetation is introduced or eliminated. They consist of simulating 5 000 years under a bare surface scenario, followed by 5 000 years of a dynamic vegetation scenario (revegetation scenario), or vice versa (degradation scenario).

Table 5.2: Set of experimental runs carried out with CHILD

Initial topographic setting	Scenarios simulated				
Topo1	DV	SV	BS	REV	DEG
Topo2	DV	SV	BS	REV	DEG

DV = Dynamic vegetation, SV = Static vegetation, BS = Bare surface, REV = Revegetation, DEG = Degradation.

5.2.1 Rainfall and climate variability

The simulations discussed in Chapter 4 use daily rainfall observations instead of the Barlett-Lewis (BL) rainfall generating algorithm used in the simulations presented in this chapter. The reason is that in Chapter 4 the vegetation model was being compared to observations, and usage of observed rainfall was appropriate. In this chapter, in contrast, the goal is to model the cumulative effect of vegetation dynamics and geomorphic processes over thousands of years. A rainfall record of that length is not available. Instead, synthetically generated rainfall is used. As discussed in more detail in Chapter 3, a Barlett-Lewis algorithm is selected because it represents accurately the intra-storm rainfall intensity variability which is characteristic of

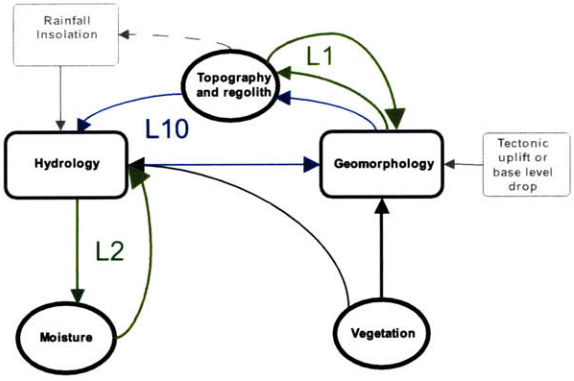

Figure 5-4: Scheme of the landscape system represented with CHILD in the static vegetation scenario.

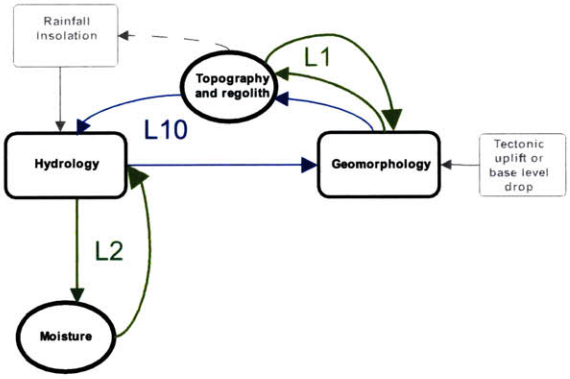

Figure 5-5: Scheme of the landscape system represented with CHILD in the bare surface scenario.

monsoon convective rainfall. This variability is critical for the generation of runoff in semiarid regions. Two time series of historic and BL generated rainfall are provided in Figure 5-6 for reference.

The use of the BL generated rainfall results in higher ecosystem productivity, as shown in Figure 5-7. The reason for this is that the BL generated rainfall is distributed in time slightly different than the rainfall observations between 1997 and 2007. First, it does not have consecutive dry years (2001-2003). These dry years are clearly visible when the annual precipitation is computed (see the annually accumulated precipitation in Figure 5-8). Such droughts reduce ecosystem productivity. Second, the BL rainfall is more evenly distributed within the year. This results in less leakage, more transpiration (as shown in Figure 5-8), and consequently, more carbon assimilation.

The BL algorithm provides rainfall variability, as Figures 5-6 and 5-8 show. However, the algorithm is designed and parametrized to capture interstorm variability, not to capture long term climate variability. Therefore it does not capture changes

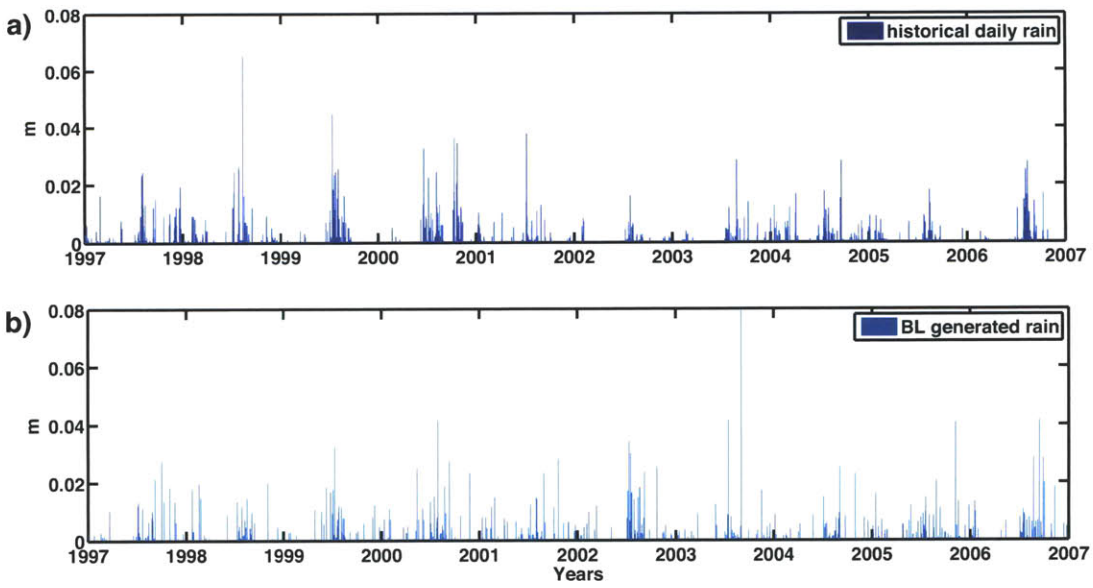

Figure 5-6: Rainfall used to force CHILD in a 33 year simulation: a) historical and b) Barlett-Lewis (BL) generated rainfall. The BL rainfall shown corresponds to individual storms. In the BL generated rainfall, within each storm, rainfall intensity varies (not shown).

in climate at longer time scales known to affect vegetation and geomorphic dynamics. For example, a drought recurrence interval of approximately 52 years has been estimated for the American southwest with tree ring data spanning 600 years, and periods of higher erosion rates are associated to such droughts. More drastic climate changes and associated geomorphic responses at the millenial scale have also been suggested [*McHugh and Goodin*, 2003; *Milne et al.*, 2003; *Monger*, 2003]. Such climatic variability is likely to affect the vegetation-geomorphic interactions discussed in this chapter. However, this work investigates the vegetation-geomorphic interactions in the landscape system under a constant climate. Future investigations may address this interesting issue of climate variability in the last 600 years, or at millenial time scales.

5.2.2 Water use efficiency as a function of temperature

The dynamic vegetation processes of CHILD were slightly modified for the simulations presented in this chapter, in contrast to the model presented in Chapter 3 and used in the simulations presented in Chapter 4. The water use efficiency (WUE) was assumed constant previously. Now, it is assumed a function of temperature (T). The reasoning behind this addition to the model is that as temperature increases, so does the specific humidity inside leaves, where air is under moisture saturation conditions. As a consequence, the gradient in vapor pressure between the leave and

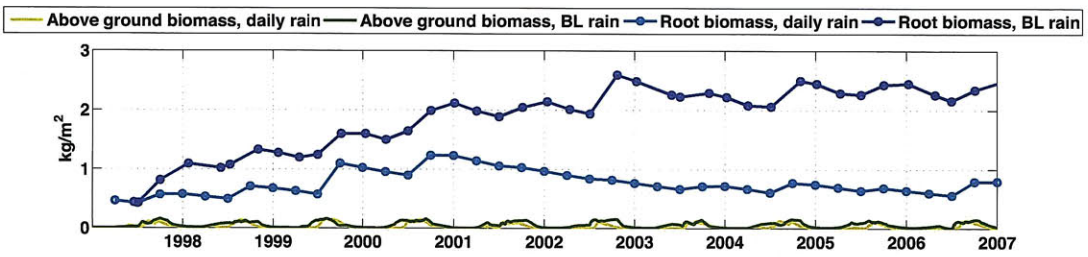

Figure 5-7: Time series of above ground and root biomass for two simulations, one using historical rainfall, and the other one using BL generated rainfall (1997-2007). The above ground biomass shown corresponds to the basin averaged biomass for each time step. Root biomass shown corresponds to the mean north facing terrain root biomass every 0.25 years. In these simulations mean north and south facing terrain biomass is similar.

the surrounding air increases, and more water is transpired by a plant for a given stomatal opening. While the amount of water transpired increases with temperature, the amount of carbon influx into the leave remains relatively constant. This results in a lower WUE as temperature in the leave increases [*Ponton et al.*, 2006; *Williams and Albertson*, 2005]. Assuming that the gradient in specific humidity between leaves and the surrounding air is proportional to the specific humidity inside the leave, q^* (which is the saturated specific humidity at the leaf temperature), and that WUE decreases linearly with that gradient, then WUE as a function of temperature can be expressed mathematically by

$$WUE(T) = WUE_o \frac{q^*(T_o)}{q^*(T)} \tag{5.1}$$

where WUE_o is the water use efficiency at a reference temperature T_o. Assuming that temperature in the leave is that in the air (a rough approximation at the daily scale), then q^* is estimated as a function of air temperature T. In the simulations WUE_o is assumed for $T_o = 20^oC$, and is equal to 0.005 $kgDM/kgH_2O$. Using this equation to estimate WUE, productivity differences between north and south-facing hillslopes increase significantly, as the time series in Figure 5-9 shows.

The spatial effects of the variability of WUE as a function of temperature are illustrated in Figure 5-10. This figure shows the time averaged vegetation cover for four different times of the year, on Topo2. The simulation is for a period of 33 years under the dynamic vegetation scenario. In the simulation, on average more vegetation grows on the north facing terrain at the beginning of the monsoon (beginning of summer), at the end of the monsoon (beginning of fall), and during winter, but more vegetation grows on south facing terrain at the beginning of the spring.

In the model, in some years when winter precipitation is high, moisture accumulates in the soil because vegetation is dormant and the potential evapotranspiration

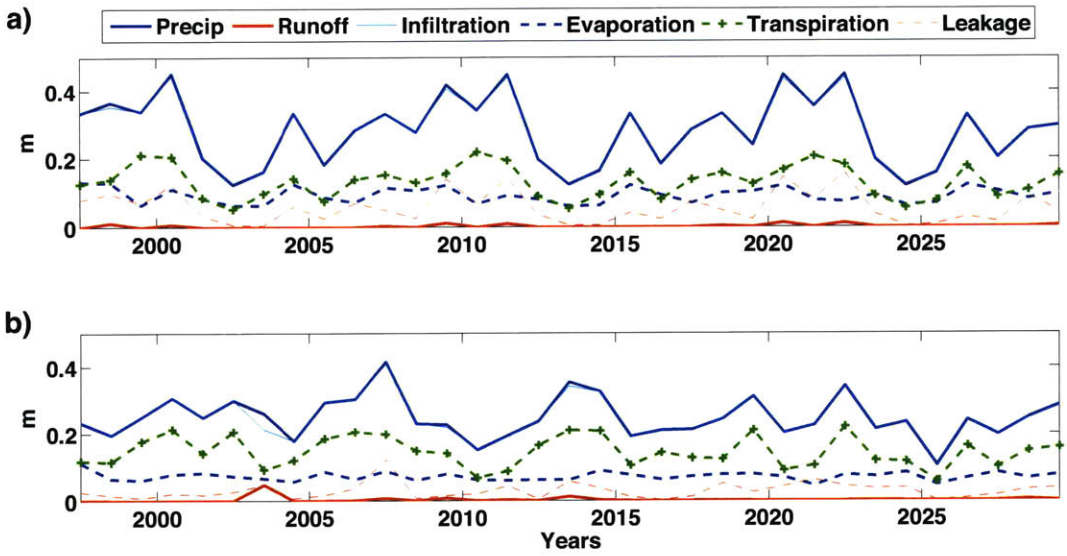

Figure 5-8: Annual accumulation of precipitation, infiltration, evaporation, transpiration and leakage in the basin in meters: a) using daily observed rainfall and b) using the BL algorithm. The initial topography in this simulation corresponds to the Kendall basin DEM with a 30 m resolution.

(PET) is low. That moisture can then be used by vegetation early in the spring. When winter moisture is available and spring growth does occur, vegetation growth is generally limited by available energy (reflected in PET) and moisture. This is shown in the higher average green vegetation on the south facing hillslope at the beginning of the spring in Figure 5-10. During the summer and early fall, vegetation growth is limited only by moisture availability, not energy. This is reflected in Figure 5-10 by less vegetation cover on the drier, sunny south facing terrain. Notice that it is in this period when the most biomass is produced due to the high energy availability (reflected in high PET) and monsoon rains. Despite the intensity of the monsoon rains in the modeled setting, soil moisture is lost rapidly due to leakage and evapotranspiration, and losses are higher in the south facing terrain. During winter, vegetation is dormant and its spatial distribution mainly reflects its previous fall disposition.

Vegetation growth in spring is higher when the WUE is dependent on temperature instead of a constant value, due to the low temperatures in spring. This amplifies the effects of higher evapotranspiration rates on south facing terrain early in the spring on vegetation distribution. The dependency of WUE on temperature also amplifies the differences in vegetation growth in the summer and fall between the north and south facing terrain, because the sunny drier south facing terrain is also hotter and thus has a lower WUE.

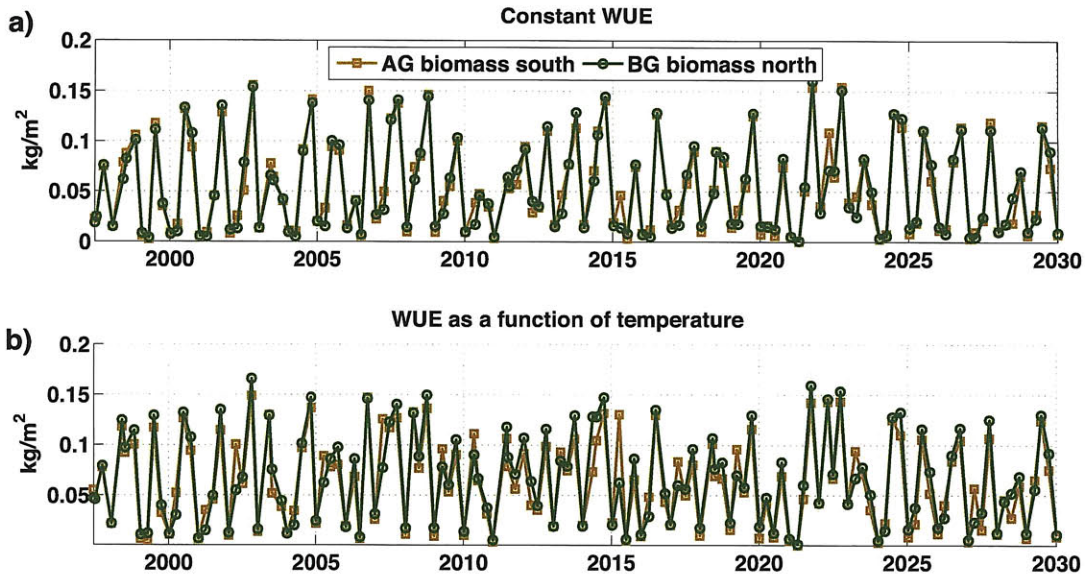

Figure 5-9: Above ground (AG) biomass in north and south facing terrain throughout 33 three years of simulation in CHILD, corresponding to current climatic conditions at the Kendall site: a) using a constant WUE and b) using a WUE that changes with temperature. The initial topography in this simulation corresponds to the synthetic field Topo2 described below in the experimental set up.

5.2.3 Feedback mechanism between ecosystem productivity and fraction of precipitation used by plants

Before discussing the long-term evolution of the landscape, a significant difference in usage of water by vegetation that manifests at smaller time scales is presented. This feedback mechanism only takes places when the vegetation dynamic processes are active.

The amount of total rainfall transpired by plants is dependent on the timing of rainfall, rainfall intensity, soil properties and vegetation. *Loik et al.* [2004] reported that the ratio of evaporation to transpiration (E:T) increases when rainfall intensity is low and/or interstorm durations are long. This is because under those conditions, in contrast to high intensity rainfall or rain events with short inter-storm periods, rainfall stays in the upper soil layers where higher evaporation losses occur.

A similar increase in the E:T ratio occurs in CHILD at an annual scale but for different reasons. In CHILD the annual E:T ratio increases during dry years, indicating that a smaller amount of the rainfall is transpired. Figure 5-11a illustrates the change in the E:T ratio during the first 33 years of the dynamic vegetation scenario over Topo1. Little annual precipitation leads to less grass leaves and as a consequence less transpiration. A lower transpiration rate leads to even less leaf biomass. This closes feedback mechanism between ecosystem productivity and fraction of the water used by plants. This feedback, absent in the static vegetation scenario (Figure 5-11b),

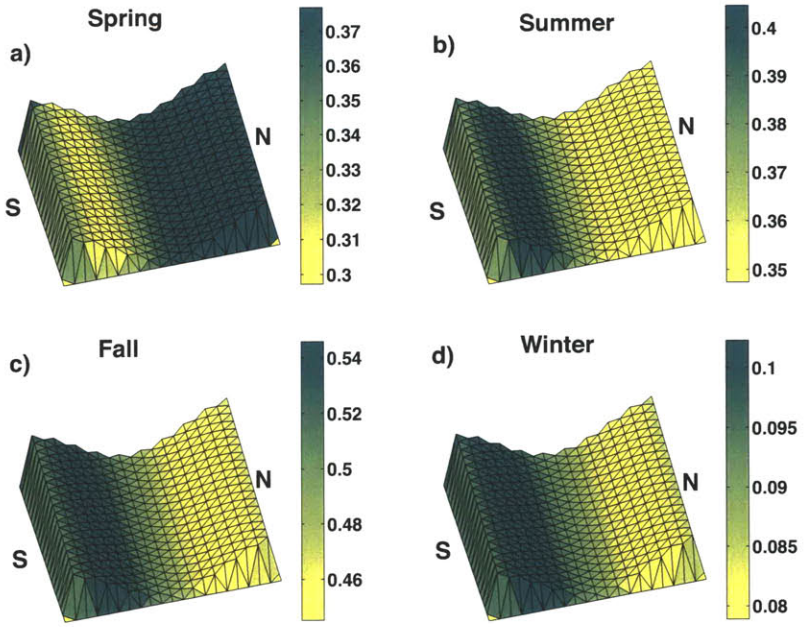

Figure 5-10: Time averaged vegetation cover fraction in the synthetic field Topo2 (see the experimental set up section below) for the 33 year simulation in CHILD, corresponding to current climatic conditions at the Kendall site using a WUE that changes with temperature, at the beginning of a) spring, b) summer, c) fall and d) winter.

leads to an increase in the E:T ratio during dry years, and also to a decrease in the E:T ratio in wet years. This feedback corresponds to L11, as described in Figure 5-1 and table 5.2.

For CHILD to capture the phenomenom described by Loik et al. [*Loik et al.*, 2004], a more detailed description of the vertical distribution of moisture is needed. Currently, as previously discussed in Chapter 3, CHILD assumes a 'bucket' model.

5.3 Results and discussion

The evolution of the landscape on each of the ten different simulations was monitored at every 100 years time steps during the 10 000 years of the simulation. The elevation, regolith depth, and root biomass maps at each 100 year time interval provided a picture of the changes taking place. The use of root biomass in the analysis of these simulations provides the advantage, over leaf biomass, that it changes slowly from year to year, thus, making it a better indication of the spatial distribution of vegetation productivity at yearly time scales. Figures 5-12 and 5-13 provide an example of the variability of the root and leaf biomass in the dynamic vegetation scenarios on Topo1 and Topo2, respectively, at different times of the simulation (years 0 - 10, 5 000 - 5 010, and 10 000 - 10 010).

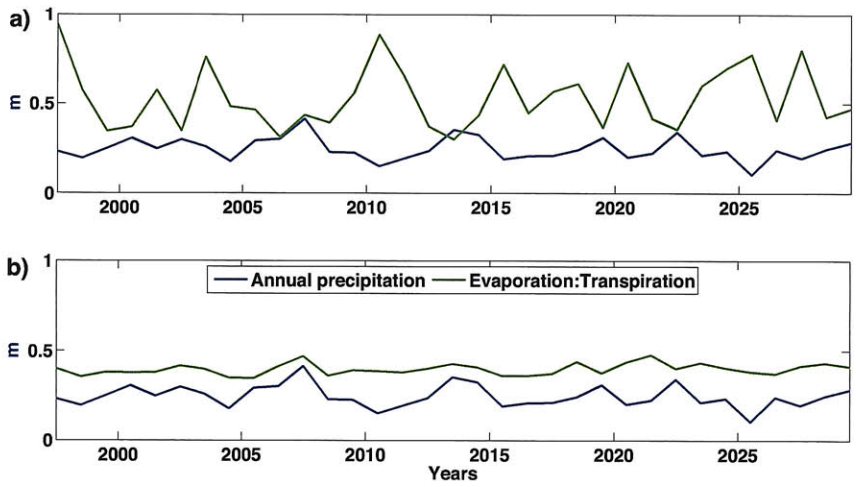

Figure 5-11: Precipitation and the ratio between annual evaporation and transpiration (E:T) corresponding to a) the same simulation depicted in Figure 5-8b, and b) the same simulation, but with a static or constant vegetation equal to the average AG vegetation cover of a).

Vegetation time series

Green biomass is similar in the north and south facing terrain. Yet, small differences of vegetation productivity are reflected as larger differences in the root biomass, which is larger in north facing terrain always, except during years 5000-5009 of the revegetation scenarios. Those years correspond to the first 10 years after vegetation has been introduced to the revegetation scenarios (years 5000-5009 in Figures 5-12b and 5-13b). During those 10 years, when vegetation develops starting from a nearly zero vegetation cover, slightly more vegetation grows in the south facing terrain.

More vegetation grows in the south facing terrain during those 10 years, and only during those years, because of two reasons. First, as is discussed in the following sections, bedrock outcrops form during the the first 5 000 years of simulation with no vegetation in the revegetation simulations. The bedrock outcrops generate runoff that infiltrates immediately downstream of the bedrock outcrop, forming moist areas. In those moist areas, during years 5000-5007, the growth of the initially light vegetation cover is limited by energy. Therefore, vegetation grows faster in the sunny south facing terrain, as reflected in Figures 5-12b and 5-13b. Second, as root biomass increases, so does transpiration and the vegetation's water requirement. Eventually growth is mainly water-limited, and vegetation growth becomes slower in the sunny south facing terrain ($\sim$ year 5008).

Figures 5-12 and 5-13 also show the evolution of root biomass in the east and west facing terrain (labeled as BG east/west aspects in the figures). In Topo1, the east/west aspects root biomass is in between that of the north and south aspects (except in years 5000 through $\sim$5007 of the revegetation scenario). This was expected

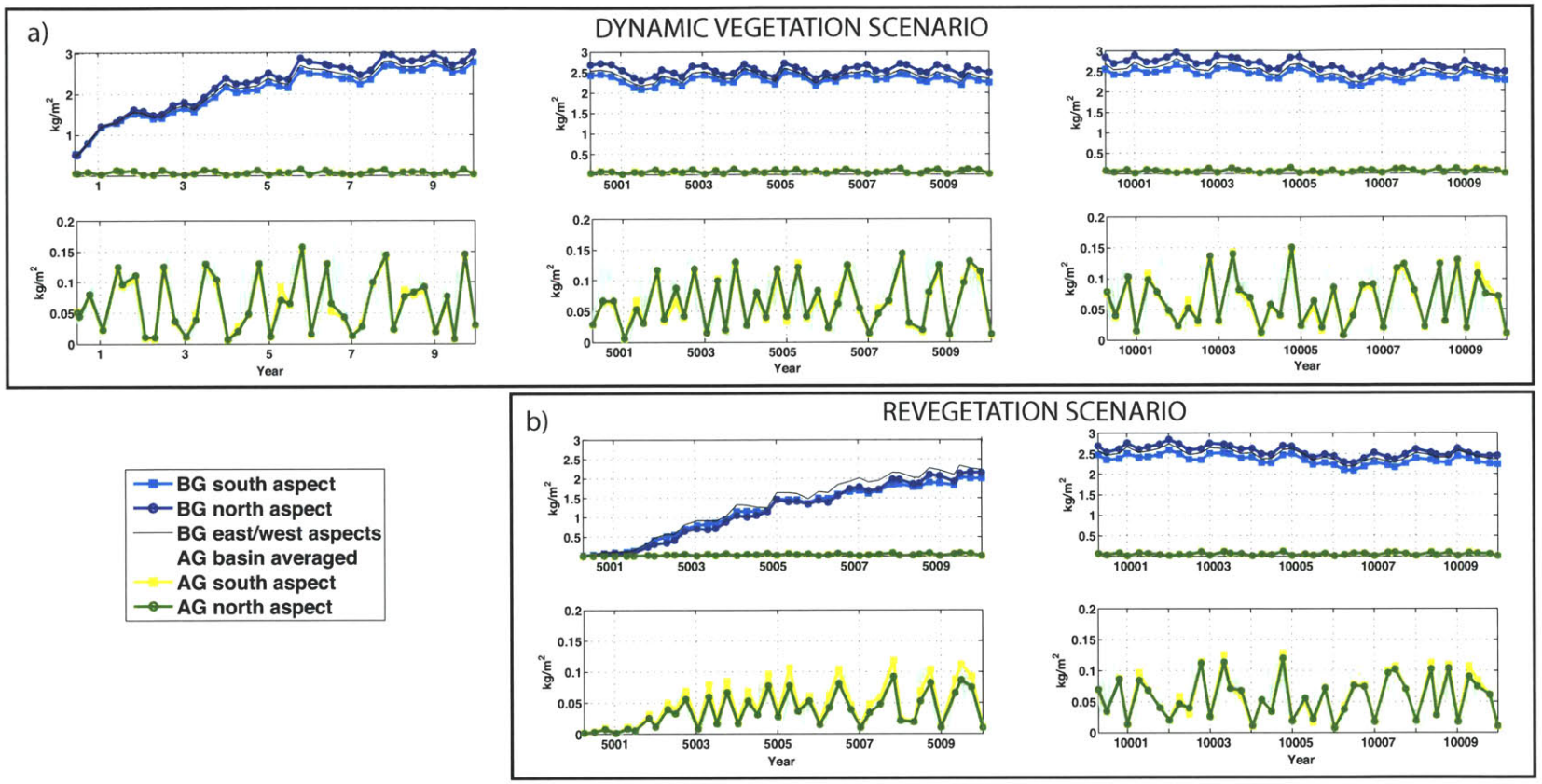

Figure 5-12: Time series representing the root and leaf biomass in the a) dynamic vegetation and b) revegetation scenarios of the simulations corresponding to Topo1. The figure shows the north and south aspect averaged root and leaf biomass at 0.25 year intervals, and the basin averaged leaf biomass at every time step of the simulation. The root and leaf biomass are presented in separate graphs of different scales in the y axis because their magnitudes differ by one order of magnitude.
BG = below ground (root) biomass, AG = above ground (leaf) biomass.

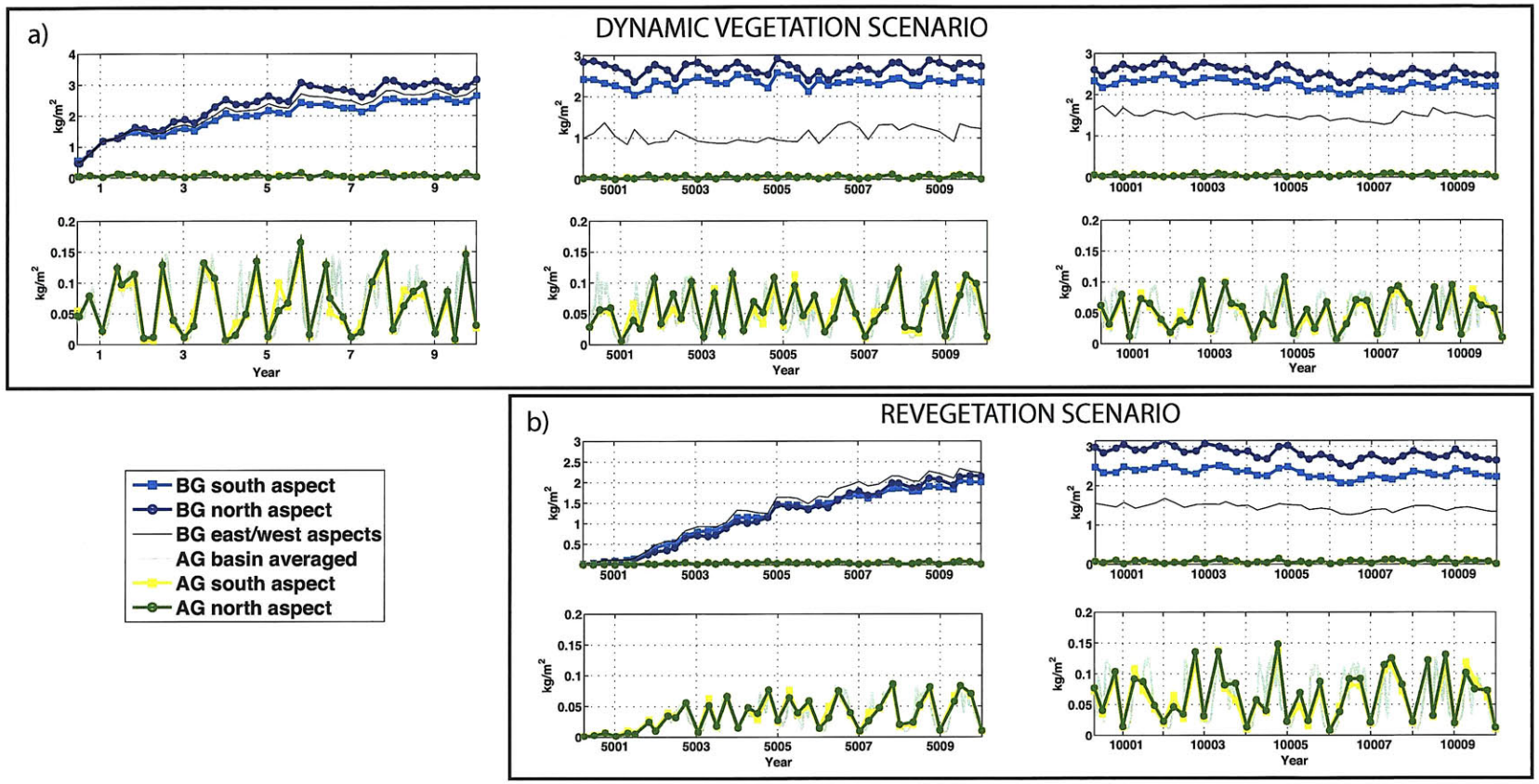

Figure 5-13: Time series representing the root and leaf biomass in the a) dynamic vegetation and b) revegetation scenarios of the simulations corresponding to Topo2. The figure shows the north and south aspect averaged root and leaf biomass at 0.25 year intervals, and the basin averaged leaf biomass at every time step of the simulation. The root and leaf biomass are presented in separate graphs of different scales in the y axis because their magnitudes differ by one order of magnitude.
BG = below ground (root) biomass, AG = above ground (leaf) biomass.

because the solar angle of incidence in the east and west aspects is intermediate between the north and south aspects. In Topo2, where west aspects do not occur, root biomass in the east aspect is also in between that of the north and south aspects in the dynamic vegetation scenario during the first years before bedrock outcrops develop (see years 0-9 in Figure 5-13a). Once bedrock outcrops develop, root biomass in the east aspect becomes approximately half of that in north and south aspects (except in years 5000-5009 in the revegeation scenario). This is because the bedrock outcrops in the Topo2 simulations appear on the ridges upstream of the north and south facing hillslopes of the domain (see Figure 5-3 for reference). These outcrops produce runoff that infiltrates in the hillslopes, and not in the valley, resulting in higher biomass productivity in the hillslopes. Because the hillslopes face north and south, and the valley east, vegetation cover is higher in the north and south aspects than on the east aspect.

5.3.1 Surface heterogeneity

The heterogeneous distribution of vegetation in space affects the degree to which geomorphic processes act on the land surface and this has been seldom considered in landscape evolution models until recently. Another aspect seldom considered in landscape evolution models, which was found in these simulations to produce larger changes in the surface properties than vegetation, and to have significant effects on landscape evolution, is the contrast between exposed bedrock and regolith covered terrain. For reference, maps of regolith depth, bedrock erosion, and total erosion (sediment and bedrock) and deposition for Topo1 and Topo2 are provided in Figures 5-14, 5-15, 5-16, 5-17, 5-18 and 5-19.

Bedrock exposure

In all the simulation scenarios with the exception of the static vegetation scenario, the regolith mantle was removed from some parts of the domain. This resulted in regions with bedrock at the surface. Because bedrock is impermeable in the model, all the rainfall that fell on these surfaces became runoff. In contrast, a very small fraction of the precipitation on regolith covered terrain became runoff. For example, in the simulation shown in Figure 5-8b, in which all the terrain is covered by regolith, only one year out of 33 had significant runoff. This difference in runoff production results in a significant increase in fluvial erosion on the bedrock, and sediment and moisture accumulation immediately downstream of the exposed bedrock-regolith interface.

The effect of bare surface, or rock outcrops and terrain with a high concentration of rock fragments, on ecosystems of arid regions is well documented (e. g., *van Wesemael et al.* [1998]; *Yair* [1990, 1995]). The runoff produced in these areas with little or no soil mantle infiltrates where it runs into a permeable soil mantle. This results in concentrated amounts of moisture downstream of the runoff-generating areas, benefiting vegetation and other life forms at that location. Some ecosystems

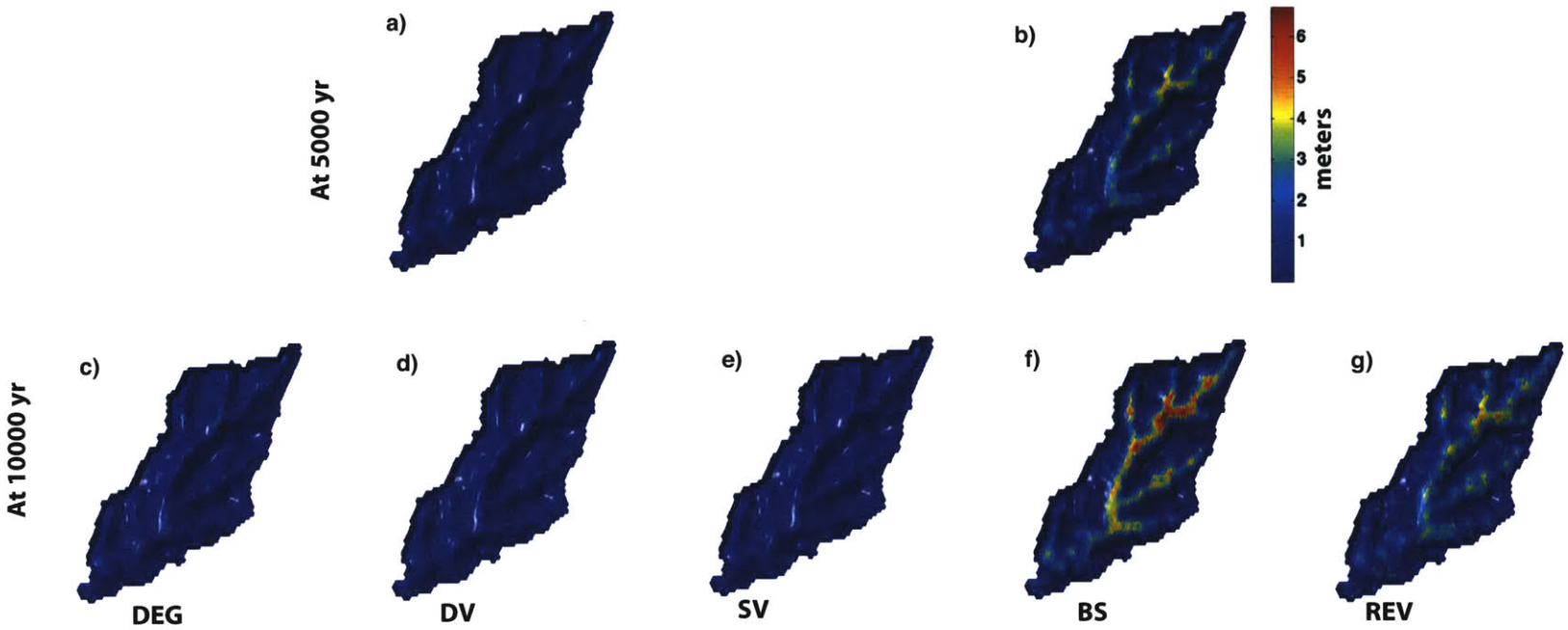

Figure 5-14: Regolith depth after 5 000 and 10 000 years for 5 different scenarios corresponding to Topo1.
DV = Dynamic vegetation, SV = Static vegetation, BS = Bare surface, REV = Revegetation, DEG = Degradation.

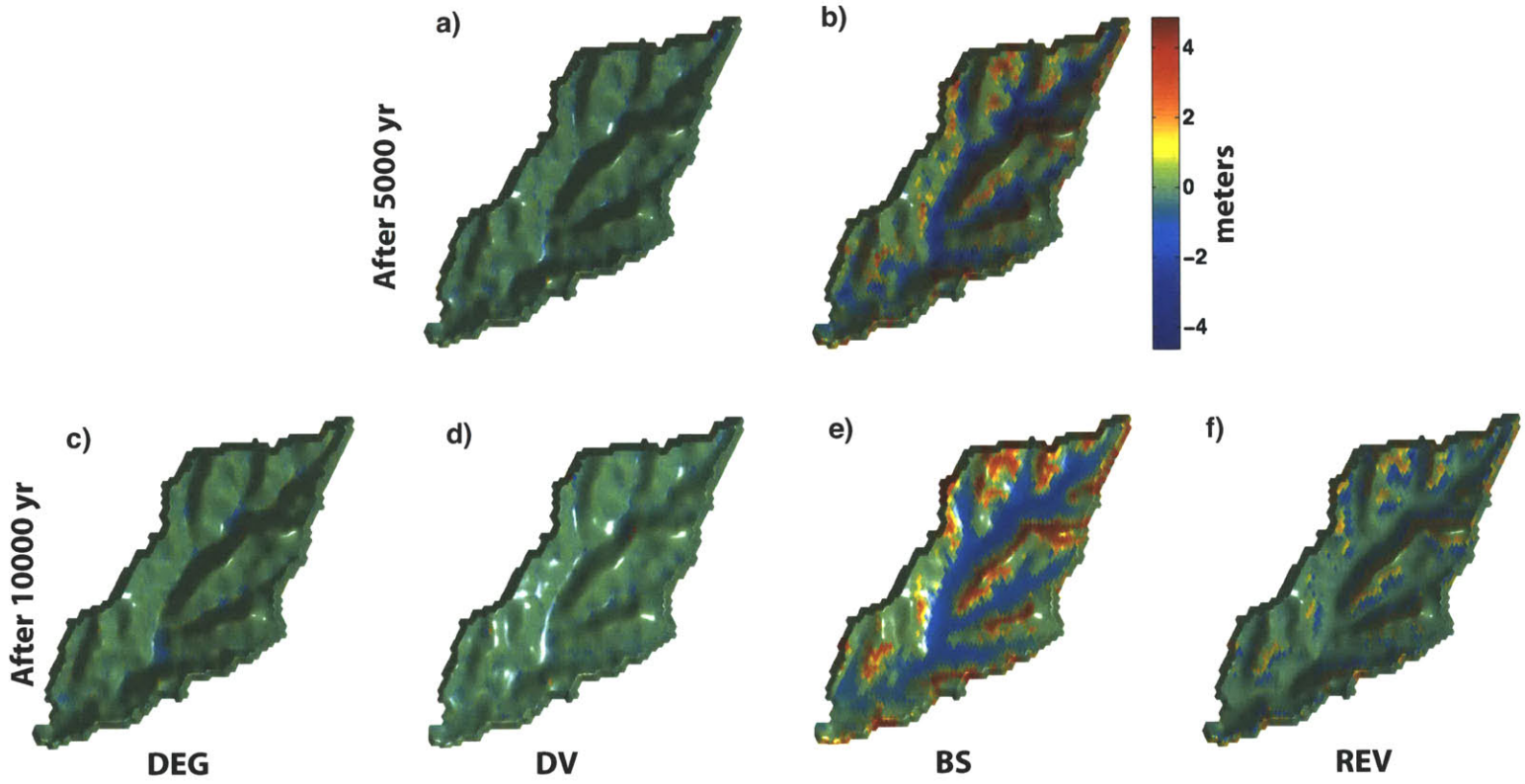

Figure 5-15: Total erosion and deposition (net changes in elevation) during 5 000 years for four different scenarios starting with Topo1. Positive values (warm hues) indicate erosion, and negative values (cool hues) deposition.
DV = Dynamic vegetation, BS = Bare surface, REV = Revegetation, DEG = Degradation.

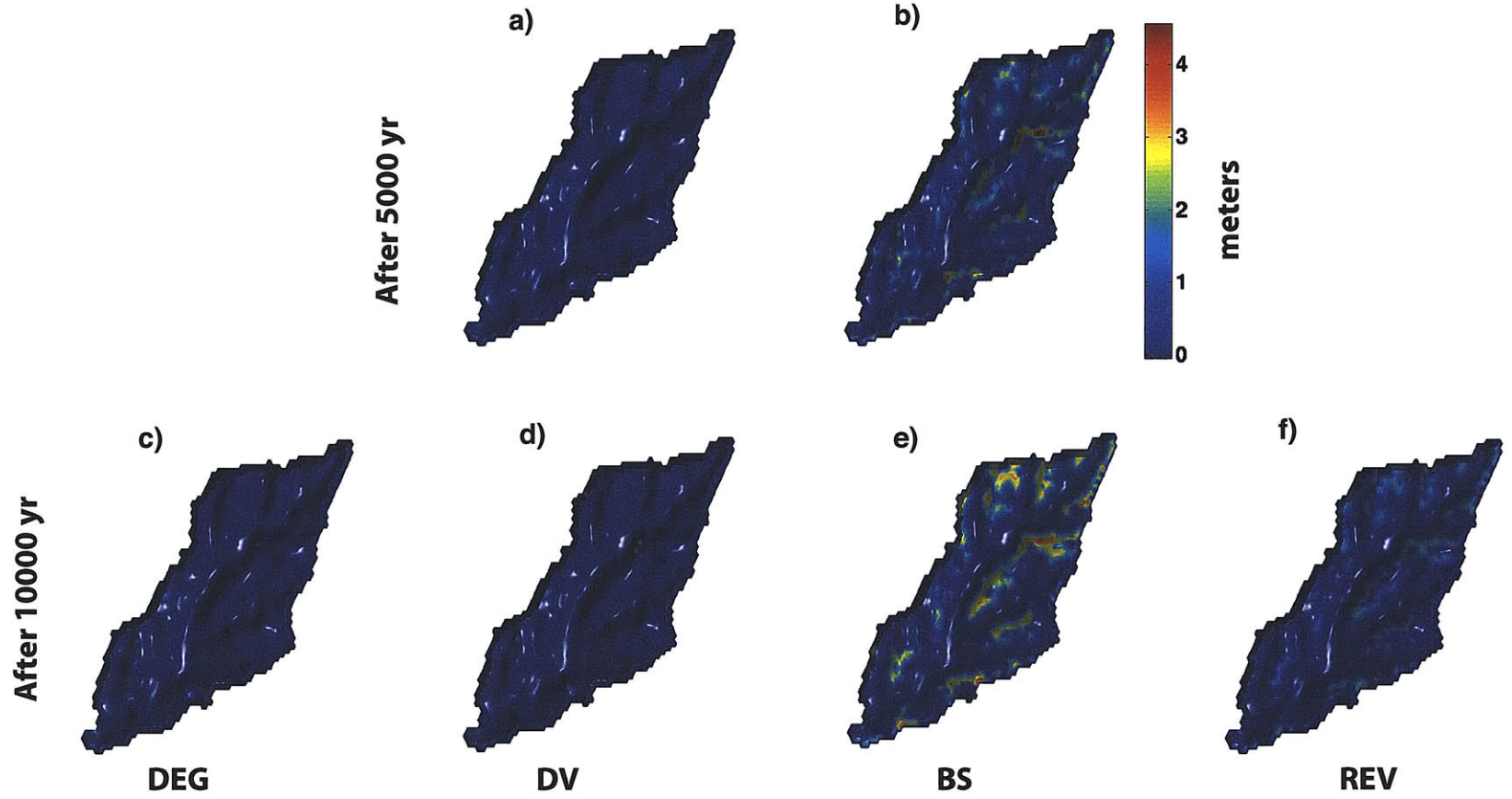

Figure 5-16: Bedrock erosion in 5 000 years corresponding to four different scenarios starting with Topo1.
DV = Dynamic vegetation, BS = Bare surface, REV = Revegetation, DEG = Degradation.

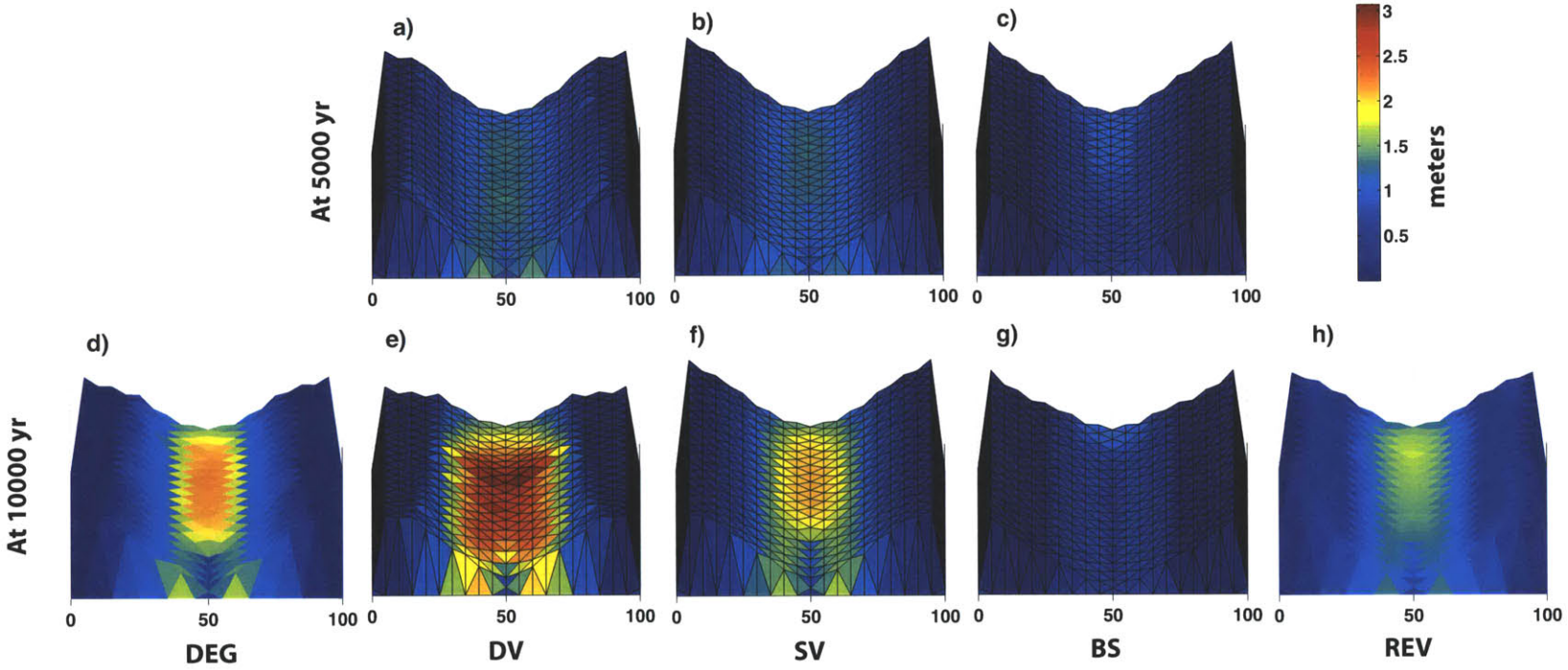

Figure 5-17: Regolith depth after 5 000 and 10 000 years of simulation for the 5 different scenarios considered in Table 5.2 starting with Topo2.

DV = Dynamic vegetation, SV = Static vegetation, BS = Bare surface, REV = Revegetation, DEG = Degradation.

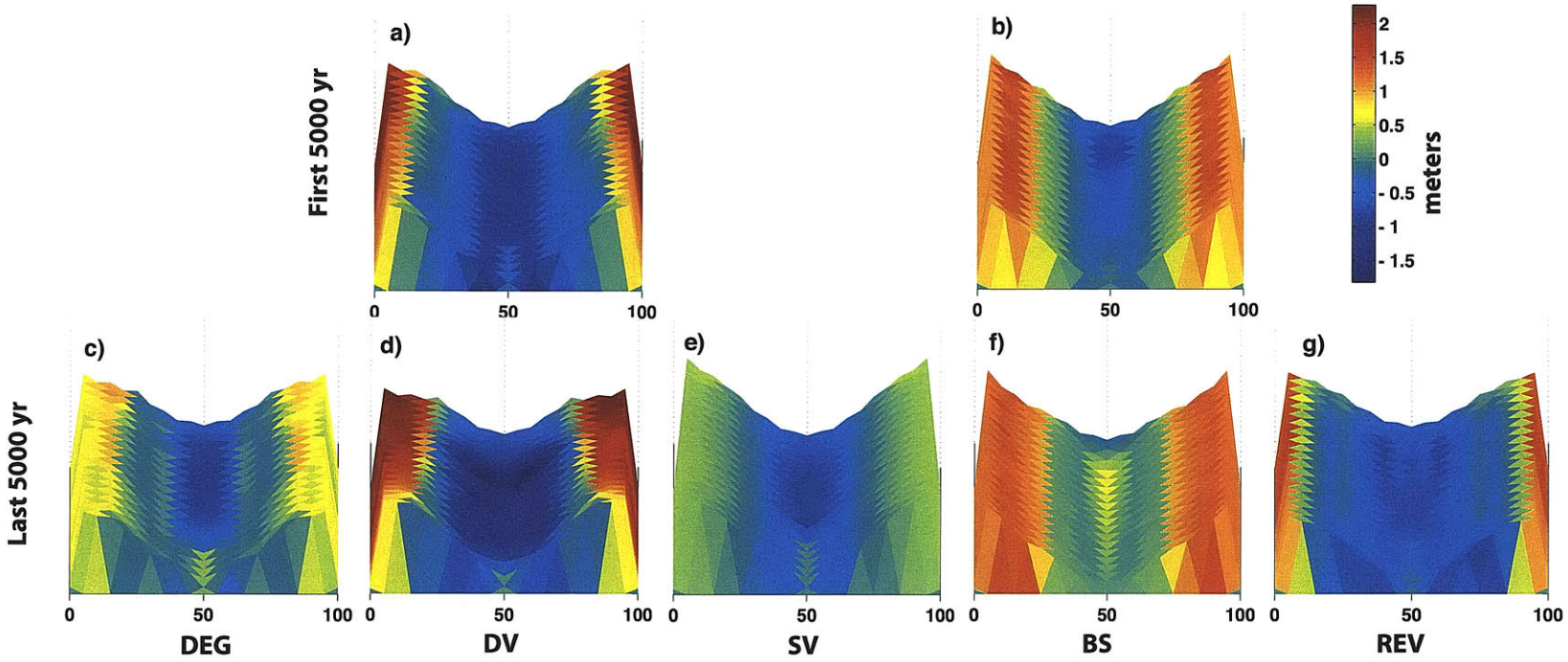

Figure 5-18: Changes in elevation in 5 000 years for the different scenarios starting with Topo2. Positive values (warm hues) indicate erosion, and negative values (cool hues) deposition.
DV = Dynamic vegetation, SV = Static vegetation, BS = Bare surface, REV = Revegetation, DEG = Degradation.

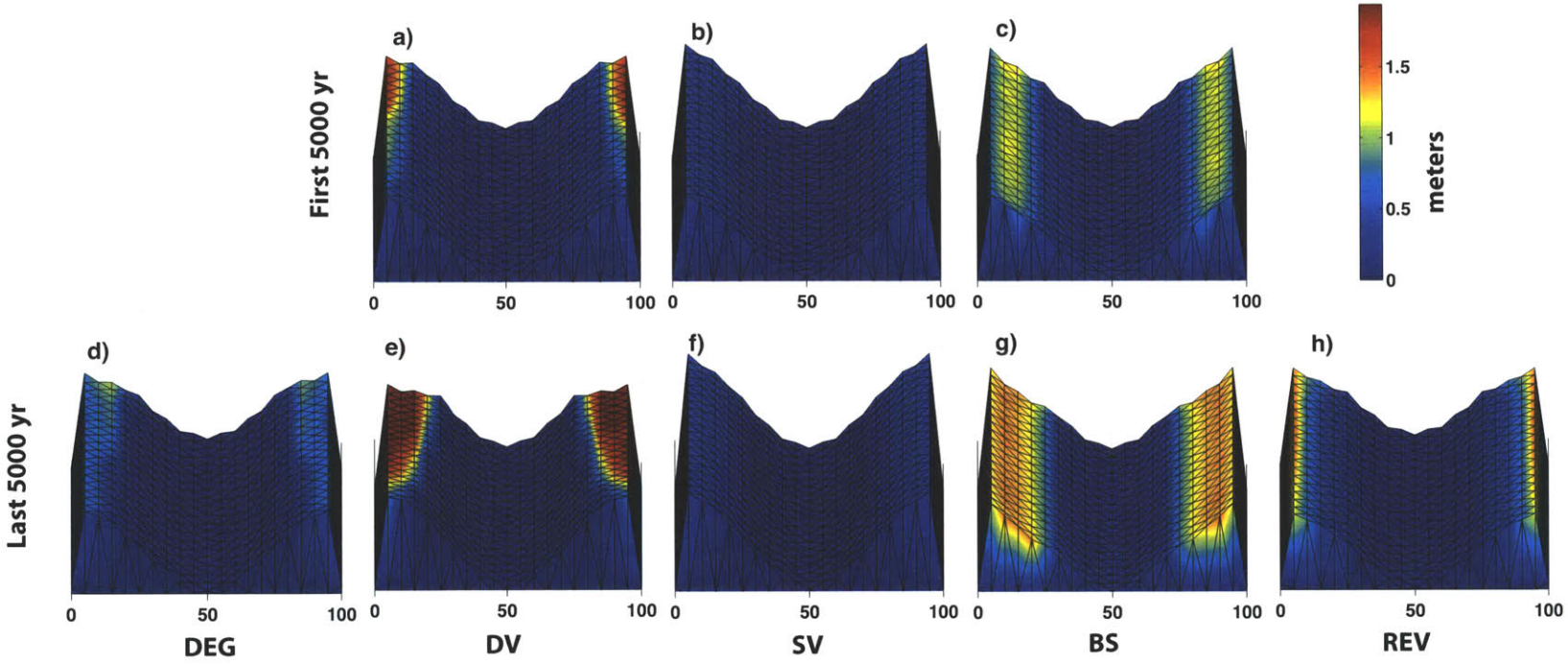

Figure 5-19: Bedrock erosion in 5 000 years for the different simulation cases starting with Topo2.
DV = Dynamic vegetation, SV = Static vegetation, BS = Bare surface, REV = Revegetation, DEG = Degradation.

actually depend on this mechanism of moisture accumulation for subsistence [*Yair and Kossovsky*, 2002]. In addition, fluvial erosion is active on the runoff producing areas, and negligible elsewhere [*Yair and Kossovsky*, 2002; *Kuhn et al.*, 2004].

The effects of bare bedrock on ecosystem productivity in the scenarios where vegetation dynamics are active are illustrated in Figures 5-20, 5-21, 5-22 and 5-23. The first two figures correspond to Topo1 at year 10 000 of the simulation, and the following two to Topo2 at various times in the simulation. In the case of the dynamic vegetation scenario for Topo1 (Figure 5-20), only individual modeling elements with steep slopes had exposed bedrock, where as in the revegetation scenario (Figure 5-21), larger portions of the terrain consist of bedrock. The larger bedrock areas in the second case produce more moisture accumulation at the bedrock-regolith horizontal interface. This larger accumulation is reflected in the ecosystem productivity, as root biomass in the second case reaches values twice as high as in the first case.

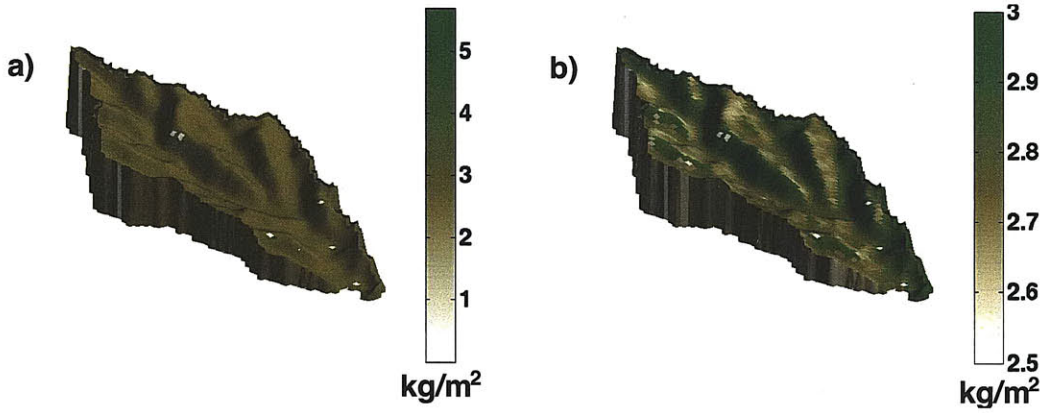

Figure 5-20: Root biomass distribution corresponding to Topo1 dynamic vegetation scenario at year 10 000, in kg/m^2. The color bar in a) shows the total range of root biomass values, where as the color bar in b) shows a narrower range of values to make clearer the difference among north and south facing hillslopes.

The values of root biomass shown in the figures are a few times larger than those expected for semiarid grassland ecosystems. Thus, it is likely that under such accumulation of moisture, other plant functional types that are not represented in the model grow, in particular woody vegetation. Other possibility is that grass growth under these circumstances becomes limited by factors such as nutrients or light, limitations not considered in the present model.

Regolith removal and extension

Bedrock effects on the landscape depend on the extent of exposed bedrock, which is limited by the distribution of a regolith mantle. Redistribution of regolith leads to regolith removal when erosion processes are intense, as is the case in the absense of vegetation, and when the initial regolith mantle is thin. Zones prone to erosion, such

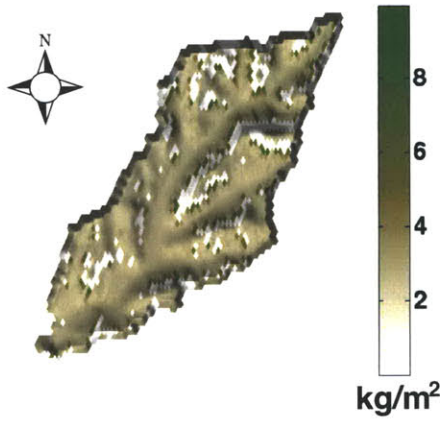

Figure 5-21: Root biomass distribution corresponding to the Topo1 revegetation scenario at year 10 000, in kg/m^2.

as steep terrain, and zones with little sediment supply such as ridges, are more likely to lose their regolith mantle than gentle sloping terrain or terrain with large drainage areas. This is clear in Figure 5-24, that shows the distribution of bedrock erosion in Topo1 during the years 5 000 through 10 000 of the bare surface scenario simulation. Bedrock erosion is a reflection of zones where the regolith mantle has been removed. Those regions correspond to zones with steep slopes and small contributing areas.

Once bedrock is exposed, the high runoff generation can lead to further regolith removal and bedrock exposure extension. In the absence of vegetation, this feedback loop corresponds to L10, as described in Figure 5-1 and Table 5.2, and continues until the sediment supply limits the removal of the regolith, or runoff diverts and flows somewhere else. In the presence of vegetation dynamics, however, vegetation is abundant at the bedrock-regolith horizontal interface, and its abundance increases with upstream bedrock surface. This limits the removal of regolith, and in some circumstances, allows for an extension of the regolith mantle into bare bedrock terrain. As water flows into the regolith covered terrain, it infiltrates and deposits its sediment load. This leads to the accumulation of sediment at the interface and eventually the extension of the regolith mantle. In contrast with the zones prone to regolith removal, zones prone to regolith extension are gentle sloping terrain and zones with upstream sources of sediment.

One example of this regolith extension mechanism takes place in the Topo2 revegetation scenario. In this simulation, during the first 5 000 years of simulation without vegetation, bands of exposed bedrock formed along the ridges. At year 5 000 the dynamic vegetation processes were added to the system. Figure 5-23 shows the evolution of the vegetation in the following 5 000 years. After 4 300 years of evolution with vegetation (year 9 300 in the simulation), a significant portion of the previously exposed bedrock is covered with regolith and vegetation. This mechanism that leads to regolith mantle expansion is part of the loop L100, as described in Figure 5-1 and Table 5.2.

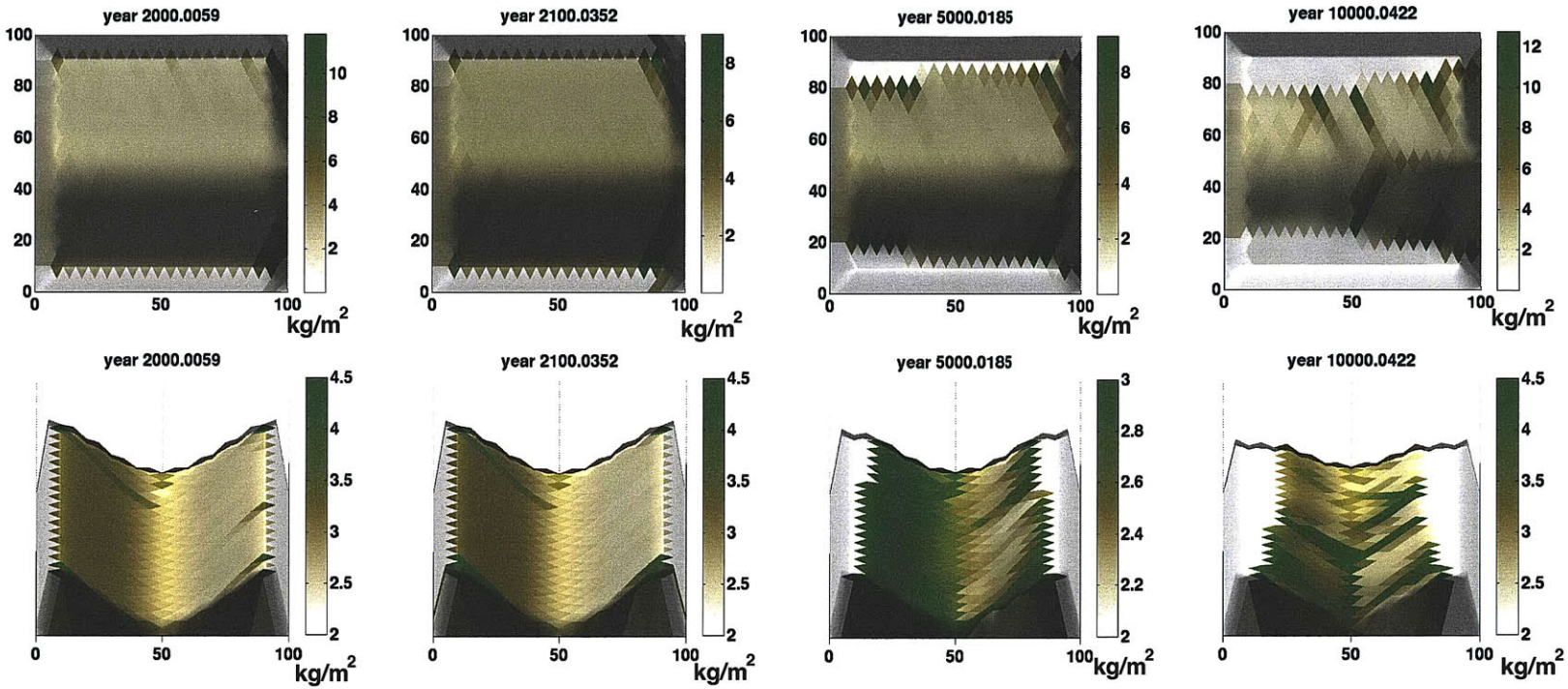

Figure 5-22: Root biomass distribution corresponding to the Topo2 dynamic vegetation scenario at various times along the simulation, in kg/m^2. The top panels are top views of the simulation, where as the bottom panels are views from the east into the simulation domain. The color scale of the bottom panels shows a reduced range in root biomass values to highlight differences in vegetation values within that range.

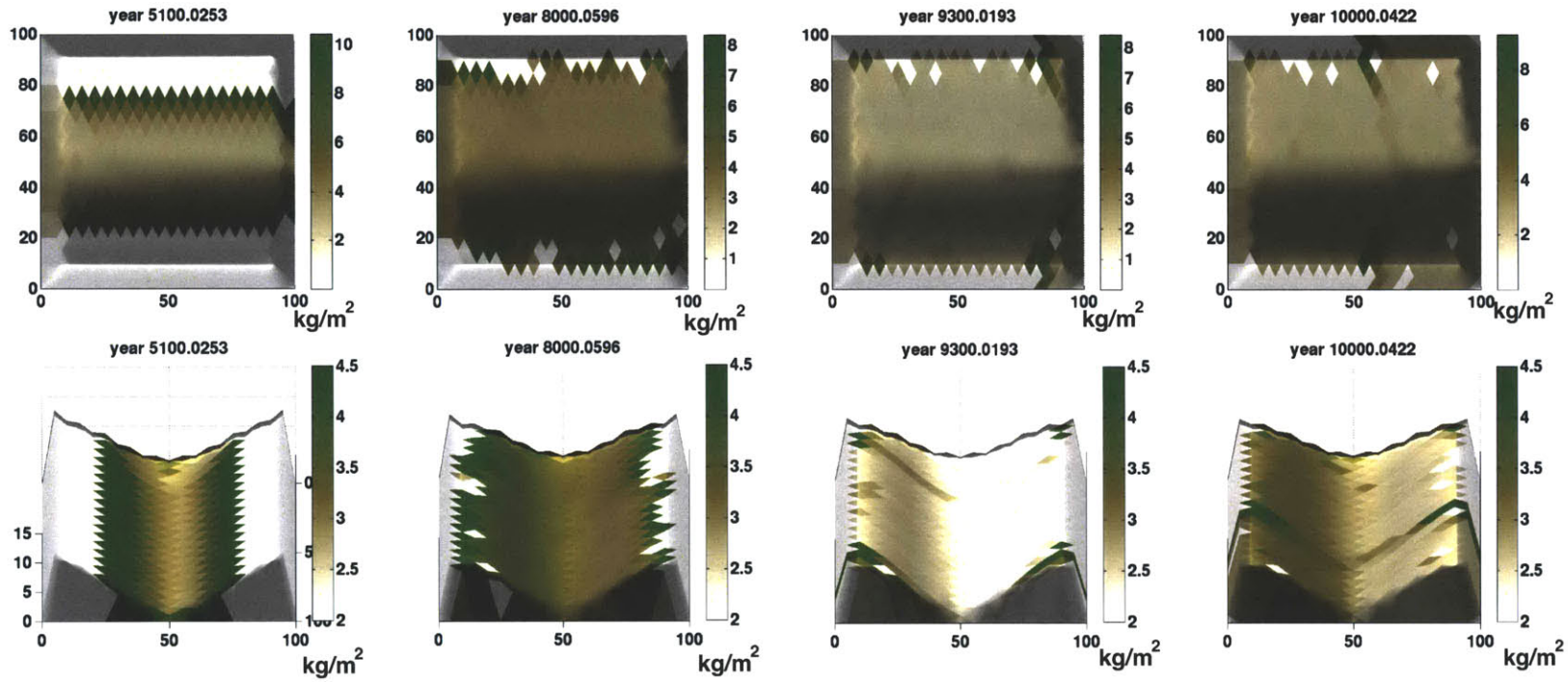

Figure 5-23: Root biomass distribution corresponding to the Topo2 revegetation scenario at various times along the simulation, in kg/m^2. The top panels are top views of the simulation, where as the bottom panels are views from the east into the simulation domain. The color scale of the bottom panels shows a reduced range in root biomass values to highlight differences in vegetation values within that range.

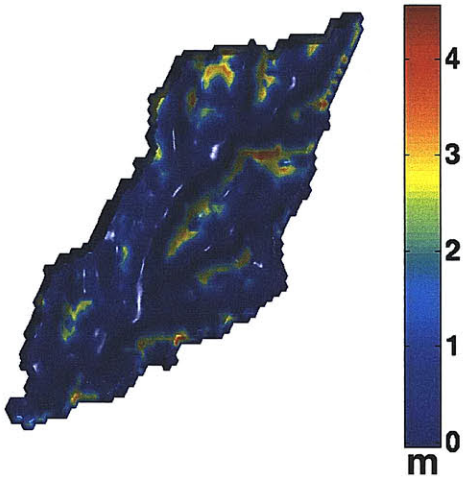

Figure 5-24: Bedrock erosion distribution corresponding to the last 5 000 years of the Topo1 bare surface scenario, in meters.

In addition to vegetation, regolith depth is a controlling factor of regolith removal. This was evident in the degradation scenarios corresponding to Topo1 and Topo2. In those simulations, vegetation cover during the first 5 000 years of the simulation (equivalent to the first 5 000 years of the dynamic vegetation scenarios) resulted in regolith accumulation in the terrain, and some bedrock weathering. Bedrock weathering increased regolith depth in the order of tens of centimeters, which is significant relatively to the initial regolith depth in these simulations ($0.3m$). These changes in regolith depth reduced the bedrock extension significantly in comparison to bedrock extension in the first 5 000 years of the bare surface scenario. This is reflected in the bedrock erosion rates in the 5 000 years of landscape evolution without vegetation in the degradation scenario, that indicate smaller regions of exposed bedrock than those in the first 5 000 years of the landscape evolution under the bare surface scenario (compare Figures 5-16b and 5-16c, and 5-19c and 5-19d).

In these simulations bedrock erodibility is high ($0.05\ m\ yr^{-1}Pa^{-1}$) and corresponds to soft bedrocks. If the bedrock erodibility were orders of magnitude lower, as is the case of hard rocks, (e.g., $10^{-5}\ m\ yr^{-1}Pa^{-1}$ [*Tucker and Slingerland*, 1997]), bedrock erosion would be negligible in these simulations. Under those circumstances regolith removal would be more extensive in the bare surface scenarios, due to the lack of sediment supply at the bedrock-regolith horizontal interface, and regolith extension would occur at a much slower rates in the cases when vegetation dynamics were present in the system.

Patterns of erosion and deposition

Patterns of exposed bedrock and vegetation at the bedrock-regolith horizontal interface lead to localized erosion (on the bedrock) and deposition (at the bedrock-regolith

horizontal interface), and as a consequence to patterns of erosion and deposition. This is illustrated in Figures 5-24, 5-25a and 5-25b .

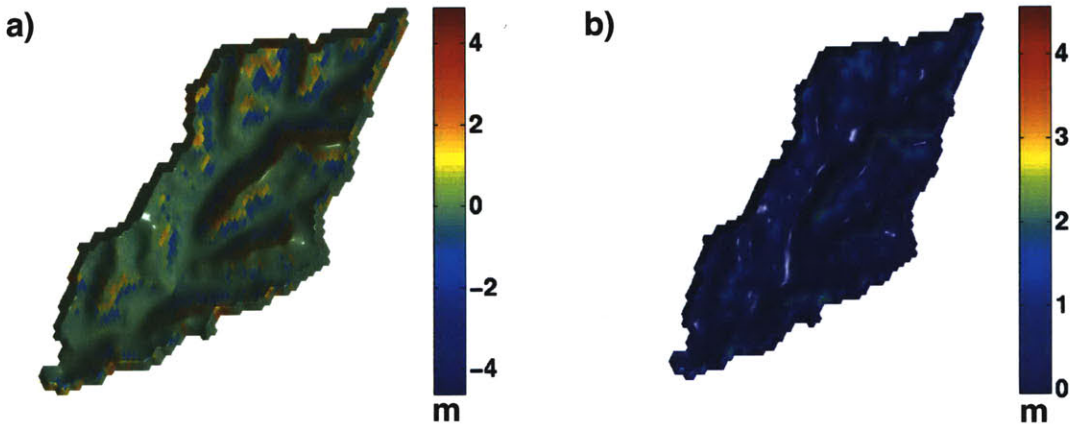

Figure 5-25: Maps of erosion and sedimentation corresponding to the last 5 000 years of the Topo1 revegetation scenario, in meters. Positive values mean erosion, and negative values deposition. a) Absolute erosion and deposition , b) bedrock erosion only.

Exposed bedrock resulted in large quantities of bedrock erosion and generation of sediment. In the bare surface scenarios, the produced sediment moved away from the hillslopes. In the small synthetic domain (Topo2), sediment left the domain (Figures 5-18b and 5-18f), whereas in the larger 30 m DEM simulation domain (Topo1), sediment deposited in the valley network, producing significant valley aggradation (Figures 5-15b and 5-15e). In the vegetated scenarios, in contrast, sediment movement was slower. In the small synthetic domain (Topo2), sediment deposited in the valley (Figures 5-18a, 5-18d, 5-18e and 5-18g), whereas in the larger topographic domain (Topo1), sediment deposited at the bedrock-regolith limit (Figures 5-15a, 5-15d and 5-15f), where vegetation was abundant. The above generated clearly different patterns of erosion and deposition among the various simulation scenarios.

5.3.2 Vegetation bands

Another vegetation pattern forms, besides the one that forms at the bedrock-regolith horizontal interface previously described. This pattern clearly manifests in the Topo2 simulation during the vegetation dynamics and revegetation scenarios, and consists of bands of vegetation that start close to the top of the ridge, and descend towards the valley bottom, as shown in Figures 5-22 and 5-23. Vegetation is is most abundant in the upper side of the band, at the bedrock-regolith horizontal interface, where it begins, and gradually decreases in abundance in the downstream direction. In addition, once these bands form, they migrate in the direction parallel to the valley axis, at rates of approximately 5 m every 100 years.

In the dynamic vegetation scenario (Figure 5-22), these bands begin to form around the year 2 100 of the simulation. Initially, the vegetation bands appear on the eastern edge of the elevation domain. This is because runoff generated on the bare bedrock along the ridges drains to the east. Runoff from those bare bedrock regions does not flow directly towards the valley, as in the bare surface scenario, because sediment accumulates at the bedrock-regolith boundary. The sediment accumulation creates an mound at the boundary, and this prevents water from crossing the interface. Instead, water flows along the bare bedrock area in the east direction, until it reaches the artificial impermeable eastern boundary of the modeling domain (the only outlet of the modeling domain is the eastern end of the valley axis). Once it reaches the eastern boundary, it begins to drains in the downward direction, creating vegetation strips (on the north and south facing hillslopes).

As these vegetation bands capture sediment, they increase their elevation relative to the contiguous areas, and eventually, the water flow changes its course, resulting in the westward migration of the vegetation strips. By the year 5 000, a change in the thickness of the bare bedrock region along the western end of the ridges creates a new drainage configuration that results the creation of additional vegetation bands. These bands sometimes move in the valley's upstream direction (towards the west), as described above. But some times they move in the valley's downstream direction (towards the east), due to the broadening of the bare bedrock region developing along the ridges.

The effects of the runoff generated on the bedrock outcrops on vegetation distribution, and the implications of the resulting vegetation distribution interplay with the erosion and sedimentation processes, can occur only when the vegetation dynamics are represented in the landscape system.

5.3.3 Effects of the vegetation cover at the basin scale

The slope area diagram is a widely used tool in geomorphology that clearly defines regions in a basin dominated by diffusive erosion processes, and fluvially dominated processes. Slope and drainage area adjust as these two erosive processes shape the basin, resulting in an increase in terrain slope with drainage area in the diffusive dominated terrain, which corresponds to convex shaped hillslopes generally in the regions with smaller drainage area. In contrast, an inverse relationship between drainage area and slope is found in the fluvial erosion dominated terrain. Fluvial erosion dominated terrain consists of either concave hillslopes or valley and channel networks.

Slope area diagrams for each simulation scenario are presented in Figures 5-26 and 5-27, for the Topo1 and Topo2 initial conditions, respectively. These figures show, with large circles linked with lines, the mean slope corresponding to different drainage areas. The points show the slope of each individual mesh element of the model, as a function of drainage area. The Topo1 simulations correspond to a basin where the terrain has previously adjusted to diffusion and fluvial erosive processes. Because of that, and because this basin is large enough to exhibit a clear drainage structure,

the slope area diagram is more useful than for the Topo2 simulations. In the Topo1 initial conditions, the transition from diffusive to fluvial dominated terrain is at a drainage area of approximately 2 000 m^2. The Topo2 domain is too small to show such organization in the slope area diagram. In addition it is a synthetic domain that has not adjusted to the erosive processes.

As the simulations evolve, slopes in Topo1 become more organized in terms of the slope-area relationship. The slopes in Topo2 sometimes lose order, in particular in the dynamic vegetation and degradation scenarios, where significant erosion at the ridges and sedimentation at the valleys produce a basin desorganized in terms of the slope area diagram. Despite these differences, some common organizational tendencies manifest in the slope area diagrams for both initial topographic settings.

When fluvial erosion is maximum, that is in the bare surface scenarios, slopes organize as a function of drainage area corresponding to a fluvially dominated erosion processes (slope decreases with drainage area). The organization of slopes is reflected in a reduction in the spread of slopes of individual modeling elements (dark blue dots). In the Topo1 bare surface simulation, the slope for drainage areas larger than 100 000 m^2 becomes nearly constant, probably due to the filling of the valley bottoms with sediment. Signatures such as this are likely to be found in arid landscapes or recently degraded terrain (that is, where vegetation has been recently removed).

When fluvial erosion is limited by vegetation, changes in the slope area diagram are smaller, except when vegetation dynamics trigger intense bedrock erosion in a large portion of the simulation domain. That is the case of the vegetation dynamics and degradation scenarios corresponding to Topo2.

The slope area diagram indicates a subtle difference between the dynamic vegetation and static vegetation scenarios corresponding to Topo1. This is the reduction in the spread of slopes in the dynamic vegetation scenario, particularly for large drainage areas, but not in the static vegetation scenario. This implies that there is more fluvial erosion in the dynamic vegetation scenario, particularly along the drainage network. This becomes evident when the differences between the elevation fields of the dynamic vegetation and static vegetation senarios at year 10 000 are calculated. These differences are shown in Figure 5-28.

Finally this basin scale analysis indicates that differences in the slope area diagram between the dynamic vegetation and degradation scenarios, or the bare surface and revegetation scenarios, corresponding to Topo1, are small. Each of these two sets of scenarios share the same landscape evolution system during the first 5 000 years of simulation (see the 'Experimental setup' section for reference). This implies that little change took place in the organization of the basin in the last 5 000 years of these four simulation scenarios. This underscores four things. First, that the build up of the soil mantle in the first 5 000 years of the degradation scenario prevents the removal of regolith during the following 5 000 years of the simulation, when the system is void of vegetation. Second, bedrock exposure seriously affects the basin organization in terms of the slope-area relationship. The main reason why erosion is limited in last 5 000 years of the degradation scenario even though the surface is void of vegetation is that

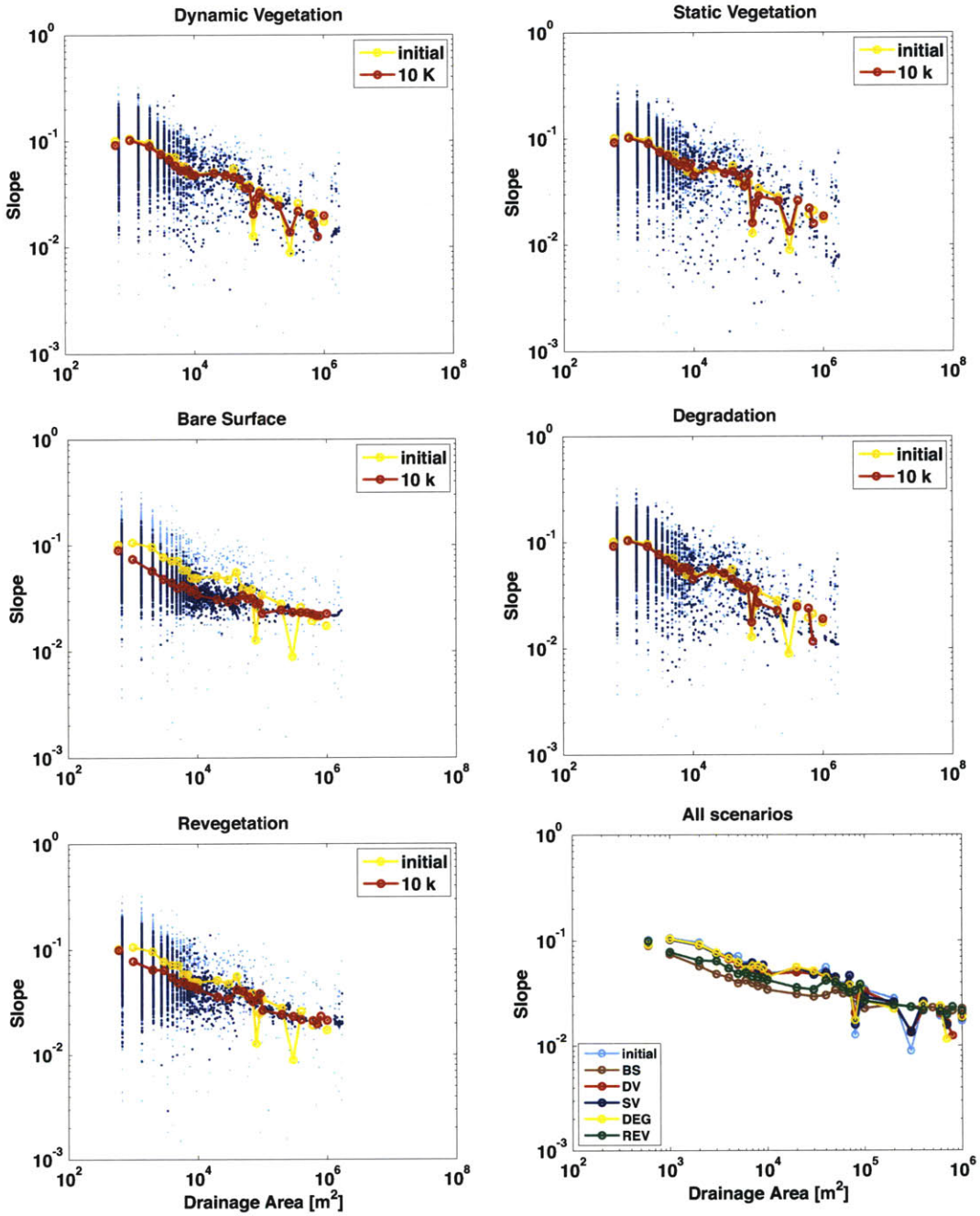

Figure 5-26: Slope area diagram for each scenario starting with Topo1. The light blue and dark blue dots represent the initial and final conditions of each mesh element of the model, respectively. Yellow and red circles linked with lines correspond to the mean slope for different drainage areas of the initial and final conditions, respectively.

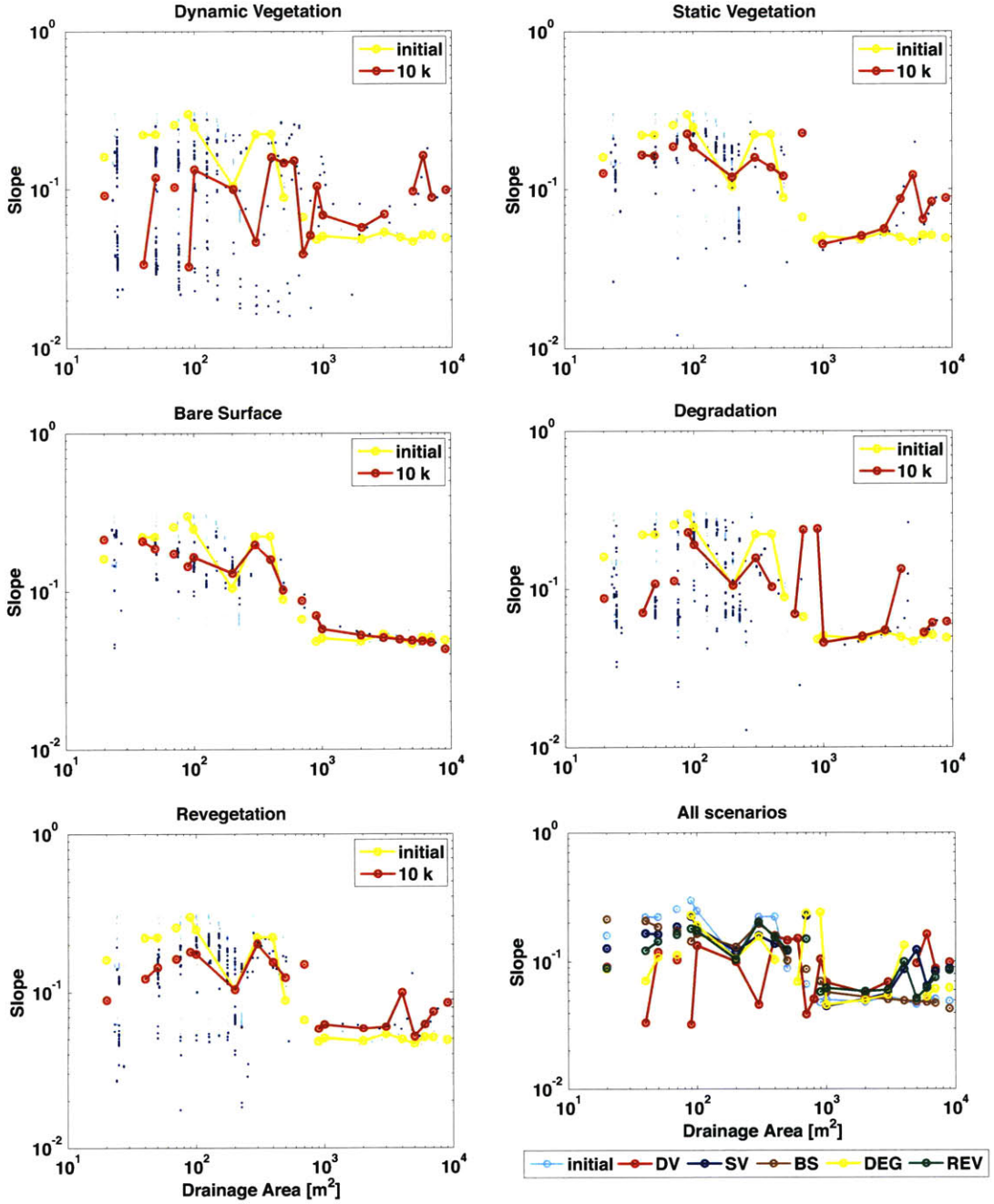

Figure 5-27: Slope area diagram for each scenario starting with the Topo2. The light blue and dark blue dots represent the initial and final conditions of each mesh element of the model, respectively. Yellow and red circles linked with lines correspond to the mean slope for different drainage areas of the initial and final conditions, respectively.

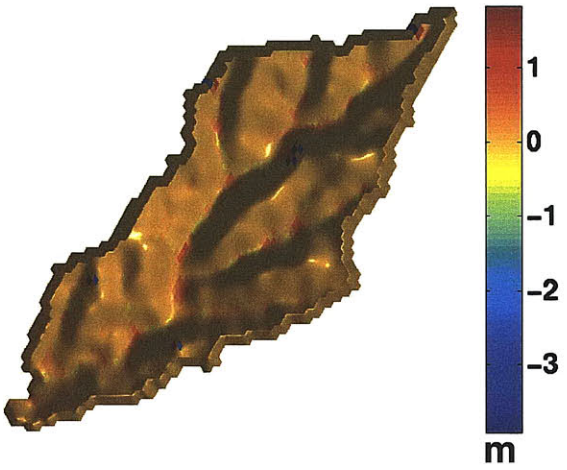

Figure 5-28: Differences in elevation after 10 000 years of simulation between the dynamic vegetation and static vegetation scenarios that start with Topo1.

bedrock exposure is limited and hence surface erosion is not common. Third, when bedrock is exposed, as in the first 5 000 years of the revegetation scenario, changes in the basin organization occur fast. In the revegetation scenario, the extension of the fluvially dominated processes all the way up to the ridges is a legacy of the first 5 000 years of simulation without vegetation. Fourth, the dynamic vegetation slowed down erosion in the last 5 000 years of the revegetation scenario, when vegetation was added to the landscape system, and maintained steeper slopes in the terrain in contrast to the bare surface scenario. This is clear in the bottom right panel of Figure 5-26.

5.3.4 Relationships between vegetation, slope, aspect and drainage area

In Chapters 2 and 4 the relationships between ecosystem productivity and topographic attributes were investigated. With the remote sensed data analysis of Chapter 2 it was found that vegetation productivity increases with drainage area, and decreases with insolation. Because insolation is lowest in terrain with a north aspect, vegetation was most abundant in that aspect. Moreover, changes in solar radiation as a function of slope were reflected in changes in vegetation, with more vegetation as solar radiation decreased. Furthermore, this data analysis indicated a correlation between vegetation cover and slope, with steeper slopes in the better vegetated terrain.

In Chapter 4 similar relationships between vegetation and solar radiation were detected in the model simulations, however, the sensitivity of vegetation productivity to drainage area was not as large as in the remote sensed data analysis. This was attributed to the uniformity of the root zone depth assumed in the model, that contrasts with the varying root zone depth expected in the field.

Deeper soils increase vegetation productivity (e.g., *Porporato et al.* [2001]; *Khumalo et al.* [2009]). Furthermore, soil horizon development processes and soil properties that change in time, and that are a function of the microclimate within a basin, and of vegetation, also affect vegetation productivity [*Jenny*, 1958]. The changes in soil properties result in a heterogeneous but organized distribution of soil properties such as hydraulic conductivity, moisture store space, and nutrient availability [*Riveros-Iregui and McGlynn*, 2009]. This organization of soil properties is probably reflected in the positive relationship between vegetation productivity and drainage area in the analysis of remotely sensed data, and it is not represented in CHILD completely.

The only representation of changes in soil properties in the model is the rooting soil depth, which equals the regolith depth. However, in the simulations presented in Chapter 4 and in this chapter, the root zone depth remains mostly constant. This is because in order to reflect as best as possible the soil profile at Kendall, a maximum root zone depth was set to 15 cm (this is discussed in more detail in Chapter 4). This limits significantly the variability of the root zone depth. Since regolith in most of the terrain is deeper than 15 cm, the root zone depth is mainly homogeneous and set to 15 cm, and thus, does not change as a function of drainage area. Regolith depth, on the other hand, increases in the channels in time scales of thousands of years, as Figures 5-14a, 5-14d, 5-17a, and 5-17e illustrate. It is very likely that if productivity increased as a function of drainage area, due to deeper root zones, more sediment would deposit in those zones, potentially increasing the root zone depth, and thus, fostering further vegetation productivity.

In the simulations, the effect of drainage area on regolith mantled simulations is further limited because in regolith mantled landscapes, runoff is rare, as Figure 5-8b illustrates. Therefore, water accumulation along the drainage network is rare. Subsurface redistribution is active in the model and occurs when moisture exceeds the field capacity. This moisture redistribution mechanism can lead to an increase in moisture in the downstream direction, and thus, an increase in ecosystem productivity with drainage area. Yet in the simulations presented, the anisotropy ratio is low (10), the terrain is not steep (the maximum slopes are 18 degrees), and the root zone layer is narrow, and so lateral soil moisture redistribution is likely to be negligible. If the anisotropy ratio were increased two orders of magnitude, perhaps the lateral soil moisture redistribution would cause an increase of ecosystem productivity with drainage area.

Nevertheless, the emergence of bedrock outcrops and its effects on vegetation productivity affects vegetation distribution. To investigate the effects of changes in the regolith depth and the elevation field on the distribution of vegetation along the 10 000 years of simulation of the dynamic vegetation scenario that starts with the Topo1 setting, the distribution of the below ground biomass as a function of aspect, slope and drainage area was calculated for years 100, 5 000 and 10 000. The results are shown in Figures 5-29, 5-30, and 5-31.

The relationships between vegetation and terrain attributes in the dynamic vege-

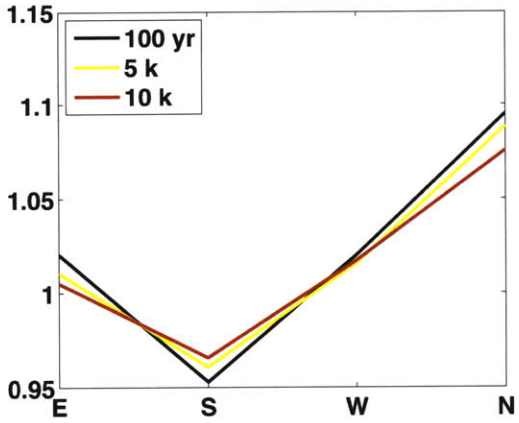

Figure 5-29: Relative below ground biomass as a function of aspect at different times during the dynamic vegetation scenario for Topo1.

tation scenario corresponding to Topo1 at year 100 are similar to those presented in Chapter 4. This is reasonable because the topographic setting Topo1 was also used in those simulations. The relationships between vegetation and aspect (Figure 5-29), and vegetation and drainage area (Figure 5-31), change little at years 5 000 and 10 000. However, the relationship between vegetation and slope changes at years 5 000 and 10 000. At these times in the simulation the relative root biomass for south facing terrain with slopes larger than 7.5° is high. This is due to the localized increase in biomass downstream of exposed bedrock, occurring mostly in south facing terrain (Figure 5-30). This change in the vegetation slope relationship suggests that the relationships found in the analysis of remote sensed data presented in Chapter 2 can be affected severely by irregularities in the surface properties of the terrain such as bedrock outcrops.

Figures for the analysis of the spatial distribution of vegetation as a function of aspect, slope and drainage area for the dynamic vegetation scenario corresponding to Topo2 are not presented because the results can be summarized in words. The analysis indicates that the north facing terrain is more productive than the south facing terrain, and that the difference in productivity between the opposing north and south facing hillslopes decreases with time, probably due to the control of bare bedrock generated runoff on vegetation growth in the latter years of the simulation. The distribution of vegetation productivity as a function of slope is in agreement with the change in insolation with slope but only at the beginning of the simulation: relative root biomass decreases with slope in the south facing terrain, and it increases with slope in the north facing terrain. When runoff from bare bedrock becomes the dominant control on vegetation distribution in the latter years of the simulation, relative root biomass increases with slope for both north and south facing aspects. Finally, the analysis indicates that vegetation distribution is relatively uniform as the drainage area increases, but only at the beginning of the simulation. When the runoff

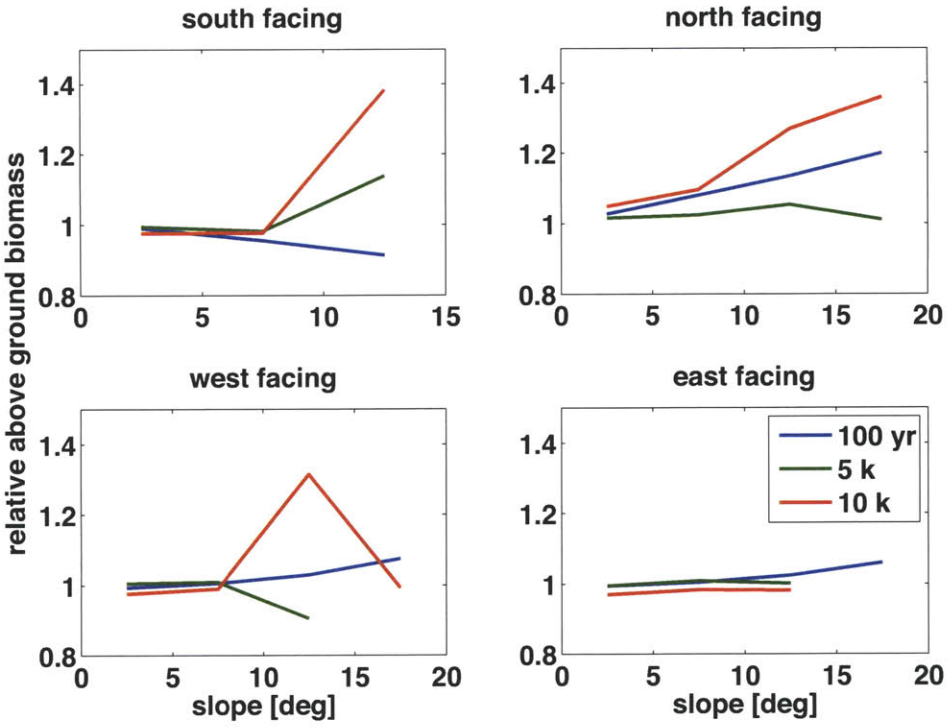

Figure 5-30: Relative below ground biomass as a function of slope at different times during the dynamic vegetation scenario for Topo1.

from bare bedrock zones begin to control vegetation distribution in the domain, the relationship between relative root biomass and drainage area becomes erratic.

Effects of vegetation cover on terrain steepness

A relationship between terrain steepness and vegetation cover was found in the analysis of remotely sensed data in Chapter 2. In the simulations presented in this chapter the distribution of bare bedrock, in addition to the distribution of vegetation, controlled the changes in regolith depth and elevations. In these simulations, even though differences in vegetation between north and south appear, they did not impact topography as much as the distribution of bare bedrock in the landscape.

Nevertheless vegetation limits erosion in the steeper north facing terrain. Mean slopes for different aspects were calculated for the initial and final conditions of each scenario represented with the model. These calculations are shown in Figure 5-32. For the Topo1 setting, Figure 5-32a illustrates how mean slope decreases uniformly for all aspects when vegetation limits erosion (dynamic vegetation, static vegetation and degradation scenarios), but it decreases $\sim 50\%$ more in the steeper north facing terrain than in the south facing terrain when vegetation is absent in the simulation (bare surface scenario).

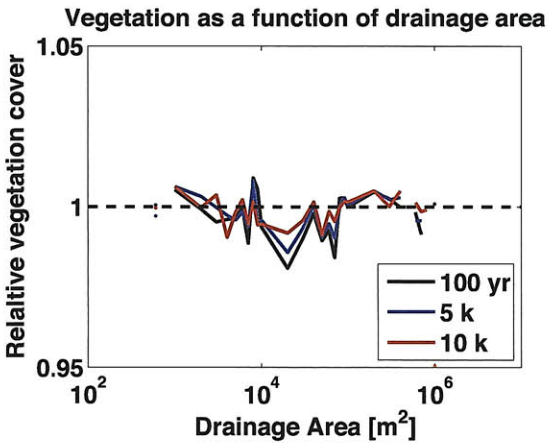

Figure 5-31: Relative below ground biomass as a function of drainage area at different times during the dynamic vegetation scenario for Topo1.

Under bare surface conditions, a bias in erosion between north and south facing terrain with similar slopes can rise from differences in evaporation rates between the two aspects. More evaporation on the south facing terrain increases the available storage space in the soil. This increase in storage capacity can reduce the frequency of saturation runoff generation, and thus result in reduced erosion. Such bias could have manifested in the Topo2 bare surface scenario, however, it did not, as Figure 5-32b illustrates. The mechanism described above probably was not strong enough to cause any significant difference in mean slopes between the opposing hillslopes, in comparison to the effect of bedrock exposure. The heterogeneity in the landscape that results from bedrock exposure dominates the patterns of erosion and deposition in the simulation, as Figures 5-17c, 5-17g, 5-18b, 5-18f, 5-19c and 5-19g illustrate. Because bedrock exposure is practically the same in the south and north facing hillslopes, the mean slopes are also the same.

In the dynamic vegetation scenario, differences in landform due to the differences in vegetation cover as a function of aspect in Topo2 were minimal (see Figure 5-32b). The mean slope of the south aspect is less than one tenth of a degree smaller than the mean slope of the north aspect, in contrast with the differences of the order of one degree found in the remotely sensed data analysis (see Figure 2-7b). This is also attributed to the large effects of bedrock exposure on the system (Figures 5-17a, 5-17e, 5-18a, 5-18d, 5-19a and 5-19e).

5.4 Conclusions

CHILD was used to simulate the evolution of the landscape for 10 000 years allowing for dynamic vegetation to interact with geomorphic processes. This means that in contrast to the simulation discussed in Chapter 4, these simulations had the geomorphic processes 'turned on'.

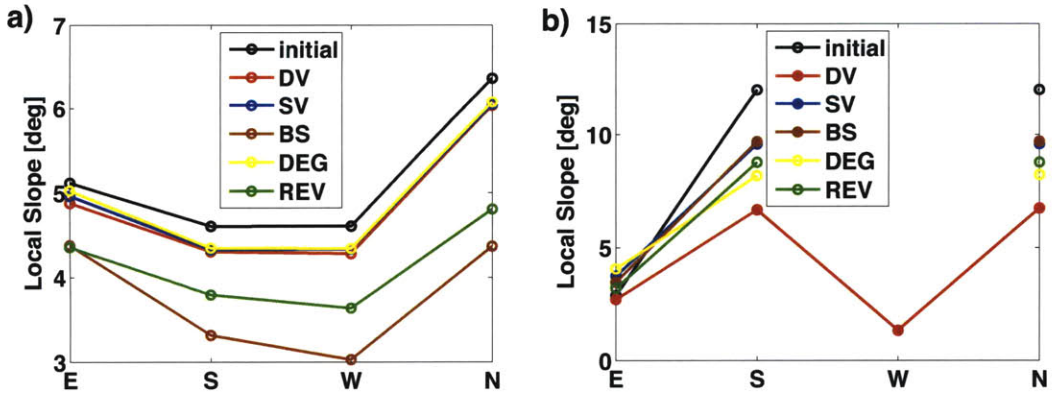

Figure 5-32: Slope as a function of aspect for all scenarios (dynamic vegetation, static vegetation, bare surface, degradation, revegetation) corresponding to a) Topo1 and b) Topo2.

Two different initial topographic conditions were used for two sets of simulations. The first initial topographic condition (Topo1) corresponds to the Digital Elevation Map (DEM) of the southeastern Arizona site. It provides a realistic setting with a wide range of topographic features to investigate (of slope, aspect and drainage area). The second initial topographic condition (Topo2) provides a more uniform setting that is useful to test the effects of vegetation differences between north and south facing terrain on geomorphic processes. In these simulations tectonic uplift played a minor role in the evolution of the landscape because the uplift rate ($0.00001m/yr$) is small relative to the time scale of the simulations.

These simulations highlighted the relevance of surface heterogeneity on geomorphologic processes. Large heterogeneity in these simulations is caused by the development of bedrock zones in the landscape. On exposed bedrock, runoff frequency is orders of magnitude higher than in regolith covered terrain. Thus, even though erodibility is an order of magnitude lower on bedrock than on regolith, exposed bedrock erodes faster than regolith covered terrain. Furthermore, the runoff generated in the bare bedrock generated an increase in soil moisture and biomass productivity downstream of the bedrock-regolith interface.

In addition to the dynamic vegetation simulations, a series of 4 additional simulations on each of the two initial elevation fields (a total of 8 more simulations) were carried out. These additional simulations consisted of a static vegetation simulation, a bare surface simulation, and what are referred to as a re-vegetation and degradation simulations. The re-vegetation simulation consisted of the evolution of the landscape during 5 000 years with no vegetation, and then 5 000 years with vegetation, where as the degradation simulation was similar but in it, a period of landscape evolution with vegetation is followed by a period of landscape evolution without vegetation.

By comparing the different simulations it is concluded that: a) differences arise between a vegetated and non-vegetated landscape, b) between a landscape where

vegetation is artificially kept uniform and constant in time, and one where vegetation changes as a function of moisture in time and space, and c) that the initial conditions play a major role in the evolution of the landscape, even if the initial topographic settings, in particular the regolith depth, are slightly different.

The main difference between the vegetated and non vegetated simulations was the extension of bedrock exposed, and its consequences in landscape evolution. The main difference between the static and dynamic vegetation simulations was that the rates of erosion in the drainage network were higher in the dynamic vegetation simulation (in the case of Topo1, since no channels exist in Topo2).

By comparing the bare surface and degradation simulations it is concluded that the exposure of bedrock in the system is sensitive to even small changes in the initial conditions, such a slightly thicker regolith mantle. In the degradadion simulations, regolith thickness increased during the 5 000 years of simulation when a dynamic vegetation was prescribed, and in the next 5 000 years, when vegetation was removed artificially from the system, the extension of bare bedrock was significantly reduced in comparison to the situation where the initial regolith depth was uniform (30 cm) (bare surface simulation).

The interplay between vegetation and water and sediment fluxes in the simulations produced two types of vegetation patterns. In the larger and more realistic domain Topo1, areas or bare bedrock formed in the zones of steeper slopes surrounding ridges, and in the downstream interface between the bedrock and the regolith, vegetation productivity was high. Vegetation patterns formed (type 1), and these densely vegetated areas captured runoff and sediment produced in the bedrock. These patterns consists of stripes of vegetation perpendicular to the direction of the slope. These natural 'dams' eventually captured enough sediment such that regolith began to deposit upstream, in the bare bedrock, resulting in the recovery of the bedrock by regolith. The recovery was fastest in the zones that had a large supply of sediment (large upstream bare bedrock) and gentle slopes. This type of pattern was also observed in Topo2

The second pattern (type 2) is clearer in the smaller (and synthetic) domain (Topo2). Bands of vegetation formed in the direction of the slope (in contrast with the pattern type 1, which forms in the direction perpendicular to the slope), and moved perpendicular to the direction of the slope at rates of approximately 5 m every 100 years. These bands emerge where runoff from zones of exposed bedrock concentrate. This runoff concentration causes the accumulation of moisture at those points. Biomass is highest where runoff leaves the bedrock and flows into the regolith mantled terrain, and gradually decreases in the downstream direction. These vegetation bands move when sediment, carried by water, deposits along the vegetation band, changes the elevation field, and produces in a new flow path that directs the runoff to a different location.

Finally, a difference between the simulations of Topo1 and Topo2 related to the spatial scale was observed. In the large domain of Topo1, the large amounts of sediment produced in the non-vegetated scenarios deposited in the valley network and caused aggradation. In the small synthetic domain (Topo2) where no valley

network developed, the sediment were transported out of the domain.

In these experiments local scale properties of the basin (exposed bedrock, regolith depth, and vegetation cover), when integrated in space, lead to basin scale effects such as denudation of the higher elevations and bedrock erosion, deposition of sediment in different parts of the basin (or not), and the appearance of vegetation patterns that evolve in time as they interplay with the erosion and sedimentation processes, water flow patterns (set by the elevation field), and soil moisture dynamics, and are driven by climate.

CHAPTER 6

CONCLUSIONS

This thesis has investigated the bidirectional interaction between vegetation and the land form. The study focuses on semiarid landscapes, where water is the main limiting factor for vegetation growth. Analysis of remote sensing data, field measurements, and modeling are combined to explore this interaction.

6.1 Spatial organization of vegetation as a function of the form of the terrain: remotely sensed observations

Chapter 2 investigates the bidirectional interaction between the spatial distribution of vegetation and terrain form, in water-limited, grass-dominated, temperate environments, at two field sites, one in south eastern Arizona, and the other in central New Mexico. The analysis is used as a basis of comparison for the numerical model developed in this work, which is presented in Chapter 3.

The main results from the analysis indicate, in agreement with the initial hypothesis, that a) vegetation growth increases with drainage area (reflected in more vegetation along channels); b) vegetation growth is inversely proportional to radiation, generally leading to maximum grass cover on north aspects and minimum on south aspects; c) more grass cover results in steeper slopes (reflected in steeper north facing terrain); and d) radiation changes as a function of slope are reflected in grass cover (reflected as an increase in vegetation with slope in north facing terrain, and a vegetation decrease with slope in south facing terrain).

A possible future development of this type of analysis is its extension to: a) different environmental settings where nutrients, light, or temperature, may be limiting factors for vegetation growth; and b) environments dominated by vegetation communities more complex than grasslands such as shrublands and forests.

6.2 A landscape evolution model

The Channel-Hillslope Integrated Landscape Development (CHILD) model is used in this investigation. The model represents the evolution of the terrain as a combination of diffusion processes, fluvial processes, tectonic uplift, and mass movements act on it. This model has been used in a number of studies to investigate, among other things, the effects of vegetation in landscape evolution. Modifications to the original model and the model itself are discussed in Chapter 3. The key modification is a new algorithm that represents vegetation dynamics where carbon assimilation is a function of transpiration. Transpiration, in turn, depends on vegetation cover, soil moisture, potential evapotranspiration, and a phenology rule (vegetation is dormant during winter). This algorithm accounts for above ground, or green leaves biomass, and for below ground, or root biomass. In addition, in order to represent the spatial and temporal dynamics of vegetation observed in the field, annual seasonality of rainfall and of solar forcing were added to the model. Moreover, the representation of the spatially variability of insolation as a function of terrain form, and its effects on soil moisture and vegetation dynamics is included. Finally, an algorithm to represent the intra-storm rainfall variability (a Barlett-Lewis algorithm) was incorporated to CHILD. Intra-storm rainfall variability is responsible for runoff generation in the semiarid settings addressed in this work.

6.3 Validation of the soil moisture and vegetation dynamics: observation and numerical simulations of a semiarid grassland

Measurements and remotely sensed data from a site in southeastern Arizona (Kendall site, described in Chapter 2) are used to validate the soil moisture and vegetation dynamics components of the modified CHILD. Chapter 4 demonstrates that the model reproduces the moisture dynamics, evapotranspiration rates, and above ground biomass well relative to measurements and remotely sensed observations. A simulation of the test site is carried out with CHILD using observed daily rainfall as the climatic forcing during 11 years (1997-2007). In these simulations the geomorphic processes were 'turned off' (see Chapter 4 for a full description of the parameters, initial and boundary conditions of this simulation).

Time series of moisture, evapotranspiration and green biomass are compared to the model. By visual inspection it is clear that evapotranspiration is best represented, followed by moisture and then by above ground biomass. Differences between the model and measurements are further discussed in Chapter 4. In agreement with measurements, simulated evapotranspiration and green biomass respond quickly to rainfall during the monsoon period, and their response to rainfall during winter is negligible in comparison, due to the low potential evapotranspiration and dormancy of vegetation in winter.

The same spatial analysis presented in Chapter 2 is also carried out for the simulated vegetation. The spatial variability of vegetation as a function of insolation was reproduced by the model, as reflected in the relationships between green biomass and aspect, and green biomass and slope. The positive relationship between vegetation cover and drainage area found in the study sites did not manifest in the model. This is attributed to the assumption in the simulation that the maximum rooting zone is 15 cm, where as in reality, the rooting zone is likely to change in space and in fact increases from the ridges to the channels (drainage area also increases from ridges to channels). The maximum rooting zone depth assumption is based in two soil profiles that describe the soil properties at two points in the site, and on the measured root distribution of grasses at another point (see Chapter 4 for details). In the model vegetation productivity increases with root zone depth, thus, if the rooting zone increased with drainage area, vegetation productivity would also increase with drainage area.

The root carbon component of grasslands is identified as valuable in the study of the evolution of the landscape. This is because roots reflect the grassland productivity integrated throughout a few years, in contrast with the above ground biomass that grow and die completely every year. Thus roots hold valuable information about the ecosystem dynamics in semiarid grassland ecosystems at time scales longer than a year.

Areas of improvement of the vegetation model were identified. Among these are the carbon transfer between roots and shoots, and the root dynamics. Based on remotely sensed vegetation dynamics and the rainfall record, it is hypothesized that soil moisture (and perhaps nutrients and species variability) have a more significant role on root to shoot carbon transfer, and on carbon assimilation, than what the model estimates.

It is possible to improve the estimations of moisture and vegetation by using more sophisticated models that use meteorological variables such as soil, leaf and air temperature, wind, and atmospheric water vapor pressure deficit. However, the use of such variables would hamper the numerical advantage of the current version of CHILD to simulate the evolution of the landscape over tens of thousands of years.

6.4 The coupled development of land form and vegetation: a case of semiarid grasslands

One of the main goals of this work was to create a new numerical model capable of representing the topography-vegetation interaction. This new model i s the modified version of CHILD.

CHILD was used to simulate the evolution of the landscape for 10 000 years allowing for dynamic vegetation to interact with geomorphic processes. This means that in contrast to the simulation discussed in Chapter 4, these simulations had the geomorphic processes 'turned on'. In addition to simulations with the dynamic

vegetation, simulations with static vegetation and no-vegetaton were performed.

From the simulations it was concluded that: a) the effects of bare bedrock can override the role of vegetation, therefore in order to study the role of vegetation, bedrock exposure must be limited; b) vegetation patterns that evolve in time form through the interplay between runoff and sediments produced in the exposed bedrock, vegetation, and changes in the elevation field; c) vegetation significantly affects the evolution of the distribution of regolith in the landscape; and d) in the simulations, less channel (fluvial) erosion occurs when vegetation is assumed static rather than dynamic.

6.5 Motivation questions

In this final section of the conclusions, the three questions that motivated this investigation as stated in the introduction are addressed. These questions have not been fully answered but partial answers to them have been achieved.

1. Do current landforms result from the topography-vegetation interaction, or would landforms have evolved to their present condition without this interaction?

Very different landscapes result when they are covered with vegetation and when they are not, as simulations presented in Chapter 5 show, and others have previously demonstrated (e.g., *Tucker and Slingerland* [1997]; *Istanbulluoglu and Bras* [2005]. For the lengths of the simulations presented here, significant differences in regolith distribution are observed in a landscape that evolves with vegetation and one that evolves without vegetation. At longer time scales, as in *Istanbulluoglu and Bras* [2005], significant differences in relief and drainage density are observed. Moreover, it is not only the presence of vegetation that affects landscape evolution, but also the bidirectional interaction between vegetation distribution and topography: smaller erosion rates in the channels were simulated when vegetation was assumed static instead of dynamic (with static vegetation corresponding to the temporal and spatial mean of the dynamic vegetation simulations).

Further stressing that current landforms result from the topography-vegetation interaction, in Chapter 5 differences between the bare surface and degradation simulations on one hand, and between dynamic vegetation and re-vegetation simulations on the other, show that previous vegetation conditions are likely to be reflected in the contemporary topography. In the first case (bare vs degradation simulations) less erosion occurred during no-vegetation conditions when the system had been previously vegetated; in the second case (dynamic vegetation vs revegetation simulations), the slope area diagram of the revegetation simulation shows that after 5 000 years of evolution with vegetation, the revegetation simulation still showed the effects of the previous 5 000 years without vegetation.

In conclusion, in a given climatic and geological setting, topography would be

different in the absence of vegetation.

2. Have current vegetation communities in a landscape adapted to the present topographic conditions and reached a steady state (which corresponds to the contemporary topography and climate)? Is this steady state dependent upon or independent of the history of the topography-vegetation interaction?

The answer to this question depends on the time scale of interest. Usually vegetation adjusts to contemporary conditions of climate, topography and underlying sediment properties in a few years. However, the adjustment depends on the plant functional type. Annuals adjust to conditions rapidly, as is their nature as short-lived species that easily and rapidly propagate. Woody vegetation species, on the other hand, require periods of relatively moist conditions to germinate, and once established, can live up to hundreds of years. Those moist periods may only occur at times scales of decades or centuries.

The range of time scales for geomorphic processes is broad as well. Usually landscape changes take thousands and millions of years. But may take place within years or days at smaller scales and localized regions of the landscape. For example, the formation of a delta may take millions of years, but a change in its main river channel can occur within one flood event.

A third time scale to consider is that of soil formation, which, as described by *Jenny* [1958], is frequently tightly linked to vegetation. Furthermore, different vegetation species grow on the soil during different phases of soil development. The time scales of soil development depend on various factors such as parent material, weather, and vegetation. But in general, soil develops in time scales that are longer than those of the establishment of vegetation. In this work, soil development was neglected, and the regolith is assumed to have uniform properties in space and time, independently of parent material, weather and climate. In addition to these factors, climate varies at various spatial scales. For the sake of this study and discussion, climate variability beyond annual variability is neglected.

Thus, assuming constant soil properties and constant climate, vegetation in semiarid grasslands adjusts relatively quickly to the current topographic setting, which usually changes at slower rates. But as illustrated by a) the patterns of vegetation that formed in the simulations of Chapter 5, and b) the reduction of regolith movement under vegetated conditions when compared to no-vegetation conditions (also in simulations of Chapter 5), once vegetation is established it influences the distribution of regolith significantly. As a consequence, the conditions to which vegetation adapts change all the time, and thus the vegetation distribution is dependent upon the vegetation-topography interaction.

3. Assuming a topography-vegetation interaction, how sensitive are the processes acting on a landscape to external disturbances in climate and land cover? How sen-

sitive is the steady state of a landscape to these external disturbances?

The number of variables that can account for external disturbances in a landscape are many, and the combination of variables modified, and the directions and magnitudes of change of each make the number of external disturbances possibilities infinite. Two experiments in Chapter 5 evaluate the effects of possible significant disturbances to the landscape. The first consists of a change from a dynamically vegetated landscape towards one void of vegetation, for example, due to a catastrophic removal of life in a region. The second consists of a change in the opposite direction. In the simulations of Chapter 5, the removal or addition of vegetation altered the resulting regolith distribution, and to a lesser extent the topography. The length of these simulations was 10 000 years, perhaps the effect of such disturbances is amplified in longer time scales. These simulations provide a basis for future explorations of these and other disturbances to the landscape system.

APPENDIX A

TABLES OF PARAMETERS

Table A.1: Model parameters, solar forcing

Climate Parameters		
Latitude Kendall	32	$[^{o}N]$
Latitude Sevilleta	34	$[^{o}N]$
$\overline{T_a}$	15.5	$[^{o}C]$
$T_{amax} - T_{amin}$	19	$[^{o}C]$
L_{T_a} for Kendall	0.0575	$[yr]$
L_{T_a} for Sevilleta	0.0136	$[yr]$
$\overline{PET}$	15.5	$[m/yr]$
$PET_{max} - PET_{min}$	19	$[m/yr]$
L_{PET} for Kendall	0.0575	$[yr]$
L_{PET} for Sevilleta	0.0136	$[yr]$

Table A.2: Model parameters, geomorphic processes

Geomorphology Parameters		
κ_f	492	$\left[\frac{m}{Pa^{1.5}yr}\right]$
p_f	1.5	[ ]
τ_{cf}	0.76	$[Pa]$
κ_B	0.05	$\left[\frac{m}{Pa^{1.5}yr}\right]$
κ_S	0.432	$\left[\frac{m}{Pa^{2.377}yr}\right]$
m_b	0.6	[ ]
n_b	0.7	[ ]
p_{db}	1	[ ]
p_{ds}	2.377	[ ]
τ_{cb}	0	$[Pa]$
τ_{cv}	10	$[Pa]$
n_s	0.05	[ ]
n_v^R	0.6	[ ]
V_R	0.95	[ ]
κ_{diff}	0.01	$[m^2yr]$
U	0.00001	$[m/yr]$
K_w	2	$[1/m]$
W_{Ro}	0.000077	$[m/yr]$

Table A.3: Model parameters, hydrologic processes

Soil hydrology Parameters		
s_{fc}	0.44	[ ]
s_*	0.158	[ ]
s_w	0.053	[ ]
s_h	0.041	[ ]
n_p	0.373	[ ]
β	10.76	[ ]
K_s	376	$[m/yr]$
a_r	10	[ ]
I_{cb}	376	$[m/yr]$
I_{cv}	752	$[m/yr]$

Table A.4: Model parameters, vegetation dynamics, Chapter 4

Vegetation Parameters		
d_g	8.76	$1/year$]
d_r	0.63875	[$1/year$]
d_d	36.5	[$1/year$]
lff	18.25	[$1/year$]
B_{gmax}	0.2	[$kgDM/m^2$]
WUE	0.00275	$\left[\frac{kgDM}{kgH_2O}\right]$
$\langle\xi\rangle^*_{30}$	0.8	[ ]
β^*_{wp}	0.7	[ ]
R_{10}	24.09	[$1/year$]
cn	29	[ ]
T_{vmin}	-2	[$\circ C$]
T_{vmax}	30	[$\circ C$]
T_{vopt}	18	[$\circ C$]

Table A.5: Model parameters, vegetation dynamics, Chapter 5

Vegetation Parameters		
d_g	8.76	$1/year$]
d_r	0.2847	[$1/year$]
d_d	36.5	[$1/year$]
lff	1.825	[$1/year$]
B_{gmax}	0.2	[$kgDM/m^2$]
WUE	0.005	$\left[\frac{kgDM}{kgH_2O}\right]$
$\langle\xi\rangle^*_{30}$	0.8	[ ]
β^*_{wp}	0.7	[ ]
R_{10}	24.09	[$1/year$]
cn	29	[ ]
T_{vmin}	-2	[$\circ C$]
T_{vmax}	30	[$\circ C$]
T_{vopt}	18	[$\circ C$]

Table A.6: Model parameters, initial conditions

Initial conditions		
$h_{s\ init}$	0.15^a	$[m]$
	0.3^b	
s_{init}	0.5	[ ]
V_{init}	0.01	[ ]
$B_{r\ init}$	0.3^a	$[kgDM]$
	0.5^b	
$B_{d\ init}$	0.3	$[kgDM]$

Notes: a. Chapter 4 simulations, b. Chapter 5 simulations

References

Abrahams, A. D., A. J. Parsons, and J. Wainwright (1995), Effects of vegetation change on interrill runoff and erosion, Walnut Gulch, southern Arizona, *Geomorphology, 13*, 37–48.

Aldrige, R., and R. J. Jackson (1968), Interception of rainfall by Manuka (*Leptospermum scoparium) at Taita, New Zeland, N. Z. Jl. of Sci., 1*, 301–317.

Angers, D. A., and J. Caron (1998), Plant-induced changes in soil structure: processes and feedbacks, *Biogeochemestry, 42*, 55–72.

Basnet, K. (1992), Effect of topography on the pattern of trees in Tabonuco (Dacryodes excelsa) dominated rain forest of Puerto Rico, *Biotropica, 31*, 31–42.

Benavides-Solorio, J., and L. H. MacDonald (2001), Post-fire runoff and erosion from simulated rainfall on small plots, Colorado Front Range, *Hydrol. Process., 15*, 2931–2952.

Bonan, G. (2002), *Ecological climatology, concepts and applications*, first ed., 678 pp., Cambridge University Press, Cambridge, United Kingdom.

Bormann, F. H., and G. E. Liekens (1979), *Patterns and Process in a Forested Ecosystem*, first ed., 253 pp., Springer-Verlag, New York.

Bosch, J. M., and J. D. Hewlett (1982), A review of catchment experiments to determine the effect of vegetation changes on water yield and evapotranspiration, *J. of Hydrol., 55*, 3–23.

Bras, R. L. (1990), *Hydrology, An Introduction to Hydrologic Science*, first ed., Addison-Wesley Publishing Company, United States of America.

Briggs, J. M., M. D. Nellis, C. L. Turner, G. M. Henebry, and H. Su (1998), A landscape perspective of patterns and processes in tallgrass prairie, in *Grassland Dynamics*, edited by A. K. Knapp, D. C. Briggs, John M. andHartnett, and S. L. Collins, first ed., pp. 265–279, Oxford University Press, New York.

Cabral, M. C., L. Garrote, R. L. Bras, and D. Entekhabi (1992), A kinematic model of infiltration and runoff generation in layered and sloped soils, *Advances in Water Resources, 15*(5), 311 – 324, doi:DOI: 10.1016/0309-1708(92)90017-V.

Caylor, K. K., P. D'Odorico, and I. Rodríguez-Iturbe (2006), On the ecohydrology of structurally heterogeneous semiarid landscapes, *Water Resour. Res., 42*.

Collins, D. B. G. (2006), Geomorphology and ecohydrology of water-limited ecosystems: a modeling approach, Ph.D. thesis, Massachusetts Institute of Technology.

Collins, D. B. G., and R. L. Bras (2008), Climatic control of sediment yield in dry lands following climate and land cover change, *Water Resour. Res., 44*.

Collins, D. G. B., R. L. Bras, and G. E. Tucker (2004), Modeling the effects of vegetation-erosion coupling on landscape evolution, *J. Geophys. Res.*, *109*(F0), 3004, doi:10.1029/2003JF000028.

Cosby, B. J., G. M. Hornberger, R. B. Clapp, and T. R. Ginn (1984), A statistical exploration of the relationships of soil moisture characteristics to the physical properties of soils, *Water Resour. Res.*, *20*.

Coulthard, T. J. (2001), Landscape evolution models: a software review, *Hydrological Processes*, *15*(1), 165–173.

Coulthard, T. J., M. G. Macklin, and M. J. Kirkby (2002), A cellular model of holocene upland river basin and alluvial fan evolution, *Earth Surface Processes and Landforms*, *27*(3), 269–288.

Cox, J. R., G. W. Frasier, and K. G. Renard (1986), Biomass distribution at grassland and shrubland sites, *Rangelands*, *8*(2), 67–69.

Dick-Peddie, W. A. (1993), *New Mexico Vegetation: Past, Present and Future*, first ed., 244 pp., University of New Mexico Press, Albuquerque, New Mexico.

Duan, Q. Y., V. K. Gupta, and S. Sorooshian (1993), Shuffled complex evolution approach for effective and efficient global minimization, *Journal of Optimization Theory and Applications*, *76*(3), 501–521.

Dunne, T., W. Zhang, and B. F. Aubry (1991), Effects of rainfall, vegetation, and microtopography on infiltration and runoff, *Water Resour. Res.*, *27*.

Eagleson, P. S. (1978), Climate, soil, and vegetation 2. the distribution of annual precipitation derived from observed storm sequences, *Water Resour. Res.*, *14*.

Eagleson, P. S. (2002), *Ecohydrology, darwinian expression of vegetation form and function*, first ed., 443 pp., Cambridge University Press, Cambridge, United Kingdom.

Einstein, H. A., and N. Barbarossa (1952), River channel roughness, *Trans., ASCE*, *117*, 1121–1146.

Emmerich, W. E. (2008), Soil survey of Walnut Gulch Experimental Watershed, Arizona, a special report, revised in 2008, *Tech. rep.*, National Cooperative Soil Survey.

Flores-Cervantes, J. H., E. Istanbulluoglu, and R. L. Bras (2006), Development of gullies on the landscape: A model of headcut retreat resulting from plunge pool erosion, *J. Geophys. Res.*, *111*.

Foster, G. R. (1982), Modeling the erosion process, in *Hydrologic Modeling of Small Watersheds, ASAE Monogr.*, vol. 5, edited by H. C. T, pp. 295–380, Am. Soc. of Agric. Eng.

Francis, C. F., and J. B. Thornes (1990), Runoff hydrographs from three mediterranean vegetation cover types, in *Vegetation and Erosion, Processes and Environments*, edited by J. Thornes, John Wiley & Sons, New York.

Gibson, D. J. (2009), *Grasses and grassland ecoloby*, first ed., 305 pp., Oxford University Press, New York.

Goodrich, D. C., T. O. Keefer, C. L. Unkrich, M. H. Nichols, H. B. Osborn, J. J. Stone, and J. R. Smith (2008), Long-term precipitation database, Walnut Gulch Experimental Watershed, Arizona, United States, *Water Resour. Res.*, *44*(W0), 5S04, doi:10.1029/2006WR005782.

Greenway, D. R. (1990), The agency of organic beings: a selective review of recent work in geomorphology, in *Slope Stability*, edited by M. G. Anderson and K. S. Richards, John Wiley & Sons Ltd., Chinchester.

Gurnell, A. M., P. A. Hughes, and P. J. Edwards (1990), The hydrological implications on heath vegetation composition and management in the New Forest, Hampshire, in *Vegetation and Erosion, Processes and Environments*, edited by J. Thornes, John Wiley & Sons, New York.

Gutiérrez-Jurado, H. A., E. R. Vivoni, J. F. Harrison, and H. Guan (2006), Ecohydrology of root zone water fluxes and soil development in complex semiarid rangelands, *Hydrological Processes*, *20*(15), 3289–3316.

Gutiérrez-Jurado, H. A., E. R. Vivoni, E. Istanbulluoglu, and R. L. Bras (2007), Ecohydrological response to a geomorphically significant flood event in a semiarid catchment with contrasting ecosystems, *Geophys. Res. Lett.*, *34*(L24S25), doi: 10.1029/2007GL030994.

Hack, J. T., and J. C. Goodlett (1960), Geomorphology and forest ecology of a mountain region in the Central Appalachians, *Prof. pap.*, U.S. Geol. Surv.

Hanson, G. J., and A. Simon (2001), Erodibility of cohesive streambeds in the loess area of the midwestern usa, *Hydrological Processes*, *15*(1), 23–38.

Heilman, P., M. H. Nichols, D. C. Goodrich, S. N. Miller, and D. P. Guertin (2008), Geographic information systems database, walnut gulch experimental watershed, arizona, united states, *Water Resour. Res.*, *44*.

Heimsath, A. M., W. E. Dietrich, K. Nishiizumi, and R. C. Finkel (1997), The soil production function and landscape equilibrium, *Nature*, *388*(6640), 358–361.

Hidalgo, J. C. G., L. Pellicer, and M. V. Lopez (1990), Spatial distribution patterns of morphogenetic processes in a semiarid region, in *Vegetation and Erosion, Processes and Environments*, edited by J. Thornes, pp. 399–417, John Wiley & Sons, New York.

Hillel, D. (1998), *Environmental Soil Physics*, 771 pp., Elsevier Sciences & Technology Books.

Holifield, C. D., S. McElroy, M. S. Moran, R. Bryant, T. Miura, and W. E. Emmerich (2003), Temporal and spatial changes in grassland transpiratino detected using landsat tm and etm+ imagery, *Can. J. Remote Sensing*, *29*(2).

Howard, A. D. (1988), Groundwater sapping experiments and modeling, in *Sapping features of the Colorado Plateau, a comparative planetary geology field guide*, edited by A. D. Howard, R. C. Kochel, and H. E. Holt, pp. 71–83, NASA Scientific and Technical Information Division.

Howard, A. D. (1994), A detachment-limited model of drainage basin evolution, *Water Resour. Res.*, *30*.

Huang, C., C. Gascuel-Odoux, and S. Cros-Cayot (2002), Hillslope topographic and hydrologic effects on overland flow and erosion, *CATENA*, *46*(2-3), 177 – 188, doi:DOI: 10.1016/S0341-8162(01)00165-5.

Islam, S., D. Entekhabi, R. L. Bras, and I. Rodríguez-Iturbe (1990), Parameter estimation and sensitivity analysis for the modified bartlett-lewis rectangular pulses model of rainfall, *J. Geophys. Res.*, *95*.

Istanbulluoglu, E., and R. L. Bras (2005), Vegetation-modulated landscape evolution: Effects of vegetation on landscape processes, drainage density, and topography, *J. Geophys. Res.*, *110*(F0), 2012, doi:10.1029/2003JF000028.

Istanbulluoglu, E., and R. L. Bras (2006), On the dynamics of soil moisture, vegetation, and erosion: Implications of climate variability and change, *Water Resour. Res.*, *42*.

Istanbulluoglu, E., R. L. Bras, H. Flores-Cervantes, and G. E. Tucker (2005), Implications of bank failures and fluvial erosion for gully development: Field observations and modeling, *J. Geophys. Res.*, *110*.

Istanbulluoglu, E., O. Yetemen, E. R. Vivoni, H. A. Gutiérrez-Jurado, and R. L. Bras (2008), Eco-geomorphic implications fo hillslope aspect: Inferences from analysis of landscape morphology in central New Mexico, *Geophys. Res. Lett.*, *35*(L14403), doi:10.1029/2008GL034477.

Ivanov, V. Y., E. R. Vivoni, R. L. Bras, and D. Entekhabi (2004), Catchment hydrologic response with a fully distributed triangulated irregular network model, *Water Resour. Res.*, *40*.

Ivanov, V. Y., R. L. Bras, and D. C. Curtis (2007), A weather generator for hydrological, ecological, and agricultural applications, *Water Resour. Res.*, *43*(W10406), doi:10.1029/2006WR005364.

Ivanov, V. Y., R. L. Bras, and E. R. Vivoni (2008a), Vegetation-hydrology dynamics in complex terrain of semiarid areas: 1. a mechanistic approach to modeling dynamic feedbacks, *Water Resour. Res.*, *44*(W03429), doi:10.1029/2006WR005588.

Ivanov, V. Y., R. L. Bras, and E. R. Vivoni (2008b), Vegetation-hydrology dynamics in complex terrain of semiarid areas: 2. energy-water controls of vegetation spatiotemporal dynamics and topographic niches of favorability, *Water Resour. Res.*, *44*(W03430), doi:10.1029/2006WR005595.

Jenny, H. (1958), Role of the plant factor in the pedogenic functions, *Ecology*, *39*(1), 5–16.

Johnson, W. C., R. L. Burgess, and W. R. Keammerer (1976), Forest overstory vegetation and environment on the missouri river floodplain in north dakota, *Ecological Monographs*, *46*(1), 59–84, doi:10.2307/1942394.

Keefer, T. O., M. S. Moran, and G. B. Paige (2008), Long-term meteorological and soil hydrology database, Walnut Gulch Experimental Watershed, Arizona, United States, *Water Resour. Res.*, *44*(W0), 5S07, doi:10.1029/2006WR005702.

Kennedy, B. (1976), Valley-side slopes and climate, in *Geomorphology and Climate*, edited by E. Derbyshire, pp. 171–201, John Wiley & Sons, Bristol, Great Britain.

Khumalo, G., J. Holechek, M. Thomas, and F. Molinar (2009), Soil depth and climatic effects on desert vegetation dynamics, *Rangeland Ecology & Management*, *61*(3), 269–274.

Kirkby, M. J., K. Atkinson, and J. G. Lockwood (1990), Aspect, vegetation and erosion on semiarid hillslopes, in *Vegetation and Erosion*, edited by J. B. Thornes, pp. 25–39, Wiley, Chichester.

Kirkby, M. J., R. J. Abrahart, J. D. Bathurst, C. G. Kilsby, M. L. McMahon, C. P. Osborne, J. B. Thornes, and F. I. Woodward (2002), MEDRUSH, a basin scale physically-based model for forecasting runoff and sediment yield, in *Mediterranean desertification: a mosaic of processes and responses*, edited by N. A. Geeson, C. J. Brandt, and J. B. Thornes, pp. 203–227, John Wiley, Chinchester.

Knapen, A., J. Poesen, G. Govers, G. Gyssels, and J. Nachtergaele (2007), Resistance of soils to concentrated flow erosion: A review, *Earth-Science Reviews*, *80*(1-2), 75 – 109, doi:DOI: 10.1016/j.earscirev.2006.08.001.

Knapp, A. K., and T. R. Seastedt (1998), Introduction: Grasslands, Konza Prairie, and Long-Term Ecological Research, in *Grassland Dynamics*, edited by A. K. Knapp, D. C. Briggs, John M. andHartnett, and S. L. Collins, first ed., pp. 3 – 15, Oxford University Press, New York.

Knapp, A. K., J. M. Briggs, J. M. Blair, and C. L. Turner (1998), Patterns and controls of aboveground net primary production in tallgrass prairie, in *Grassland*

Dynamics, edited by A. K. Knapp, D. C. Briggs, John M. andHartnett, and S. L. Collins, first ed., pp. 193 – 221, Oxford University Press, New York.

Kuhn, N. J., A. Yair, and M. K. Grubin (2004), Spatial distribution of surface properties, runoff generation and landscape development in the zin valley badlands, northern negev, israel, *Earth Surface Processes and Landforms*, *29*(11), 1417–1430.

Laflen, J. M., W. J. Elliot, J. R. Simanton, C. S. Holzhey, and K. D. Kohl (1991), WEPP: Soil erodibility experiments for rangeland and cropland soils, *Journal of Soil and Water Conservation*, *46*(1), 39–44.

Laio, F., A. Porporato, L. Ridolfi, and I. Rodríguez-Iturbe (2001a), Plants in water-controlled ecosystems: active role in hydrologic processes and response to water stress: II. probabilistic soil moisture dynamics, *Advances in Water Resources*, *24*(7), 707 – 723, doi:DOI: 10.1016/S0309-1708(01)00005-7.

Laio, F., A. Porporato, C. P. Fernandez-Illescas, and I. Rodríiguez-Iturbe (2001b), Plants in water-controlled ecosystems: active role in hydrologic processes and response to water stress: IV. discussion of real cases, *Advances in Water Resources*, *24*(7), 745 – 762, doi:DOI: 10.1016/S0309-1708(01)00007-0.

Lancaster, N., and A. Bass (1998), Influence of vegetation cover on sand transport by wind: field studies at Owens lake, California, *Earth Surface Processes and Landforms*, *23*, 62–82.

Larcher, W. (2003), *Physiological plant ecology, ecophysiology and stress physiology of functional groups*, fourth ed., 513 pp., Springer-Verlag.

Lauenroth, W. K., O. E. Sala, D. P. Coffin, and T. B. Kirchner (1994), The importance of soil water in the recruitment of bouteloua gracilis in the shortgrass steppe, *Ecological Applications*, *4*(4), 741–749, doi:10.2307/1942004.

Leopold, L., and T. Maddock (1953), The hydraulic geometry of stream channels and some physiographic implications, *U. S. Geological Survery Professional paper*, *252*.

Leopold, L. B., M. G. Woman, and J. P. Miller (1964), *Fluvial processes in geomorphology*, 522 pp., W. H. Freeman, New York.

Loik, M. E., D. D. Breshears, W. K. Lauenroth, and J. Belnap (2004), A multi-scale perspective of water pulses in dryland ecosystems: climatology and ecohydrology of the western usa, *Oecologia*, *141*(2), 269–281.

Lull, H. W. (1964), Ecological and silvicultural aspects, sect 6, in *Handbook of Applied Hydrology*, McGraw-Hill, New York.

McHugh, M. J., and D. G. Goodin (2003), Interdecadal-scale variability: an assessment of LTER climate data, in *Climate variability and ecosystem response at long-term ecological research sites*, edited by D. Greenland, D. G. Goodin, and R. C. Smith, first ed., pp. 213 – 225, Oxford University Press.

McMahon, D. R. (1998), Soil, landscape and vegetation interactions in a small semi-arid draiange basin:Sevilleta National Wildlife Refuge, New Mexico, Master's thesis, New Mexico Institute of Mines and Technology.

Meyer-Peter, E., and R. Müller (1948), Formulas for bed-load transport, in *Proceedings of 2nd Meeting*, pp. 39–64, IAHR, Stockholm, Sweden.

Milne, B. T., D. I. Moore, J. L. Betancourt, J. A. Parks, T. W. Swetnam, R. R. Parmenter, and W. T. Pockman (2003), Multidecadal drought cycles in South-central New Mexico: Patterns and concequences, in *Climate variability and ecosystem response at long-term ecological research sites*, edited by D. Greenland, D. G. Goodin, and R. C. Smith, first ed., p. 459, Oxford University Press.

Molchanov, A. A. (1971), Cycles of atmospheric precipitation in different types of forests of natural zones of the u.s.s.r., in *Productivity of Forests Ecosystems*, edited by P. Duvigneaus, pp. 49–68, UNESCO, Paris.

Molnár, P., and J. A. Ramírez (2001), Recent trends in precipitation and streamflow in the rio puerco basin, *Journal of Climate*, *14*(10), 2317–2328.

Monger, H. C. (2003), Millenial-scale climate variability and ecosystem response at the Jornada LTER Site, in *Climate variability and ecosystem response at long-term ecological research sites*, edited by D. Greenland, D. G. Goodin, and R. C. Smith, first ed., p. 459, Oxford University Press.

Montaldo, N., R. Rondena, J. D. Albertson, and M. Mancini (2005), Parsimonious modeling of vegetation dynamics for ecohydrologic studies of water-limited ecosystems, *Water Resour. Res.*, *41*.

Montandon, L., and E. Small (2008), The impact of soil reflectance on the quantification of the green vegetation fraction from ndvi, *Remote Sensing of Environment*, *112*(4), 1835 – 1845, doi:DOI: 10.1016/j.rse.2007.09.007, remote Sensing Data Assimilation Special Issue.

Moody, J. A., and D. A. Martin (2001), Post-fire, rainfall intensity-peak discharge relations for three mountainous watersheds in the western USA, *Hydrol. Process.*, *15*, 2981–2993.

Moorcroft, P. R., G. C. Hurtt, and S. W. Pacala (2001), A method for scaling vegetation dynamics: The ecosystem demography model (ed), *Ecological Monographs*, *71*(4), 557–586, doi:10.1890/0012-9615(2001)071[0557:AMFSVD]2.0.CO;2.

Moran, M. S., R. Bryant, K. Thorme, W. Ni, Y. Nouvellon, M. P. Gonzalez-Dugo, J. Qi, and T. R. Clarke (2001), Long-term remote sensing database, Walnut Gulch Experimental Watershed, Arizona, United States, *Remote Sensing of Environment.*, *78*, 71–82.

Moran, M. S., C. D. H. Collins, D. C. Goodrich, J. Qi, D. T. Shannon, and A. Olsson (2008), Long-term remote sensing database, Walnut Gulch Experimental Watershed, Arizona, United States, *Water Resour. Res.*, *44*(W0), 5S10, doi: 10.1029/2006WR005689.

Mosley, M. P. (1982), The effect of a New Zealand beech forest canopy on the kinetic energy of water drops and on surface erosion, *Earth Surface Processes and Landforms*, *7*(2), 103–107.

Muldavin, E., G. Shore, K. Taugher, and B. Milne (1998), A vegetation classification and map for the Sevilleta National Wildlife Refug, New Mexico, *Final report*, New Mexico Natural Heritage Program and Sevilleta Long Term Ecological Research Program, Biology Department, University of New Mexico, Albuquerque, New Mexico.

Nearing, M. A., J. R. Simanton, L. D. Norton, S. J. Bulygin, and J. Stone (1999), Soil erosion by surface water flow on a stony, semiarid hillslope, *Earth Surface Processes and Landforms*, *24*(8), 677–686.

Newman, B. D., et al. (2006), Ecohydrology of water-limited environments: A scientific vision, *Water Resour. Res.*, *42*.

Nouvellon, Y., S. Rambal, D. L. Seen, M. S. Moran, J. P. Lhomme, A. Bgu, A. G. Chehbouni, and Y. Kerr (2000), Modelling of daily fluxes of water and carbon from shortgrass steppes, *Agricultural and Forest Meteorology*, *100*(2-3), 137 – 153, doi:DOI: 10.1016/S0168-1923(99)00140-9.

Nouvellon, Y., et al. (2001), Coupling a grassland ecosystem model with Landsat imagery for a 10-year simulation of carbon and water budgets, *Remote Sensing of Environment*, *78*, 131–149.

Oesterheld, M., J. Loreti, M. Semmartin, and O. E. Sala (2001), Inter-annual variation in primary production of a semi-arid grassland related to previous-year production, *Journal of Vegetation Science*, *12*(1), 137–142.

Pennington, D., and S. Collins (2007), Response of an aridland ecosystem to interannual climate variability and prolonged drought, *Landscape Ecology*, *22*(6), 897–910.

Ponton, S., L. B. Flanagan, K. P. Alstad, B. G. Johnson, K. Morgenstern, N. Kljun, T. A. Black, and A. G. Barr (2006), Comparison of ecosystem water-use efficiency among douglas-fir forest, aspen forest and grassland using eddy covariance and carbon isotope techniques, *Global Change Biology*, *12*(2), 294–310.

Porporato, A., F. Laio, L. Ridolfi, and I. Rodríguez-Iturbe (2001), Plants in water-controlled ecosystems: active role in hydrologic processes and response to water stress: Iii. vegetation water stress, *Advances in Water Resources*, *24*(7), 725 – 744, doi:DOI: 10.1016/S0309-1708(01)00006-9.

Prosser, I. P., and W. E. Dietrich (1995), Field experiments on erosion by overland flow and their implications for a digital terrain model of channel initiation, *Water Resour. Res.*, *31*, 2867–2876.

Prosser, I. P., and C. J. Slade (1994), Gully formation and the role of valley-floor vegetation, southeastern Austalia, *Geology*, *22*, 1127–1130.

Prosser, I. P., W. E. Dietrich, and J. Stevenson (1995), Flow resistance and sediment transport by concentrated overland flow in a grassland valley, *Geomorphology*, *13*, 71–86.

Reid, L. M. (1989), Channel incision by surface runoff in grassland catchments, Ph.D. thesis, University of Washington.

Rey, F. (2003), Influence of vegetation distribution on sediment yield in forested marly gullies, *CATENA*, *50*(2-4), 549 – 562, doi:DOI: 10.1016/S0341-8162(02)00121-2.

Ridolfi, L., P. D'Odorico, A. Porporato, and I. Rodríiguez-Iturbe (2003), Stochastic soil moisture dynamics along a hillslope, *Journal of Hydrology*, *272*(1-4), 264 – 275, doi:DOI: 10.1016/S0022-1694(02)00270-6.

Riveros-Iregui, D. A., and B. L. McGlynn (2009), Landscape structure control on soil co2 efflux variability in complex terrain: Scaling from point observations to watershed scale fluxes, *J. Geophys. Res.*, *114*.

Rodríguez-Iturbe, I., and A. Porporato (2005), *Ecohydrology of Water-controlled Ecosystems*, 460 pp., Cambridge University Press, Cambridge, UK.

Rodríguez-Iturbe, I., and J. B. Valdés (1979), The geomorphologic structure of hydrologic response, *Water Resour. Res.*, *15*, 1409 – 1420.

Rodríguez-Iturbe, I., D. R. Cox, and V. Isham (1988), A Point Process Model for Rainfall: Further Developments, *Proceedings of the Royal Society of London. A. Mathematical and Physical Sciences*, *417*(1853), 283–298, doi: 10.1098/rspa.1988.0061.

Rodríguez-Iturbe, I., A. Porporato, F. Laio, and L. Ridolfi (2001), Plants in water-controlled ecosystems: active role in hydrologic processes and response to water stress: I. scope and general outline, *Advances in Water Resources*, *24*(7), 695 – 705, doi:DOI: 10.1016/S0309-1708(01)00004-5.

Roering, J. J. (2008), How well can hillslope evolution models explain topography? Simulating soil transport and production with high-resolution topographic data, *Geological Society of America Bulletin*, *120*(9-10), 1248–1262, doi: 10.1130/B26283.1.

Sala, O. E. (2001), Productivity of temperate grasslands, in *Terrestrial Global Productivity*, pp. 285 – 300, Academic Press, San Diego, doi:DOI: 10.1016/B978-012505290-0/50013-2.

Sala, O. E., A. T. Austin, and L. Vivanco (2001), Temperate grassland and shrubland ecosystems, in *Encyclopedia of Biodiversity*, edited by S. A. Levin, pp. 627 – 635, Elsevier, New York, doi:DOI: 10.1016/B0-12-226865-2/00268-6.

Scatena, F. N., and A. E. Lugo (1995), Geomorphology, disturbance, and the soil and vegetation of two subtropical wet steep watersheds of Puerto Rico, *Geomorphology*, *13*, 199–213.

Scholes, R. J., and B. H. Walker (1993), *An African Savanna, Synthesis of the Nylsvley study*, 306 pp., Cambridge University Press, Cambridge, United Kingdom.

Scott, R. L., W. J. Shuttleworth, T. O. Keefer, and A. W. Warrick (2000), Modeling multiyear observations of soil moisture recharge in the semiarid American Southwest, *Water Resour. Res.*, *36*(8).

Selby, M. J. (1970), Design of a hand-portable rainfall-simulating infiltrometer, iwth trial results from the Octutira catchment, *Jl. Hydrol. (N.Z.)*, *9*, 117–132.

Selby, M. J. (1993), *Hillslope materials and processes*, second ed., Oxford University Press, Oxford, England.

Sellers, W. D. (1965), *Physical Climatology*, 277 pp., University of Chicago Press.

Shmida, A., and T. L. Burgess (1988), Plant growth , form strategies and vegetation types in arid environments, in *Plant form and vegetation structure : adaptation, plasticity and relation to herbivory*, edited by J. J. Barkman, M. J. A. Werger, and I. S. on Vegetational Structure, pp. xii, 356 p. :, SPB Academic Pub., The Hague.

Sigafoos, R. S. (1961), Vegetation in relation to flood frequency near Washington, D. C., *U. S. Geological Survery Professional paper*, *424-C*.

Sitch, S., et al. (2003), Evaluation of ecosystem dynamics, plant geography and terrestrial carbon cycling in the lpj dynamic global vegetation model, *Global Change Biology*, *9*(2), 161–185.

Small, E. E. (2005), Climatic controls on diffuse groundwater recharge in semiarid environments of the southwestern united states, *Water Resour. Res.*, *41*.

Sólyom, P. B., and G. E. Tucker (2004), Effect of limited storm duration on landscape evolution, drainage basin geometry, and hydrograph shapes, *J. Geophys. Res.*, *109*.

Sorriso-Valvo, M., R. Bryan, A. Yair, F. Iovino, and L. Antronico (1995), Impact of afforestation on hydrological response and sediment production in a small calabrian catchment, *CATENA*, *25*(1-4), 89 – 104, doi:DOI: 10.1016/0341-8162(95)00002-A, experimental Geomorphology and Landscape Ecosystem Changes, Proceedings Memorial Symposium Prof. Jan Ploey.

Stone, J. J., M. H. Nichols, D. C. Goodrich, and J. Buono (2008), Long-term runoff database, walnut gulch experimental watershed, arizona, united states, *Water Resour. Res.*, *44*.

Surkan, A. J. (1969), Synthetic hydrographs: Effects of network geometry, *Water Resour. Res.*, *5*.

Teversham, J. M., and O. Slaymaker (1976), Vegetation composition in relation to flood frequency in lillooet river valley, british columbia, *CATENA*, *3*(2), 191 – 201, doi:DOI: 10.1016/0341-8162(76)90009-6.

Trimble, S. W. (1990), Geomorphic effects of vegetation cover and management: some time and space considerations in prediction of erosion and sediment, in *Vegetation and Erosion, Processes and Environments*, edited by J. Thornes, John Wiley & Sons, New York.

Tucker, C. J. (1979), Red and photographic infrared linear combinations for monitoring vegetation, *Remote Sensing of the Environment*, *8*, 127–150.

Tucker, G. E., and R. L. Bras (1998), Hillslope processes, drainage density, and landscape morphology, *Water Resour. Res.*, *34*.

Tucker, G. E., and R. L. Bras (2000), A stochastic approach to modeling the role of rainfall variability in drainage basin evolution, *Water Resour. Res.*, *36*.

Tucker, G. E., and R. Slingerland (1996), Predicting sediment flux from fold and thrust belts, *Basin Research*, *8*(3), 329–349.

Tucker, G. E., and R. Slingerland (1997), Drainage basin responses to climate change, *Water Resour. Res.*, *33*.

Tucker, G. E., S. T. Lancaster, N. M. Gasparini, and R. L. Bras (2001), The channel-hillslope integrated landscape development (child) model, in *Landscape Erosion and Evolution Modeling*, edited by R. S. Harmon and W. W. I. Doe, pp. 349–388, Kuwer Acad., New York.

Vacca, A., S. Loddo, G. Ollesch, R. Puddu, G. Serra, D. Tomasi, and A. Aru (2000), Measurement of runoff and soil erosion in three areas under different land use in sardinia (italy), *CATENA*, *40*(1), 69 – 92, doi:DOI: 10.1016/S0341-8162(00)00088-6.

van Wesemael, B., J. Poesen, A. S. Benet, L. C. Barrionuevo, and J. Puigdefbregas (1998), Collection and storage of runoff from hillslopes in a semi-arid environment: geomorphic and hydrologic aspects of the aljibe system in almeria province, spain, *Journal of Arid Environments*, *40*(1), 1 – 14, doi:DOI: 10.1006/jare.1998.0429.

Viles, H. A. (1990), The agency of organic beings: a selective review of recent work in geomorphology, in *Vegetation and Erosion, Processes and Environments*, edited by J. Thornes, John Wiley & Sons, New York.

Weiss, J. L., D. S. Gutzler, J. E. A. Coonrod, and C. N. Dahm (2004), Seasonal and inter-annual relationships between vegetation and climate in central new mexico, usa, *Journal of Arid Environments*, *57*(4), 507 – 534, doi:DOI: 10.1016/S0140-1963(03)00113-7.

Willgoose, G., R. L. Bras, and I. Rodríguez-Iturbe (1991), A physical explanation of an observed link area-slope relationship, *Water Resour. Res.*, *27*(7).

Willgoose, G., R. L. Bras, and I. Rodríguez-Iturbe (1994), Hydrogeomorphology modelling with a physically based river evolution model, in *Processes Models and Theoretical Geomorphology*, edited by M. J. Kirkby, John Wiley & Sons.

Williams, C. A., and J. D. Albertson (2005), Contrasting short- and long-timescale effects of vegetation dynamics on water and carbon fluxes in water-limited ecosystems, *Water Resour. Res.*, *41*.

Wistendahl, W. A. (1958), The floodplain of the Raritan River, New Jersey, *Ecological Monographs*, *28*, 129–153.

Yair, A. (1990), The role of topography and surface cover upon soil formation along hillslopes in arid climates, *Geomorphology*, *3*(3-4), 287 – 299, doi:DOI: 10.1016/0169-555X(90)90008-E, proceedings of the 21st Annual Binghamton Symposium in Geomorphology.

Yair, A. (1995), Short and long term effects of bioturbation on soil erosion, water resources and soil development in an arid environment, *Geomorphology*, *13*(1-4), 87 – 99, doi:DOI: 10.1016/0169-555X(95)00025-Z, biogeomorphology, Terrestrial and Freshwater Systems.

Yair, A., and A. Kossovsky (2002), Climate and surface properties: hydrological response of small arid and semi-arid watersheds, *Geomorphology*, *42*(1-2), 43 – 57, doi:DOI: 10.1016/S0169-555X(01)00072-1.